STUDY ON DEVELOPING NANO COATED SOLAR PHOTOVOLTAIC CELL AND OPTIMIZING ITS PROCESS PARAMETERS TO IMPROVE THE ENERGY ABSORBING EFFICIENCY

Thesis submitted to the

PONDICHERRY UNIVERSITY

for the award of the degree of

DOCTOR OF PHILOSOPHY

IN

MECHANICAL ENGINEERING

by

M.JEEVARANI,

under the guidance of

Dr. R.ELANSEZHIAN

(Supervisor)

DEPARTMENT OF MECHANICAL ENGINEERING

PONDICHERRY ENGINEERING COLLEGE

PUDUCHERRY – 605 014

INDIA

JULY 2014

Dr. R.ELANSEZHIAN, Associate Professor (Supervisor)
Department of Mechanical Engineering
Pondicherry Engineering College
Puducherry – 605 014, India

BONAFIDE CERTIFICATE

Certified that this thesis entitled "**STUDY ON DEVELOPING NANO COATED SOLAR PHOTOVOLTAIC CELL AND OPTIMIZING ITS PROCESS PARAMETERS TO IMPROVE THE ENERGY ABSORBING EFFICIENCY**", submitted for the award of the degree of Doctor of Philosophy in Mechanical Engineering of Pondicherry University, Puducherry is a bonafide and authentic record of the individual work done by **M.JEEVARANI**, under my supervision and guidance during the requisite period under the regulations in force. This work is original and this thesis or any part thereof has not been submitted elsewhere for the award of any Degree or Diploma, Fellowship, Associateship of this university or any other university.

Place : Puducherry
Date : 10.07.2014

Dr. R.ELANSEZHIAN
Supervisor

DECLARATION

I do hereby declare that the thesis entitled "**STUDY ON DEVELOPING NANO COATED SOLAR PHOTOVOLTAIC CELL AND OPTIMIZING ITS PROCESS PARAMETERS TO IMPROVE THE ENERGY ABSORBING EFFICIENCY"** submitted to Pondicherry University for the award of Degree of Doctor of Philosophy is a record of original and independent research work done by me under the supervision and guidance of **Dr. R. ELANSEZHIAN** (Supervisor) and it has not previously formed the basis for the award of any Degree or Diploma, Fellowship, Associateship or other similar titles to any candidate of this university or any other university.

Place : Puducherry **M.JEEVARANI**
Date : 10.07.2014

Dedicated

To my beloved

Parents,

Husband Anand

And Daughter Abinaya

ACKNOWLEDGEMENTS

I have immense pleasure in expressing my profound gratitude and sincere thanks to my guide **Dr. R. Elansezhian** for his valuable guidance, unflinching encouragement, useful suggestions, keen interest and timely help in completing this thesis successfully. It has been a great pleasure to work with him and I will always cherish my association with him. His perpetual energy, moral support, dedication and continuous guidance enabled me to complete this work successfully.

I would like to express my sincere appreciation to **Prof. A. Selvaraju**, Head, Department of Mechanical Engineering, for all the administrative support. I am thankful to the members of my Doctorial committee **Prof. K. Mahadevan and Prof. N. Sathyanarayana** for their useful suggestions. Their involvement with originality has triggered and nourished my intellectual maturity that will benefit me for my academic career. It's a great opportunity for me to pay respect to all my teachers who have helped me to shape my career.

I would like to specially acknowledge the help and cooperation extended by **Dr. Kannan**, X-ray Diffraction lab, and **Dr. Suresh Babu**, for his support to use the spin coating and UV-Visible measurement facility in his research lab, Centre for Nano Science, Pondicherry University. I would like to thank **Dr.N.Periyasamy** for his support to use I-V characteristics facility in his research lab, Centre for Green Energy Technology. I would like to thank **Mr. N. Kirubakaran,** SEM lab, **Mr. Nagarajan**, thin film lab, **Mr. N. Tamilselvan and Mr. B. Kaniamuthan** (research scholar),

nano photovoltaics lab, for extending their help and cooperation during this research work.

I would also like to thank **Dr. Mohan**, electroplating department, CECRI, Karaikudi, **Dr. Arout selvan**, Scientist, DRML, Hyderabad, for helping to carry out some of the experiments in their organizations. I would like to thank **Dr. Rajasekaran**(CECRI) who showed the proper way to do my research work and I would like to thank **Mr. Pavul raj** (research scholar, CECRI), who showed constant support to make surface roughness and coating thickness measurements. I would like to thank **Mr. Paramananda Jena** for his valuable support to identify elements using XRD software.

It is a great pleasure for me to work with a friendly and cheerful group of fellow scholars and I thank **Miss. Karpagavalli, Miss. Sathyaprasanna, Mr. Muraliraja, Mr. Anand, and Mr. Mohan** for their support and encouragement during the course of this research work. I wish to thank my sister **M. Kanimozhi** for helping me in documentation of this thesis. I wish to thank everybody who helped directly or indirectly to make my research work successful.

My deepest gratitude goes to my parents for their unflagging love and support throughout my life; this dissertation is simply impossible without them. I extend my gratitude to my beloved husband who gave full support to me in all difficult family situations and helping me by giving his valuable suggestions to shape this research work. Special and lovable thanks to my daughter who suffered along with me by travelling to various places in the course of my research work. Thanks to Almighty for making my life through more bountiful.

M.JEEVARANI

ABSTRACT

In this research, experimental investigations were carried on optimizing process parameters of electroless coating of copper and spin coating of TiO_2 on copper coated solar PV cells. A comprehensive experimental study of electroless copper coating and spin coating of TiO_2 on solar PV cells under specific coating conditions have been carried out and reported in this paper.

Copper was coated over solar PV cells using electroless method, which acts as conducting medium. Process parameters such as pH, temperature and effect of surfactants concentration were varied and corresponding coating thickness and voltage were measured. The preliminary experiments were conducted by varying the level of pH, temperature and surfactants and their effects were studied using full factorial method. The pH was varied at 4 different values such as 4-5, 5-6, 8-9, 9-10 and temperature was varied at different values such as 75 ºC, 80 ºC, 85 ºC, 90 ºC. The surfactant Sodium do-decyl sulphate was used and its concentration was varied from 0-1.4g/l. Coating thickness, voltage, surface roughness, surface tension and contact angle were measured for the samples with different surfactant concentrations. The preliminary experiments were conducted to fix the activation and immersion time of the sample .The control parameters and their levels were fixed for three factors such as pH, temperature and surfactant concentration.

Design matrix was framed with 3 factors and 2 levels (2^3 Factorial Design). Design of experiment (DOE) was conducted to optimize the various process parameters for electroless coating of Cu on solar PV cells and the analysis was made using Analysis of Variance method (ANOVA). Minitab software was used for the analysis and the mathematical equations were framed relating different process parameters.

Titanium di-oxide is prepared using solgel method and it is coated on the PV cells using spin coating. The sol-gel processing made use of a low temperature chemical method for production of inorganic oxide materials. The process may involve single or multi component oxides in crystalline or amorphous form and is suitable for thin film coating production. TiO_2 is an excellent material for

environmental purification, photo-electrochemical solar energy conversion and optical application.

Titanium-iso prop oxide - 6.3ml (SOURCE), ethanol - 50ml (SOLVENT), and acetic acid - 5ml (COMPLEXING AGENT) were the principal materials used in the study. Ethanol was subjected to magnetic Stirring for around 50 minutes and then 5ml of acetic acid was added and allowed to mix for 10 minutes. Titanium-iso prop oxide was added to the mixture and allowed to mix for 20 minutes to form the sol-gel. This formed gel was used later for spin coating. Preliminary experiments were conducted by coating the samples at different rpm ranges, from 1000 rpm to 5000 rpm, using intervals of 500 rpm with spinning time ranging from 20 -120 sec at an interval of 20 sec. The samples were heated to different temperatures from 50 ^{o}C to200 ^{o}C, since the coating thickness depends on the evaporation of the solvent at high temperature. The control parameters and their levels were fixed for three factors such as spinning speed, spinning time and temperature. Design matrix was framed with 3 factors and 2 levels (2^3 Factorial Design). Design of experiment (DOE) was conducted to optimize the various process parameters for spin coating of TiO_2 on copper coated solar cells. The analysis was made using Analysis of Variance method (ANOVA). Minitab software was used for the analysis and the mathematical equations were framed relating different process parameters.

The nano additives such as ZnO, CuO and Al_2O_3 were added at various percentages in the electroless copper bath and the samples were coated with the above nano additives. Studies were made on the influence of nano additives on solar Photovoltaic cells with respect to improvement of coating thickness, surface roughness, voltage and power generated. Comparisons were made between (i) copper coated samples, (ii) Cu + TiO_2 coated samples, (iii) Cu + Nano CuO (iv) Cu + Nano ZnO and (v) Cu + Nano Al_2O_3. (vi)Cu + Nano CuO+ TiO_2 coated samples (vii) Cu + Nano ZnO+ TiO_2 coated samples (viii) Cu + Nano Al_2O_3 + TiO_2 coated samples and (ix) non- coated sample. The comparative studies were made using SEM, EDAX, XRD and UV-VIS spectroscopy.

Surface morphology and the cross section of the samples were studied using Scanning Electron Microscope (Hitachi S-3400N) analysis and the elemental

composition of the samples were identified using Energy-dispersive X-ray spectroscopy (EDAX). The various XRD patterns of the samples were studied using (RIGAKU ULTIMA IV) X-ray Diffractometer. The absorbance, reflectance and the transmission characteristics of the samples were studied using UV-VIS spectrometer (Perkin Elmer lambda 650 S) UV/VIS spectrometer. The surface roughness of the sample was measured using surface roughness meter (Mitutoyo portable surface roughness tester). The coating thickness was measured using Positector 6000 instrument. The voltage and current was measured using multimeter (Exitech) with decade box arrangements under environmental conditions. The I-V characteristics were measured using a solar simulator (class AAA, ORIEL SYSTEMS).

CONTENTS

ACKNOWLEDGEMENTS ..... **i**
ABSTRACT ..... **iii**
CONTENTS ..... **vi**
LIST OF TABLES ..... **xi**
LIST OF FIGURES ..... **xii**
ABBREVIATIONS ..... **xvii**
NOTATIONS ..... **xix**
Chapter 1 : INTRODUCTION **1**
1.1 NEED FOR SUSTAINABLE ENERGY SOURCES: 2
1.2 ENVIRONMENTAL IMPACT OF FOSSIL FUELS: 2
1.3 SOLAR ENERGY AND ITS ADVANTAGES 2
1.4 SOLARENERGYAND ITS CONVERSION CHALLENGES 3
1.4.1 Energy Cost: 3
1.4.2 Energy Fluctuation: 3
1.4.3 Location Dependency: 4
1.4.4 Huge Investment Requirement 4
1.5 GROWTH OF SOLAR PV INDUSTRY AND Si REQUIREMENT 4
1.6 PLACE OF PHOTOVOLTAICS IN ENERGY SUPPLY. 5
1.7 LOSSES IN SOLAR CELL 6
1.7.1 Loss of low energy photons 7
1.7.2 Loss due to excess energy of photons 7
1.7.3 Voltage loss 7
1.7.4 Fill Factor loss 7
1.7.5 Loss by reflection 8
1.7.6 Loss due to incomplete absorption 8
1.7.7 Loss due to metal coverage 8
1.7.8 Recombination losses 8
1.8 MINIMIZATION OF OPTICAL LOSSES 8
1.8.1 Anti–reflective coating(ARC) 9
1.8.2 Surface Texuring 10
1.9 ELECTROLESS COATING MECHANISM 11
1.10 SPIN COATING THEORY 12
1.11 ORGANISATION OF THESIS 13
1.12 OUTLINE OF RESEARCH METHODOLOGY 14
Chapter 2 : LITERATURE REVIEW **15**
2.1 ELECTROLESS COPPER COATING 16

2.2 EFFECT OF P^H VALUES 18
2.3 EFFECT OF OPERATING TEMPERATURES 19
2.4 SURFACTANTS 20
2.5 SODIUM DO-DECYL SULPHATE (SDS) 21
2.6 ANTI REFLECTION COATING 22
2.7 TITANIUM DI-OXIDE 22
2.8 MECHANISM OF PHOTOCATALYSIS. 23
2.9 APPLICATIONS OF TITANIUM DI-OXIDE 24
2.9.1 Self-cleaning function 24
2.9.2 Anti-fogging glass 24
2.9.3 Photocatalytic Anti Bacterial Effect 25
2.10 INTRODUCTION TO THE SOL – GEL TECHNOLOGY 25
2.11 STEPS IN PRODUCING Si WAFERS 26
2.12 MULTICRYSTALLINE Si INGOTS 28
2.13 SOLAR CELL CHARACTERISTICS 29
2.13.1. Short circuit current(I_{sc}) : 29
2.13.2 Open circuit Voltage V_{oc} : 29
2.13.3 Fill factor FF: 30
2.13.4 Efficiency η: 30
2.14 ANALYTICAL TECHNIQUES 30
2.14.1 Solar simulator : I-V measurement 31
2.14.2 UV –Visible Spectroscopy 32
2.15 INTRODUCTION TO DESIGN OF EXPERIMENTS 33
2.15.1 Full factorial design 33
2.15.2 Main effect plot 34
2.15.3 Interaction Plot 34
2.16 SUMMARY 34
Chapter 3 : EXPERIMENTAL DETAILS 35
3.1 PROBLEM DEFINITION 35
3.2 PROPOSED SOLUTION 35
3.3 COATING TECHNIQUES USED 35
3.4 BASIC GOVERNING EQUATION 35
3.5 MANUFACTURING OF MULTICRYSTALLINE SOLAR CELL 36
3.5.1 Wafer dicing: ID and wire sawing 36
3.6 ELECTROLESS COPPER COATING PROCESS 37
3.6.1 Preparation of the Substrates 37
3.6. 2 Cleaning of the Substrates 38

3.6.3 Activation / Catalyzation of the Substrate 38
3.6.4 Electroless Copper Coating Bath and Operating Conditions 39
3.7 SPIN COATING PROCESS 41
3.8 MEASUREMENT OF P^H 43
3.9 COATING THICKNESS MEASUREMENT 43
3.10 SURFACE ROUGHNESS MEASUREMENTS 44
3.11 ESTIMATION OF CONTACT ANGLE 45
3.12 PENDANT DROP SHAPE METHOD 46
3.13 ESTIMATION OF SURFACE TENSION 47
3.14 SCANNING ELECTRON MICROSCOPE (SEM) 49
3.15 X-RAY DIFFRACTOGRAM (XRD) 50
3.16 MEASUREMENT OF I_{SC} AND V_{OC} 50
3.17 I-V MEASUREMENT 52
3.18 UV-VISIBLE SPECTROSCOPY 53
3.19 SUMMARY 54
Chapter 4 : EXPERIMENTAL RESULTS AND DISCUSSIONS 55
4.1 PRELIMINARY EXPERIMENTS FOR ELECTROLESS PROCESS 55
4.1.1 Preliminary Experiments by varying pH of the Bath 55
4.1.2 Preliminary Experiments by Varying Temperature of the Bath 56
4.1.3 Preliminary Experiments by Varying Surfactant Concentration. 58
4.1.3.1 SEM Micrograph at Different Surfactant Concentration 60
4.1.4 Measurement of Various Properties for Different Activation Time. 62
4.1.4.1 SEM Micrograph for Different Activation Time 64
4.1.5 Measurement of Various Properties for Different Immersion Time 64
4.2 ELECTROLESS COPPER COATING ON MULTICRYSTALLINE SOLAR CELL 66
4.3 PRELIMINARY EXPERIMENTS FOR SPIN COATING PROCESS 69
4.3.1 Preliminary Experiments by Varying Spinning Speed 69
4.3.2 Preliminary Experiments by Varying Spinning Time 70
4.3.3 Preliminary Experiments by Varying Temperature 72
4.4 SPIN COATING OF TIO_2 ON COPPER COATED SOLAR CELL 73
4.5 X-RAY DIFFRACTION ANALYSIS 75
4.6 UV-VISIBLE SPECTROSCOPY ANALYSIS 76
4.7 I-V CHARACTERISTICS 78
4.8 SUMMARY 80
Chapter 5 : DESIGN OF EXPERIMENTS 81

5.1 DESIGN OF EXPERIMENTS FOR ELECTROLESS COPPER COATING ON SOLAR CELLS 81
5.1.1 Control Parameters and Their Levels 81
5.1.2 Design Matrix 82
5.1.3 Measurement of Various Properties for Electroless Copper Coated Solar cells at Different Run Labels. 83
5.1.4 Analysis of Electroless Copper Coating Process Using ANOVA 83
5.1.4.1 Main Effects Plot for Various Output Responses 83
5.1.4.2 Interaction Plot for Various Output Responses 85
5.2 DESIGN OF EXPERIMENTS FOR SPIN COATING OF TiO_2 ON COPPER COATED SOLAR CELLS 86
5.2.1Control Parameters and Their Levels 87
5.2.2 Design Matrix 87
5.2.3 Measurement of Various Output Responses for Different Run Labels 88
5.2.4 Analysis of Spin Coating Of TiO_2 on Copper Coated Solar Cell Using ANOVA 88
5.2.4.1 Main Effect Plot 88
5.2.4.2 Interaction Plot 90
5.3 SUMMARY 92
Chapter 6 : COMPARATIVE STUDIES 93
6.1 COMPARITIVE STUDY WITH THE ADDITION OF NANO ADITIVES TO THE ELECTROLESS COPPER BATH 93
6.1.1 Measurement of Various Properties of Copper Coated Solar Cell With Addition of Nano Additives 93
6.1.2 SEM Images of Copper Coated Solar Cell With the Addition of Nano Additives 96
6.1.3 Energy-Dispersive X-Ray Analysis Results of Copper Coated Solar Cell With the Addition of Nano Additives 96
6.1.4 Comparison of UV-Visible Spectroscopy of Copper Coated solar Cell with Addition of Nano Additives 98
6.2 COMPARITIVE STUDY WITH THE SPIN COATED TiO_2 ON COPPER COATED SOLAR CELL WITH NANO ADDITIVES 99
6.2.1 SEM and EDAX analysis 99
6.2.2 UV-Visible Spectroscopy analysis 100
6.3 SUMMARY 101
Chapter 7 : CONCLUSION 102
7.1 EFFECT OF COPPER TEXTURING 102
7.2 OPTIMIZATION OF ELECTROLESS PROCESS 102
7.3 EFFECT OF TiO_2 COATING 102
7.4 OPTIMIZATION OF SPIN COATING 102

7.5 ADDITION OF NANO ADDITIVES 103
7.6 FUTURE SCOPE..... 103
APPENDIX 104
REFERENCES..... 109
LIST OF PUBLICATIONS 115

LIST OF TABLES

Table 3.1: Compositions of plating bath used for electroless copper coatings 39
Table 4.1: Experiments by Varying Activation Time 62
Table 4.2: Experiments by Varying Immersion Time 64
Table 4.3: Measurement of Various Properties by Varying Spinning Speed 69
Table 4.4: Measurement of Various Properties by Varying Spinning Time 71
Table 4.5: Measurement of Various Properties by Temperature 72
Table 4.6: Electrical Properties of Copper Coated Solar Cell and Reference Cell 80
Table 5.1: Control Parameters 82
Table 5.2: Design Matrix for Electroless Copper Coating Process 82
Table 5.3: Properties at Different DOE Run Labels 83
Table 5.4: Control Parameters 87
Table 5.5: Design Matrix for Spin Coating Process 88
Table 5.6: Various Output Responses for Different Run Labels 88
Table 6.1: Various Parameters by the Addition of CuO Nano Additives 93
Table 6.2: Various Parameters by the Addition of Al_2O_3 Nano Additives 93
Table 6.3: Various Parameters by the Addition of ZnO Nano Additives 94

LIST OF FIGURES

Fig. 1.1: Average PV module prices (for 125 W or higher sized module) 5
Fig. 1.2: P-N Junction illuminated by solar radiation 5
Fig. 1.3: Generation of electron hole pair as a function of depth of solar cell..... 6
Fig. 1.4: Possible interactions of solar radiation falling on a solar cell 9
Fig. 1.5: Anti-Reflective Coating..... 10
Fig. 1.6: Surface Texturing 10
Fig. 1.7: ARC with surface texturing..... 11
Fig. 1.8: Electroless Coating Mechanism 11
Fig. 1.9: Comparison of electroplating with electroless plating process 12
Fig. 1.10: Outline of Research Methodology..... 14
Fig. 2.1: Effect of pH values on plating rate in additive-free electroless baths 19
Fig. 2.2: Effect of temperatures on plating rate in additive-free electroless baths 20
Fig. 2.3: A plot of conductivity against surfactant concentration 21
Fig. 2.4: Illustration of structure of anionic surfactant SDS 21
Fig. 2.5: Mechanism of Photocatalysis 23
Fig. 2.6: Applications of Titanium – Di oxide..... 24
Fig. 2.7: Steps in production of Si wafers from raw Si (Quartzite) 27
Fig. 2.8: Process for production of multicrystalline Si ingots 29
Fig. 2.9: Typical plot of a solar cell I-V curve and its parameters..... 29
Fig. 2.10: Setup of solar simulator for I-V characterization of solar cell 31
Fig. 2.11: Typical I-V curve and other parameters obtained from solar simulator..... 32
Fig. 2.12: Diagram of a single-beam UV/Vis spectrophotometer 33
Fig. 3.1: Inner Diameter Sawing..... 36
Fig. 3.2: Wire Sawing 37
Fig. 3.3: Dicing of Multicrystalline Square Wafers..... 37
Fig. 3.4: Solar Cell Samples Cut Into Required Dimensions 37
Fig. 3.5: Chemicals required for cleaning..... 38
Fig. 3.6: Beakers showing the chemicals required for activation of the substrate..... 38
Fig. 3.7: Electronic precision balance..... 39
Fig. 3.8: Magnetic stirrer with conical flask 40
Fig. 3.9: Electroless coating equipment 40
Fig. 3.10: Non coated and copper coated Solar cell samples..... 40

Fig. 3.11: TiO_2 Sol-gel solution 41
Fig. 3.12: Sample Fixed in Chuck of Spin Coating Equipment 41
Fig. 3.13: Procedure for Spin coating process 42
Fig. 3.14: Spin Coating Equipment 42
Fig. 3.15: Measurement of pH using cyberscan pH 510 43
Fig. 3.16: Coating thickness gauge 44
Fig. 3.17: Surface roughness measurement of non-coated solar cell 44
Fig. 3.18: Surface roughness measurement of copper coated solar cell 45
Fig. 3.19: Contact angle meter 46
Fig. 3.20: Schematic line drawing of Contact angle measurement set – up 46
Fig. 3.21: Image of the drop having pendant shape 47
Fig. 3.22: Final image of drop used for analysis of contact 47
Fig. 3.23: Surface Tensiometer Setup 48
Fig. 3.24: Schematic line drawing of Surface Tensiometer Setup 48
Fig. 3.25: Scanning Electron Microscope 49
Fig. 3.26: RIGAKU ULTIMA IV X-ray Diffractometer with solar cell 50
Fig. 3.27: Measurement of I_{SC} and V_{OC} with decade box arrangements 51
Fig. 3.28: Solar cell exposed to environmental conditions 51
Fig. 3.29: Circuit diagram for voltage and current measurement 52
Fig. 3.30: Oriel Sol3A sun simulator used for I-V measurement 52
Fig. 3.31: Perkin Elmer lambda 650 S UV/VIS spectrometer 53
Fig. 3.32: Optical design of 150 mm integrating sphere 54
Fig. 4.1: Coating thickness of electroless coated by varying pH 55
Fig. 4.2: Voltage of electroless coated copper by varying pH 55
Fig. 4.3: SEM micrograph of electroless copper samples with (500X) magnification by varying pH (a) 4-5 (b) 5-6 (c) 8-9 (d) 9-10 56
Fig. 4.4: Voltage of electroless copper coated sample by varying temperature 56
Fig. 4.5: Coating thickness of electroless copper coated sample by varying temperature 57
Fig. 4.6: SEM micrograph of electroless copper coated solar PV cell with magnification 1000X at temperatures (a) 75^{o}C (b) 80^{o}C (c) 85^{o}C (d) 90^{o}C 57
Fig. 4.7: Effect of surfactant on surface roughness 58
Fig. 4.8: Effect of surfactant on surface tension 58
Fig. 4.9: Effect of surfactant on contact angle 59

Fig. 4.10: Effect of surfactant on coating thickness..... 59
Fig. 4.11: Effect of surfactant on coating thickness..... 59
Fig. 4.12: SEM micrograph of electroless copper coated solar PV cell with magnification 1000X at different surfactant concentration 60
Fig. 4.13: Mapping of copper coated silicon surface with surfactant SDS (a) Without surfactant (b) 0.75 g/l (c) 1.2g/l 61
Fig. 4.14: Voltage and Current Density by Varying Activation Time..... 62
Fig. 4.15: Surface Roughness for Various Activation Time..... 63
Fig. 4.16: Coating Thickness for Various Activation Time..... 63
Fig. 4.17: EDAX Diffractogram of solar cell with activation time of 2 minutes 63
Fig. 4.18: SEM Micrograph of Electroless Copper Coated Solar PV Cell with Magnification 1000X by Varying Activation Time..... 64
Fig. 4.19: Voltage and Current Density by varying immersion Time 65
Fig. 4.20: Surface Roughness for Various Immersion Time 65
Fig. 4.21: Coating Thickness For Various Immersion Time 65
Fig. 4.22: SEM image of copper coated solar cell across the grid..... 66
Fig. 4.23: EDAX diffractogram of copper coated on grid surface 66
Fig. 4.25: Mapping of deposition of cu particles on silicon surface and the grid..... 67
Fig. 4.26: Cross section SEM image of copper coated on grid lines 67
Fig. 4.24: EDAX Diffractogram at the silicon surface 67
Fig. 4.27: SEM image of copper coated solar cell showing the copper nano particles at 5000X..... 68
Fig. 4.28: SEM image showing the size of copper nano particles on silicon surface at20,000X..... 68
Fig. 4.29: Variation of coating thickness and voltage with spinning speed 69
Fig. 4.30: Variation of coating thickness and surface roughness with spinning speed 70
Fig. 4.31: Variation of coating thickness and surface roughness with spinning time 71
Fig. 4.32: Variation of coating thickness and voltage with spinning time 72
Fig. 4.33: Variation of coating thickness and surface roughness with temperature 72
Fig. 4.34: Variation of voltage with temperature..... 73
Fig. 4.35: SEM micrograph of spin coated TiO_2oncopper coated solar cell 74
Fig. 4.36: EDAX Diffractogram at the surface of spin coated TiO_2 on copper coated solar cell 74

Fig. 4.37: SEM micrograph showing the cross section of spin coated TiO_2 on Copper Textured solar cell 75
Fig. 4.38: Mapping of Spin Coated TiO_2 on Copper Coated Solar Cell (a) Distribution of Ti (b) Distribution of Cu 75
Fig. 4.39: XRD of Copper Coated PV Cell 76
Fig. 4.40: XRD of Spin coated TiO_2 on Copper Coated PV Cell 76
Fig. 4.41: UV-Vis Absorbance spectra for non- coated, Copper coated and TiO_2 solar cell 77
Fig. 4.42: UV-Vis Reflectance spectra for non- coated, Copper coated and TiO_2 solar cell 78
Fig. 4.43: I-V characteristics of reference cell 79
Fig. 4.44: I-V characteristics of copper coated solar cell 79
Fig. 4.45: I-V characteristics of spin coated TiO_2 on copper coated solar cell 79
Fig. 5.1: Main Effect Plot for Surface Roughness 83
Fig. 5.2: Main Effect Plot for Coating Thickness 84
Fig. 5.3: Main Effect Plot For output power 84
Fig. 5.4: Interaction plot for surface roughness 85
Fig. 5.5: Interaction plot for coating thickness 85
Fig. 5.6: Interaction plot for output power 86
Fig. 5.7: Main Effect Plot For output power 89
Fig. 5.8: Main Effect Plot for Coating Thickness 89
Fig. 5.9: Main Effect Plot for Surface Roughness 89
Fig. 5.10: Interaction plot for output power 90
Fig. 5.11: Interaction plot for surface roughness 91
Fig. 5.12: Interaction plot for coating thickness 91
Fig. 6.1: Variation of coating thickness with percentage variation of nano additives . 94
Fig. 6.2: Variation of surface roughness with percentage variation of nano additives 95
Fig. 6.3: Variation of open circuit voltage with percentage variation of nano additives 95
Fig. 6.4: SEM images of electroless copper coated solar cells with the addition of nano additives with 1000x magnification 96
Fig. 6.5: EDAX of copper coated solar cell with copper oxide nano additive 96
Fig. 6.6: EDAX of copper coated solar cell with Aluminium oxide nano additive 97
Fig. 6.7: EDAX of copper coated solar cell with Zinc oxide nano additive 97

Fig. 6.8: UV –Visible reflectance spectra of copper coated Solar cell with nano additives 98
Fig. 6.9: UV-Visible Absorbance spectra of copper coated solar cell with nano additives 98
Fig. 6.10: SEM image and EDAX of TiO_2 coated on copper coated solar cell with zinc oxide nano additive 99
Fig. 6.11: SEM image and EDAX of TiO_2 coated on copper coated solar cell with Aluminium oxide nano additive 99
Fig. 6.12: SEM image and EDAX of TiO_2 coated on copper coated solar cell with zinc oxide nano additive 100
Fig. 6.13: UV-Visible Absorbance spectra of spin coated TiO_2on copper coated solar cell with nano additives 100
Fig. 6.14: UV-Visible reflectance spectra of spin coated TiO_2 on copper coated solar cell with nano additives 101

ABBREVIATIONS

AFM	Atomic Force Microscope
AM 1.5	Air mass 1.5 condition when the sun is at 45 ^{o} above the horizon.
ANOVA	Analysis of Variance
ARC	Anti Reflective Coating
ASTM	American Society for Testing and Materials
CBO	Cross Beam Optics
CCD	Charge-Coupled Device
CMC	Critical Micelle Concentration
CTAB	Cetyl Trimethyl Ammonium Bromide
CVD	Chemical Vapour Deposition
CZ	Chzokralski process
DAS	Data Acquisition Systems
DOE	Design of Experiments
EDTA	Ethylene Diamine Tetra Acetic acid
EDAX	Energy Dispersive X-ray Spectroscopy
EGS	Electronic Grade Si
EHP	Electron-Hole Pair
FF	Fill Factor
FZ	Float Zone
ID	Inner Diameter
JCPDS	Joint Committee on Powder Diffraction Standards
LED	Light Emitting Diode
MGS	Metallurgical Grade Si
MOS	Metal Oxide Semiconductor

PV	Photovoltaic
PVD	Physical Vapour Deposition
ppb	parts per billion
ppm	parts per million
SDS	Sodium Do decyl Sulfate
SEM	Scanning Electron Microscopy
Si	silicon
STC	Standard Test Conditions
ST	Surface Tension
TEM	Transmission Electron Microscopy
UV	Ultraviolet
XRD	X-Ray Diffraction

NOTATIONS

C	Celsius
I	Intensity of light reflected from a sample
Io	Intensity of light reflected from a reference material
nm	Nano meter
M^+	Metal ions
mA	Milli ampere
mV	MilliVolts
pH	Percentage of hydrogen ions
P_{rad}	Power of solar radiation.
%R	Percentage of Reflectance
R	Reducing agent used in the compositions of bath
R_a	Average surface roughness value
%T	Percentage of Transmittance
V_{oc}	Open circuit voltage
θ	Contact angle
λ	Wavelength of monochromatic light
ρ	Density
μ	Coefficient of friction
η	Efficiency
μm	Micro meter
e-	negative-electron
h+	positive-hole

CHAPTER 1 : INTRODUCTION

Energy is required for a wide range of applications such as transportation, industrial applications, agricultural applications, household applications, household requirements and office applications. It can have many forms like heat energy, electrical energy, chemical energy, nuclear energy, light energy and so on. In the pre-industrial era, fuel wood was the major source of energy. After the discovery of steam engine, coal has become the choice of energy source. The discovery of internal combustion engine resulted in the use of petroleum products (Petrol, diesel and natural gas) to fulfill our energy requirements. The fossil fuels (Coal, Oil and Gas) are either used directly or converted to electricity and transported to be used in industries and homes. Electrical energy is the most convenient form of energy which can be converted into all forms of energy, from the point of view of transmission, distribution and control.

The use of energy plays a very important role in one's life. The availability and accessibility of sufficient amount of energy accelerate the individual's and nation's development. The relationship between social development and use of energy is very clear; nations with more use of energy are in more advanced state of development. Also, it is a well-established relationship that countries having higher per capita annual energy consumption have higher literacy rate, while countries having lower per capita energy consumption have lower literacy rates. For instance, the per capita annual energy consumption in the US is more than12,000 kWh/year, while it is just over 600 kWh/year, in India. There are several other developing countries where the situation is even worse. Therefore, significantly higher energy supply is required for the growth of developing countries and to sustain the lifestyle in the developed countries.

Since the use of energy has become an integral part of our life, its supply should be secure and sustainable. At the same time, it should be economical, environmentally friendly and socially acceptable. The current trends in energy consumption are neither secure nor sustainable. The rising consumption of fossil fuels (and associated prices), together with increasing greenhouse gas emission, threatens

our secure energy supply. The price rise could lead to worldwide recession and the negative environmental effect could cause irreversible change to the global climate. The lack of sufficient energy supply can also hold back the growth of billions of people living in the developing countries. Therefore, development of clean, secure, sustainable and affordable energy sources should be our priority in this century.

1.1 NEED FOR SUSTAINABLE ENERGY SOURCES:

The energy requirement of the world is ever increasing. The increasing energy demands put a lot of pressure on the conventional energy sources (oil, gas and coal). But the fossil fuel-based energy sources are limited in quantity and also cause environmental pollution. Therefore, there is a need for alternative energy sources which can provide us energy in a sustainable manner.

1.2 ENVIRONMENTAL IMPACT OF FOSSIL FUELS:

The fossil fuels are mainly carbon based. Fossil fuels are combusted (burned with oxygen) in order to derive useful energy, for instance, use of coal in power plants and use of petrol in automobiles. The combustion of fossil fuels results in the formation of carbon dioxide (CO_2). After combustion of the fuels, CO_2 is usually released in the atmosphere. This gas absorbs the infrared part of radiation from the earth and re-radiates it back to the earth, creating the effect of a 'Greenhouse'. Due to the greenhouse effect of carbon dioxide, the average global temperature of the earth is believed to be increasing. The pre-historic concentration of CO_2 was 280 ppm (part per million) which has now increased to 377 ppm (2006 data). The other gases like methane, nitrous oxide and chloro fluoro carbon (CFC, which causes damage to ozone layer) are also greenhouses gases, and their concentration in the atmosphere is also increasing due to human activities. The increased temperature of the earth due to the greenhouse effect will result in erratic weather patterns, floods, droughts and submerging of low-lying areas due to melting ice at poles.

1.3 SOLAR ENERGY AND ITS ADVANTAGES

Following are the advantages of using the sun's energy:

- It is an everlasting, renewable energy source.
- It is clean energy source, no potential damage to the environment.

- It is a very large source of energy. The power from the sun intercepted by the earth is about 1.8×10^{11}MW, which are many thousand times larger than our current power consumption from all sources.
- Additionally, solar energy is free, does not cause pollution and is available to all at fairly equal manner, unlike fossil fuel sources, which are concentrated at same locations only. This fact provides a chance that an individual can generate his/her own energy depending on the requirement, at his/her place of choice. This equitable availability can also play a role in social development, especially in developing countries such as India.

1.4 SOLAR ENERGYAND ITS CONVERSION CHALLENGES

The negative effects of the conventional energy sources can be overcome by making use of the sun's energy with additional advantages, but there are significant challenges to be overcome in order to make use of clean energy. These are as follows:

1.4.1 Energy Cost:

The conventional energy sources have always been the most cost-effective way to supply the large amount of electricity needed for modern life. Producing electricity from renewable resources like wind and biomass is simply more expensive. Green technology does not have the infrastructure that fossil fuels have developed over the years, making the initial cost of building green power facilities more expensive. Therefore, cost-effective energy conversion technologies need to be developed.

1.4.2 Energy Fluctuation:

Utility companies can easily stockpile coal to meet the ever-challenging demand for electricity, especially during peak demand hours. Most renewable energy sources cannot be stored to provide for future use; the amount of electricity produced depends on instantaneous wind speed or solar illumination. Therefore, a mechanism for effective energy storage and efficient recovery is required.

1.4.3 Location Dependency:

Fossil fuel power plants can be placed almost anywhere, as long as a railroad or pipeline can reach the site. In contrast, the areas, where green energy like wind and hydropower can be utilized, are limited.

1.4.4 Huge Investment Requirement:

There is also resistance to change caused by the magnitude of the investment in the existing energy infrastructure, and the daunting cost of creating a new one. Every aspect of our energy system has been optimized over the past 100 years of industrial development to suit the existing energy system. Energy assets are typically capital intensive and have long lifetime.

1.5 GROWTH OF SOLAR PV INDUSTRY AND Si REQUIREMENT

Solar PV industry has grown almost 1000 times its size since the time of inception. In 1975, the worldwide PV module production was about 2 $MW_{p,}$ and it has grown to more than 3000 MW_p in 2007. In the last 10 years, the average growth of solar PV industry was more than 30%. Most of this growth happened because of the progress in Si Wafer-based solar PV modules. As of today, more than 90% of the solar PV modules are made in monocrystalline and multicrystalline Si wafers. These wafers are made of high quality Si or what is called **electronic grade** Si.

The electronic grade Si is mainly produced for the microelectronics industry. Since the development of PV modules in 1975, the solar cell industry also started using it. The electronic grade Si manufacturers could supply Si to the solar cell industry as per the requirement. The Si is supplied from their surplus-capacity and from the Si waste produced at the different stages of Si wafer manufacturing. Because of the large growth in PV industry (over 30%) and relatively smaller growth in the microelectronics industry (less than 10%), a time had come when microelectronics industry was not able to supply enough Si to solar cell industry. This started happening in about 2004. From 2004 to 2007, the solar PV module prices gradually increased (instead of decreasing due to volume growth), due to shortage of Si. The price index of solar PV modules for sizes higher than $125W_p$ is shown in Fig.1.1. Increase in solar PV module price in the period of Si shortage can clearly be noticed.

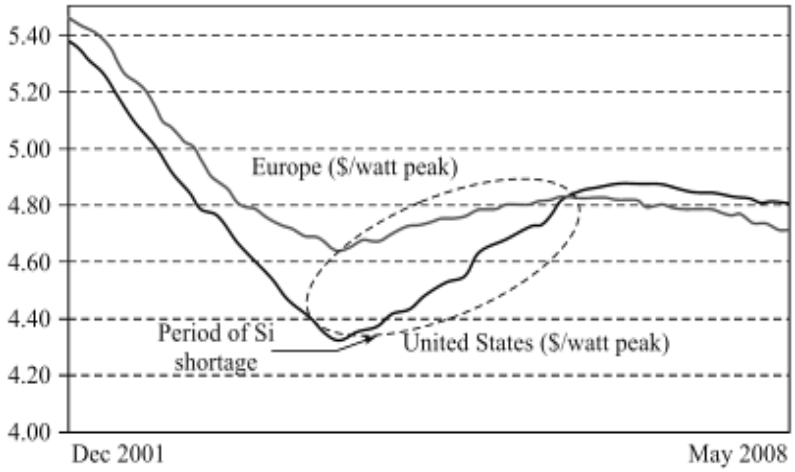

Fig. 1.1: Average PV module prices (for 125 W or higher sized module)

1.6 PLACE OF PHOTOVOLTAICS IN ENERGY SUPPLY

Sunlight can be converted to electricity due to the photovoltaic effect discovered in 1839 by Edmund Becquerel, a French scientist. Sunlight is composed of photons, or packets of energy. These photons contain various amounts of energy corresponding to the different wavelengths of light. When photons strike a solar cell, a semiconductor P-N junction device, they may be reflected or absorbed, or they may pass through the cell. Absorption of a photon in a solar cell results in the generation of electron-hole pair (EHP). This EHP, when separated from each other across the P-N junction, results in the generation of a voltage across the junction, which can drive the current in an external circuit and, therefore, power can be extracted from the solar cell, also referred to as photovoltaic (PV) device.

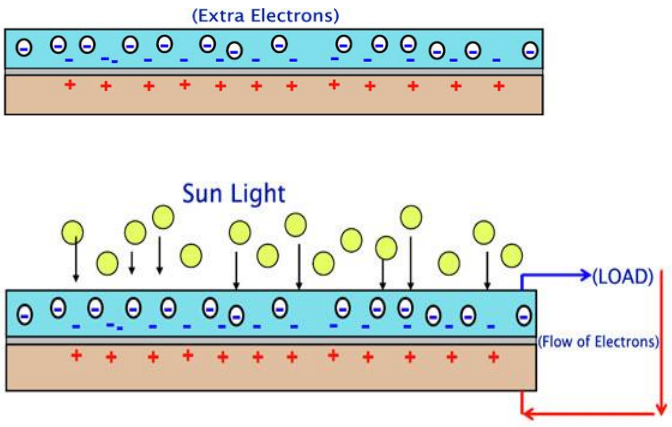

Fig. 1.2: P-N Junction illuminated by solar radiation

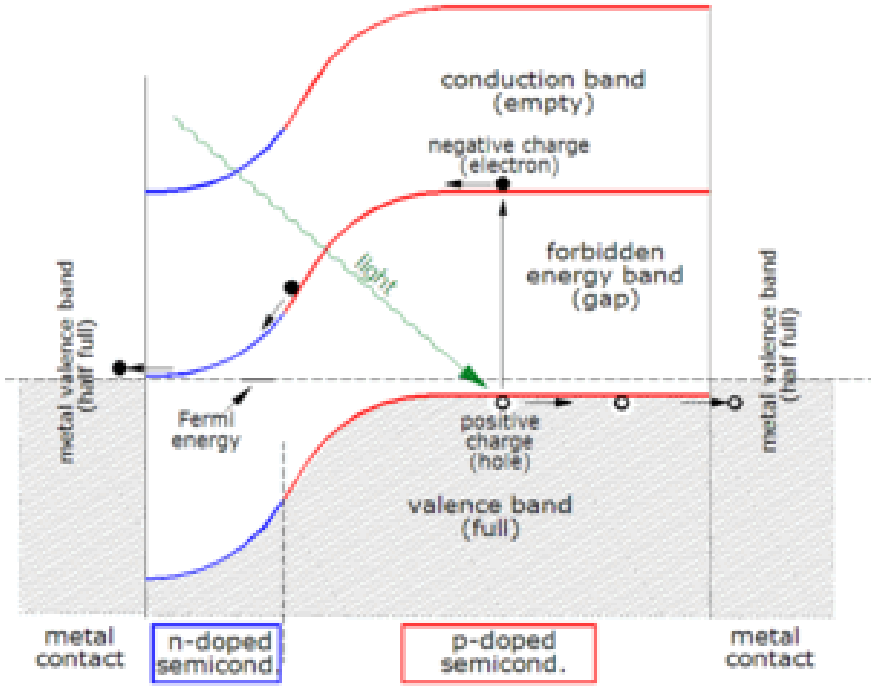

Fig. 1.3: Generation of electron hole pair as a function of depth of solar cell

If a piece of p-type silicon is placed in intimate contact with a piece of n-type silicon, then a diffusion of electrons occurs from the region of high electron concentration (the n-type side of the junction) into the region of low electron concentration (p-type side of the junction). When the electrons diffuse across the p-n junction, they recombine with holes on the p-type side. The diffusion of carriers does not happen indefinitely, however, because charges build up on either side of the junction and create an electric field. The electric field creates a diode that promotes charge flow, known as drift current that opposes and eventually balances out the diffusion of electrons and holes. This region where electrons and holes have diffused across the junction is called the depletion region because it no longer contains any mobile charge carriers.

1.7 LOSSES IN SOLAR CELL

A loss in solar cell refers to loss of photon energy (partial or full) which, due to some reason, is not able to deliver an electron out of a solar cell. This loss could be due to the fundamental reason (limited by material properties) or it could be due to the technological reason (limited by cell processing capabilities). There are several ways in which photon energy loss could occur.

1.7.1 Loss of low energy photons

The photons having energy less than the band gap energy do not get absorbed in the material and therefore, do not contribute to the generation of electron-hole pairs. This is referred as transmission loss, and is almost equal to 23% for a single junction solar cell.

1.7.2 Loss due to excess energy of photons

In an ideal case only, photon of energy equal to the band gap energy is required to excite an electron from valance band to conduction. When the photon energy E is higher than the band gap energy Eg, the excess energy=E-Eg is given off as a heat to the material. This loss is referred as the thermalization loss. For a single junction solar cell, this is equal to about 33%.

1.7.3 Voltage loss

The voltage corresponding to the band gap of a material is obtained by dividing the band gap (potential energy) by charge, i.e., Eg/q. This is referred as the band gap voltage. The actual voltage obtained from a solar cell is Voc. This happens due to the unavoidable intrinsic Auger recombination. The ratio of Voc/Eg/q lies in the range of 0.65 to 0.72.

1.7.4 Fill Factor loss

The I-V curve of ideal solar cell is square (i.e., FILL FACTOR (FF) =1), but in reality, the cell I-V curve is given by the exponential behavior. In the best case, the FF could be 0.89. This type of loss arises from the parasitic resistance (series and shunt resistance) of the cell.

The above said four losses are the fundamental losses which cannot be minimized beyond their fundamental limit. The following are the technological losses, which can be avoided by adopting special fabrication techniques. This technological loss can be divided into optical losses and electrical losses. The optical loss is referred to as the loss of photons which may result in the generation of electron-hole pairs and the electrical loss is referred to as the loss of photons, which are absorbed in solar cell, but do not contribute to the cell output power due

to either recombination or ohmic losses. The losses due to the technological reasons are as follows:

1.7.5 Loss by reflection:

A part of incident photons is reflected from the cell surface. The reflection can be minimized by using anti-reflecting coating and surface texturing.

1.7.6 Loss due to incomplete absorption:

It refers to the loss of photons which have enough energy (i.e.,>Eg) to get absorbed in the solar cell, but do not get absorbed in the cell due to limited solar cell thickness. The incomplete absorption is becoming important in the current scenario as the thickness of the cell is being reduced in order to save the active material for cost reduction purpose. This type of loss can be minimized by having appropriate light trapping schemes.

1.7.7 Loss due to metal coverage:

In wafer based solar cell, the contact to the front side of the cell (from where the light enters) is made in the form of finger and bus bar. This metal contact shadows some light which can be up to 10%. Several approaches have been adopted to minimize this loss which include one-side contacted cell, buried solar cell of transparent contact as used in thin film solar cells.

1.7.8 Recombination losses:

Not all the generated electron-hole pairs contribute to the solar cell current and voltage due to recombination. The recombination could occur in the bulk of material or at the surfaces. This type of recombination can be minimized by appropriate surface and bulk passivation techniques.

1.8 MINIMIZATION OF OPTICAL LOSSES

Solar cell is a P-N junction with metal contacts at both the sides, which is supposed to absorb all solar radiation falling on it. Any loss of radiation will result in less generation of electron-hole pair which will result in the reduction in $I_{L.}$. The loss of solar radiation due to optical loss is referred to as the solar radiation which falls on solar cell, but does not get absorbed due to some reason. The loss of radiation could be

due to the reflection from the solar cell surface, due to the transmission through solar cell or due to the reflection from the metal contact as shown in Fig. 1.4. The optical loss could be as high as 40% to 50%.These optical losses should be minimized in order to get high $I_{L.}$ The optical losses can be reduced by the following design.

- Putting anti –reflection coating on the solar cell surface,
- Texturing front surface to reduce the reflection,
- Minimizing the front metal contact coverage area to reduce contact shading, and
- Making solar cell thicker to increase absorption of low energy photons.

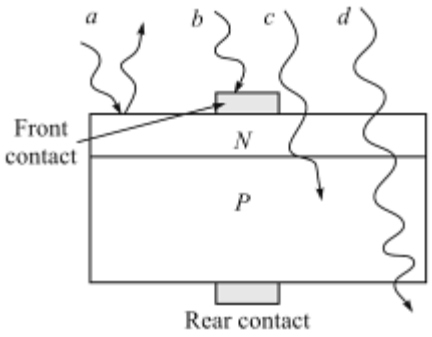

Fig. 1.4: Possible interactions of solar radiation falling on a solar cell

The above figure shows: a-reflection of radiation from front surface, b-absorption or reflection by front metal contact, c-absorption of radiation in the solar cell and d-transmission of radiation through the cell.

1.8.1 Anti–Reflective Coating(ARC)

An ARC is a thin layer of a dielectric material deposited on the surface of solar cell. It should not absorb any light and should reduce the reflection (bare si surface reflects about 30% of incient light). The reduction in reflection is based on destructive interference. In order to obtain the condition of destructive interference, thickness d_1 and refractive index n_1 of the ARC should be properly chosen. The thickness of the dielectric ARC should be such that the radiations reflected from the air-ARC interface and from the ARC- semiconductor interface have 180^o phase difference as shown in Fig. 1.5. The out of phase waves will have destructive interference resulting in zero/smaller reflected energy. This requires that for the normal incidence, the thickness of the ARC should be quarter of the wavelength i.e.

$$d_1=\frac{\lambda o}{4n_1}$$

where λ_o is the wavelength of radiation in air and λ_o/n_1 is the wavelength of radiation in the dielectric medium of refractive index n_1.

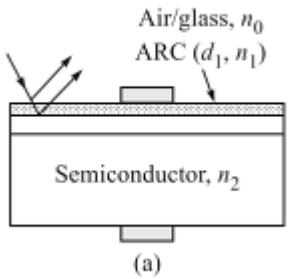

Fig. 1.5: Anti-Reflective Coating

In the above figure, minimization of reflection loses is achieved by putting anti-reflective coating(ARC) of thickness d_1 and refractive index n_1.

1.8.2 Surface Texturing

Surface texturing is another technique of reducing reflection. It is done by making the surface rougher. Reflection is reduced from a rough surface as it increases the chances of reflected rays to bounce back on the surface as demonstrated in the Fig.1.6. In thisway, rays in the second interaction with the surface may get into the cell and overall reflection get reduced.With the surface texuring alone, the weighted average reflection of the Si surface can be brought down to about 11%. Together with the surface texuring and ARC deposition as shown in Fig. 1.7, the overall reflection can be brought down to within 3%.

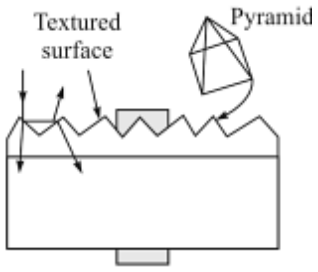

Fig. 1.6: Surface Texturing

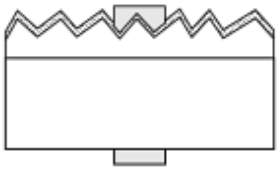

Fig. 1.7: ARC with surface texturing

1.9 ELECTROLESS COATING MECHANISM

Electroless coating processes deposit metallic coating on a substrate without the use of an external voltage or current. They are commonly referred to as chemical metal deposition because the electrons required to bring about the discharge of metal ions are produced by a chemical reaction in solution. Deposition of metal is made from solutions containing reducing agents. Such deposits form only on certain catalytically active surfaces (autocatalytic deposition). The electrons needed to reduce the metal ions are provided by the reducing agents *R* which surrender *n* electrons, while getting oxidized to $R^{(n+)}$ as shown in Fig. 1.8. The simplified form of the reaction which describes the electroless process is given as follows:

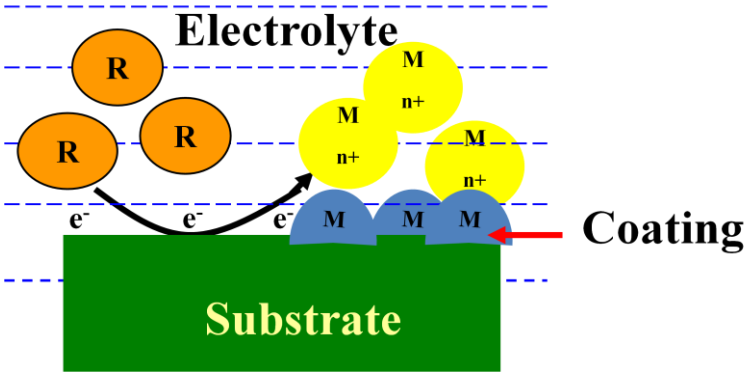

Fig. 1.8: Electroless Coating Mechanism

R-Reducing agent, M^{n+}-Metallic ions

Simplified form of the reaction:

$$R \rightarrow R^{(n+)} + ne^- \quad \text{---------- Eq(2.1)}$$

$$M^{n+} + ne^- \rightarrow M \quad \text{---------- Eq(2.2)}$$

It is properly named autocatalytic, because the oxidation of the reducing agent can start or become self-sustained only at the depositing metal surface. Plating can be done on non-catalytic base materials, after suitable activation of the surfaces involved.

Electroless deposits of nickel, copper, gold, silver, cobalt, palladium etc. and of alloys involving one or more of these metals have been produced in this process on various metallic and non metallic substrates.

In contrast to electroplating, electroless plating does not involve electric field distribution. As a consequence uniformity of coating thickness could be achieved even on intricate part geometries. A schematic comparison of electroplating and electroless plating is shown in Fig. 1.9.

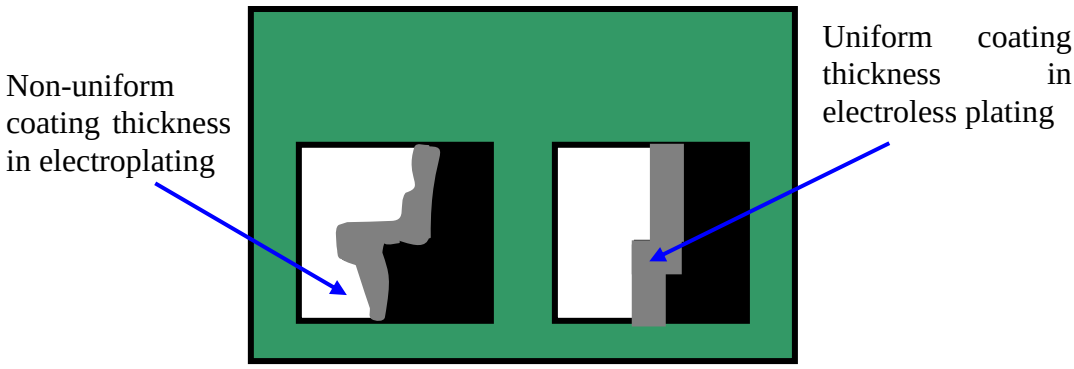

Fig. 1.9: Comparison of electroplating with electroless plating process

1.10 SPIN COATING THEORY

Spin coating involves the acceleration of a liquid puddle on a rotating substrate. The coating material is deposited in the center of the substrate either manually or by a robotic arm. The physics behind spin coating involve a balance between centrifugal forces controlled by spin speed and viscous forces which are determined by solvent viscosity.

The spin coating technique consists of four basic stages:

1. The polymer is dispensed onto the wafer
2. The polymer is spread across the wafer (by spinning at approximately 500 rpm)
3. The wafer is then spun at a higher speed (2000-4000 rpm)
4. The "edge bead" is removed using a backside wash cycle which causes solvent to curl back over the lip of the wafer and wash off the "bead" that is created due to the surface tension at the edge of the wafer.

Some variable process parameters involved in spin coating are:

- Solution viscosity

- Solid content
- Angular speed
- Spin Time

The film-forming process is primarily driven by two independent parameters – viscosity and spin speed. The range of film thicknesses easily achieved by spin coating is 1-200µm. For thicker films, high material viscosity, low spin speed, and a short spin time are needed. However, these parameters can affect the uniformity of the coat. Multiple coatings are preferred for a film thickness greater than 15µm.

1.11 ORGANISATION OF THESIS

This thesis contains seven chapters starting with an introduction to the importance of energy, and the need for sustainable energy and the crisis due to fossil fuels. It discusses about advantages of solar energy and the challenges in harvesting it. This discussion leads to the growth of PV industry, Si requirement, and losses in solar cell and how to minimize these losses. With this discussion the objective of this research starts and ends up with two coating techniques to overcome these losses which lead to high efficiency solar cell. In chapter2, a comprehensive literature review on electroless copper coatings, mechanisms involved and the effect of various parameters of electroless copper coatings are presented. Literature on TiO_2, its applications and the mechanism of Photocatalysis are presented. The details of experimental and analytical procedures used in this work are presented in chapter 3. Chapter 4 presents the results and discussions of preliminary experiments conducted to fix the parameters for DOE in electroless copper coating and spin coating of TiO_2 of solar cell, studies based on characterization of solar cell with copper coating and TiO_2 coating on solar cell. Chapter 5 presents the Minitab results of the Design of experiments (DOE) conducted for electroless copper coating and spin coating of TiO_2 on solar cell. Chapter 6 presents the comparative study conducted by the addition of nano additives to the electroless copper bath. Conclusions and the scope for future research work are highlighted in Chapter 7. The overall outline of present research study is presented in Fig. 1.10.

1.12 OUTLINE OF RESEARCH METHODOLOGY

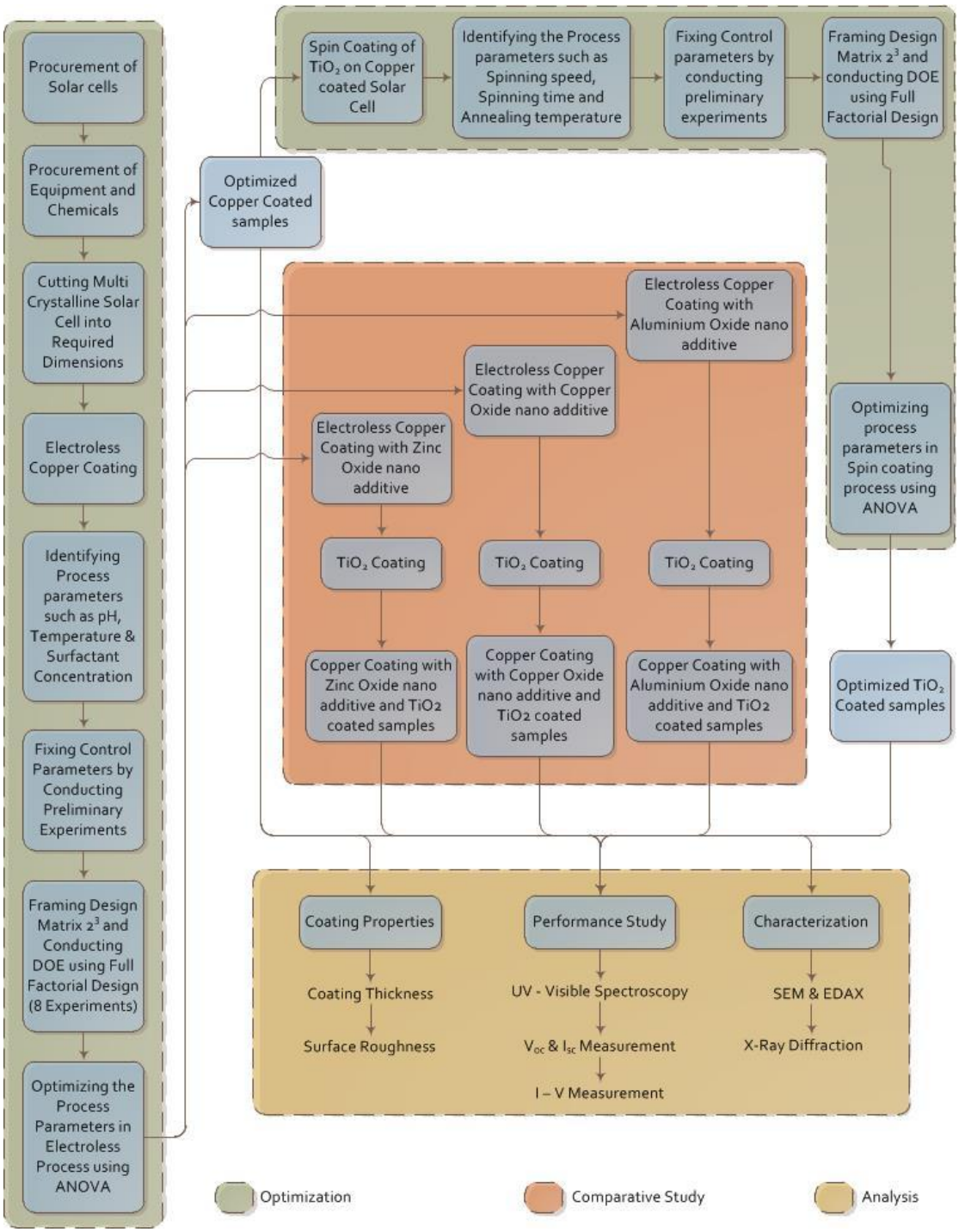

Fig. 1.10: Outline of Research Methodology

CHAPTER 2 : LITERATURE REVIEW

Photovoltaic cells convert sunlight directly into electricity. A solar cell (also called photovoltaic cell or photoelectric cell) is a solid state electrical device that converts the energy of light directly into electricity by the photovoltaic effect. The exponential growth in the PV market and necessity of a material cheaper than mono crystalline silicon make multi crystalline silicon an important alternative. The drawback is that, the silicon has a high electrical resistivity and high reflectivity due to the smooth surface of the silicon wafer (**Oskam, 1998 and Andrew, 2000**).

In this research, mask less and electroless fabrication were performed to form patterned nano particles of copper metal species on the activated surface of multi crystalline silicon wafer. The deposition was achieved spontaneously and selectively at the defect sites on the wafer surface by immersing into alkaline electroless copper bath containing trace amount of copper ion species. The copper nano particles encapsulated on the silicon surface created the roughness on the silicon surface which itself act as an anti reflection coating reducing the reflection and the dense copper particles deposited on the silver grid lines will enhance the corrosion resistance and anti bacterial properties.

Copper particles were deposited in the spaces between the particles prior to deposition of the polymer electrolyte, forming continuous copper bridges to quickly transport generated photoelectrons from the particle surfaces to the transparent electrode, reducing electron/hole recombination. Several metal deposition methods were used including sputtering, electroplating, and doctor-blade coating. This strategy resulted in significant enhancement of the solar conversion efficiency compared to a similar design constructed without the copper coating *(***Sahrul Saehana et al.,**).

High-efficiency silicon solar cells need a textured front surface to reduce reflectance since optical losses due to reflectance of incident solar radiation are one of the most important factors which limits their efficiency. Only a very limited amount of research had been carried out to improve the performance of solar cells using non-vacuum deposition techniques. Electroless coatings are pioneer and popular coatings for improving the functional performance of various components for the following reasons such as high uniformity, good surface coverage and improved corrosion

resistance. The cost of using this approach is significantly lower than PVD and CVD processes (**Hilton B, 2011**). Hence it is a worthwhile attempt to use electroless coating technique for coating on solar cells.

Here electroless process was used to texture the silicon surface and also for the coating on the grid surface. Copper indium diselenide (CIS) has been deposited on molybdenum substrates using electroless process (**Manjunatha pattabi, 2000 and balakrishnan Kavitha, 2011**).

2.1 ELECTROLESS COPPER COATING

Electroless copper deposition can be performed on a catalytic surface due to anodic oxidation of a reducing agent and cathodic reduction of copper ions. Catalytic metal (palladium) activates the silicon surface through the mechanism of contact displacement, while the surfaces of silicon dioxide remain inert. The contact displacement deposition (also known as immersion deposition, galvanic deposition, conversion, etc.) is a reaction in which electrons are supplied not by an oxidation (as in electroless deposition), but by the substrate itself (**Paunovic, 1968 and Buck, 1964).**

Since silicon is not thermodynamically favorable for the initiation of electroless copper deposition, contact displacement deposition of palladium is done to form a seed layer where the electroless process can begin (**Nathan, 2012., Paunovic, 1968., Paunovic, 1998**). The palladium activation creates catalytic sites (nucleation centers) on the silicon surface, enabling subsequent electroless copper deposition.

C.A. Deckert et al studied, for higher plating rates applied at higher temperatures, the most commonly used complexing agents that are based on ethylene di-amine tetra acetic (EDTA) . Various common reducing agents have been used in electroless baths, namely, formaldehyde, di methylamine boron, borohydride, hypophosphite and hydrazine (**F.A. Lowenheim , 1974, N.V. Mandich, 1993 and C.A. Deckert, 1995*)*** .In practice, however, all commercial electroless copper solutions for deposition of high purity copper in THP have utilized formaldehyde as the reducing agent. This is a result of combination of cost, effectiveness and ease of control of formaldehyde system. Additives that stabilize the bath against the formation of undesired cuprous oxide particles are referred to as stabilizers. This undesirable phenomenon can be

controlled simply by bubbling air or oxygen through the bath as reported by **(Innes et al., 1969 and Coombs, 1998)**.

The plating process is autocatalytic, in other words, the deposition continues once it starts. Using formaldehyde as the reducing agent, the main reaction of copper deposition can be expressed as (**Lukes, R.M**)

$$Cu2^{+} + 2HCHO + 4OH^{-} \rightarrow Cu + 2HCOO^{-} + 2H2O + H_2 \quad \text{..... Eq (2.1)}$$

where $HCOO^{-}$ (formic acid) is the oxidation product of the reducing agent.

The electrochemical mechanism can be resolved into the following two steps, which take place simultaneously at two electrodes. Initially, the copper deposition occurs at the palladium surface (**Buck, 1964**)

$$\text{Cathode: } Cu^{2+} + 2e^{-} \rightarrow Cu. \text{ ..... Eq (2.2)}$$

On the deposited copper surface, the reaction at the anode becomes

$$\text{Anode: } 2HCHO + 4\,OH^{-} \rightarrow 2HCOO^{-} + 2H_2O + H_2 + 2\,e^{-} \text{ .... Eq (2.3)}$$

with hydrogen being produced. (**Paunovic, 1968**).

Despite recently achieved reductions in consumption, screen printed silver used in solar cell front side metallization is still an important cost driver in solar cell production. A metallization scheme based on copper plating has the potential to lower these costs at similar or even improved efficiency. Plating allows the formation of very compact and highly conductive contacts (**Hanna. F et al., 2003**). Copper is just as conductive as silver, but occurs far more frequently. Thus, its price is about 100 times lower, making it less costly for solar cell production and less susceptible to price fluctuations. The recent drive towards replacing aluminium metallization by copper in silicon device technology has led to a renewal of interest in electrochemical deposition of metals onto silicon as well as onto various barrier materials (**Nathan Fritz, 2012**).

Recently, electroless deposition of copper, using only a chemical bath, has received considerable attention. Major advantages of the electroless deposition process include the formation of a uniform deposit on irregular surfaces, direct deposition on surface activated non-conductors and the formation of less porous, more corrosion resistant

deposits (**Riedel Wolf, 1991**). Copper plating can change the appearance, dimensions, or electrical conductivity of a metal part. The cost of using this approach is significantly lower than PVD and CVD process.

2.2 EFFECT OF P^H VALUES

Farrid Hanna et al. studied the effect of pH values on the rate of electroless copper deposited from the tartarate bath at 30 ^oC and EDTA bath at 50 ^oC is shown in Fig.2.1 (pH values were changed by the addition of NaOH concentrated solution to the electroless baths). The results indicate that the deposition rate increases markedly with the increase of pH value up to 12.5 for tartarate bath and 13.0 for EDTA bath. Above these values, the rates of electroless plating decrease. Electroless copper baths are characterized by a plating rate that firstly increases and passes through a peak then begins to decrease as a function of pH. This behavior can be explained in accordance with a study (**Nuzzi, F.J., 1983**) involving the following two steps:

- The initial increase of the rate up to pH 12 is due to the effect of OH^- ions as reactants in the total reaction as represented by Eq. (2.4):

$$Cu^{2+} + 2HCHO + 4OH^- \rightarrow Cu^0 + H2 \uparrow + 2H2O + 2HCOO^- \quad \ldots \text{Eq (2.4)}$$

- The decrease in the rate of deposition at pH over 12.5 is due to the consumption of OH^- ions by hydrolysis of formaldehyde to methylene glycol anions followed by its oxidation to formate ions as shown in Eqs (2.5) and (2.6).

$$HCHO + OH^- \rightarrow CH_2(OH)O^- \quad \ldots\ldots\ldots\ldots\ldots\ldots\ldots\ldots\ldots \text{Eq (2.5)}$$

$$CH(OH)O^- + OH^- \rightarrow CHOO^- + H2O + e^- \quad \ldots\ldots\ldots\ldots\ldots\ldots \text{Eq (2.6)}$$

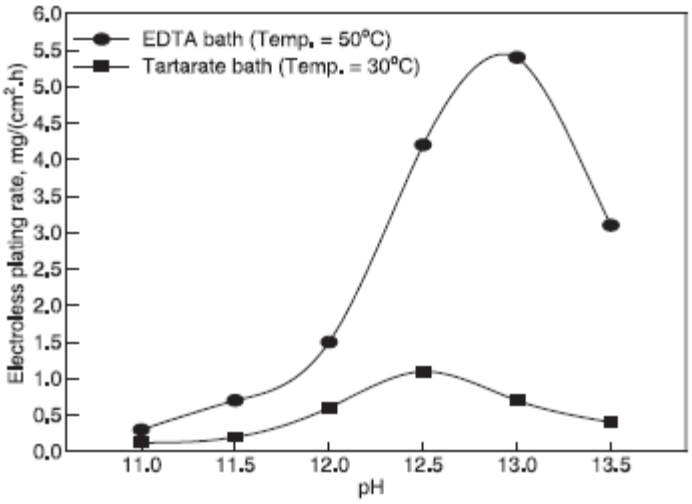

Fig. 2.1: Effect of pH values on plating rate in additive-free electroless baths

2.3 EFFECT OF OPERATING TEMPERATURES

Farrid Hanna et al., 2003 studied the effect of operating temperatures on the electroless deposition rate of copper from tartarate and EDTA additive-free baths as illustrated in the Fig.2.2. The results clearly indicate that the deposition rate increases with the increase of bath temperature up to 50 ^{o}C for the two baths studied. After 50^{o}C, the tartarate additive-free bath decomposes rapidly and the rate of deposition decreases sharply. On the other hand, EDTA bath is stable up to 70 ^{o}C and the rate of deposition decreases slightly. This behavior can be attributed to the stronger complexing ability of EDTA than tartarate (**Hung**, **1985**). From the above results, it can be concluded that 40–45 ^{o}C is the optimum operating temperature for tartarate bath and 45–60 ^{o}C for the EDTA bath. Therefore, the optimum temperatures for electroless copper plating by the tartarate and EDTA baths are 30 ^{o}C and 50 ^{o}C, respectively.

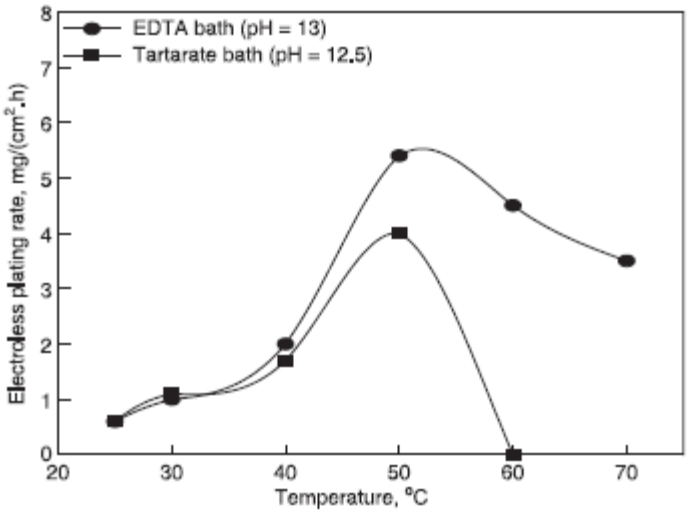

Fig. 2.2: Effect of temperatures on plating rate in additive-free electroless baths

2.4 SURFACTANTS

Surfactants are surface active agents that lower the surface tension of a liquid, allowing easier spreading, and lowering the interfacial tension between two liquids. Surfactants reduce the surface tension of water by adsorbing at the liquid–gas interface. Many surfactants assemble in the bulk solution into aggregates known as micelles. The concentration at which surfactants begin to form micelles is known as the Critical Micelle Concentration or CMC. A surfactant can be classified by the presence of formally charged groups in its head. A nonionic surfactant has no charge groups in its head and an ionic surfactant carries a net charge. If the charge is negative, the surfactant is called anionic; if the charge is positive, it is called cationic. **Tripathy et al.,1997** studied the effect of addition of Sodium Dodecyl Sulfate (SDS) on the surface morphology and reported that SDS addition in the bath improved the surface morphology**. Medina-Valtierra et al., (2007)** studied the influence of cetyl Trimethyl ammonium bromide (CTAB) on the roughness of Titania sol–gel films and reported that the sol–gel films prepared with surfactant showed a granular microstructure and are composed of irregular particles on the surface and enhanced the photocatalytic activity. In the presence of CTAB, at lower concentrations (up to 0.6 g/l) coalescence of nickel particles have been deposited on the substrate surface and at the higher concentration (above 0.6 g/l) uniformly improved surface finish of the deposited layer was achieved (**R. Elansezhian, 2009**).

2.5 SODIUM DO-DECYL SULPHATE (SDS)

Surfactants are amphiphilic molecules that possess both hydrophobic and hydrophilic properties. A typical surfactant molecule consists of a long hydrocarbon 'tail' that dissolves in hydrocarbon and other non-polar solvents, and a hydrophilic 'head group' that dissolves in polar solvents (typically water). One example of a dual character molecule having a head-group and a non-polar tail is sodium do-decyl sulphate (SDS), $Na^+ \ ^-OSO_3Cl_2H_{25}$. When a sufficient amount of SDS is dissolved in water, several bulk solution properties are significantly changed, particularly the surface tension (which decreases) and the ability of the solution to solubilise hydrocarbons, (which increases). These changes do not occur until a minimum bulk SDS concentration is reached. This concentration is called the critical micelle concentration (CMC). Below the CMC, the addition of surfactant to an aqueous solution causes an increase in the number of charge carriers ((aq) Na^+ and (aq) $^-OSO_3Cl_2H_{25}$) and consequently, an increase in the conductivity. Above the CMC, further addition of surfactant increases the micelle concentration while the monomer concentration remains approximately constant (at the CMC level). Since a micelle is much larger than a SDS monomer it diffuses more slowly through solution and so is a less efficient charge carrier. A plot of conductivity against surfactant concentration is shown in Fig (2.3).

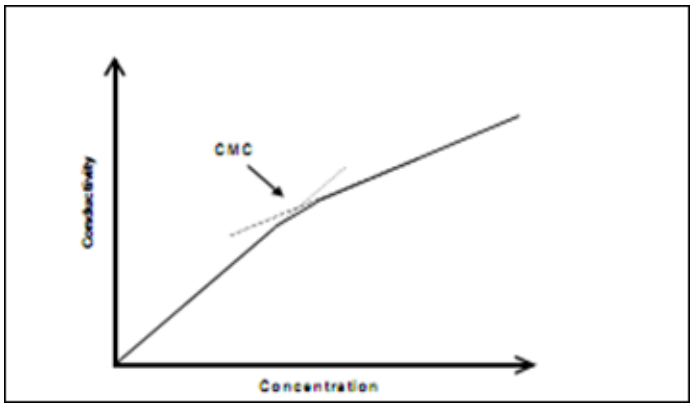

Fig. 2.3: A plot of conductivity against surfactant concentration

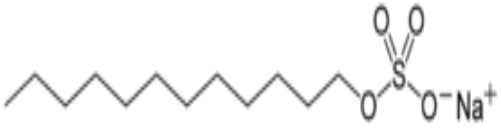

Fig. 2.4: Illustration of structure of anionic surfactant SDS

2.6 ANTI REFLECTION COATING

In this contribution, the higher reflection of a mc-Si solar cell surface is strongly reduced by the deposition of TiO_2 antireflection coating (ARC) on the front using spin coating method(**Hocinel, 2012**). TiO_2 is superior to other substances because of its high photocatalytic activity and chemical stability in aqueous solution under UV light irradiation (**R.S. Sonawane, 2002**). Titania (TiO_2) has 3 crystalline forms: anatase, brookite and rutile. Of these forms, anatase TiO_2 has been widely used as a popular catalyst, because of its various merits, such as optical and electronic properties, high photocatalytic activity, low cost, non-toxicity and chemical stability (**Funda Sayilkan et al., 2005**).

2.7 TITANIUM DI-OXIDE

In 1972, **Fujishima and Honda** discovered the photocatalytic splitting of water on TiO_2 electrodes. This event marked the beginning of a new era in heterogeneous photocatalysis. Since then, research efforts in understanding the fundamental processes and in enhancing the photocatalytic efficiency of TiO_2 have come from extensive research performed by chemists, physicists and chemical engineers. Such studies are often related to energy renewal and energy storage (**Bard, A. J., 1982, Gratzel, M., 1983, Parmon, V. N, 1989, Pelizzetti, E., 1991**).In recent years, applications to environmental cleanup have been one of the most active areas in heterogeneous photocatalysis. This is inspired by the potential application of TiO_2-based photo catalysts for the total destruction of organic compounds in polluted air and wastewaters (**Schiavello, M, 1988, and Ollis, D. F, 1991**).

TiO_2 is an excellent material for environmental purification, photo-electrochemical solar energy conversion and optical application. The sol-gel processing is a low temperature chemical method used for production of inorganic oxide materials, nanosized metal oxide semiconductors and widely used to obtain better ceramics (**Funda Sayilkan et al., 2005 and, R.Mechiakh, 2007**). When the precursor is a transition metal alkoxide, its high reactivity towards water must be controlled to obtain gels. In this sol-gel process, TiO_2 is usually prepared by hydrolysis,

condensation and polycondensation of the titanium alkoxides, Ti (OR) 4. (**Funda Sayilkan et al., 2005**).

2.8 MECHANISM OF PHOTOCATALYSIS

A photocatalyst is a substance that helps bring about a light-catalyzed reaction, such as chlorophyll in photosynthesis. Like photosynthesis, the reaction continues throughout the day once begun. When photocatalyst titanium dioxide (TiO_2) absorbs ultraviolet radiation from sunlight or illuminated light source (fluorescent lamps), it will produce pairs of electrons and holes. The electron of the valence band of titanium dioxide becomes excited when illuminated by light. The excess energy of this excited electron promoted the electron to the conduction band of titanium dioxide therefore creating the negative-electron (e-) and positive-hole (h+) pair. This stage is referred to as the semiconductor's 'photo-excitation' state. The energy difference between the valence band and the conduction band is known as the 'band gap'. Wavelength of the light necessary for photo-excitation is: 1240 (Planck's constant, h) / 3.2 eV (band gap energy) = 388 nm. The positive-hole of titanium dioxide breaks apart the water molecule to form hydrogen gas and hydroxyl radical. The negative-electron reacts with oxygen molecule to form super oxide anion. This cycle continues when light is available.

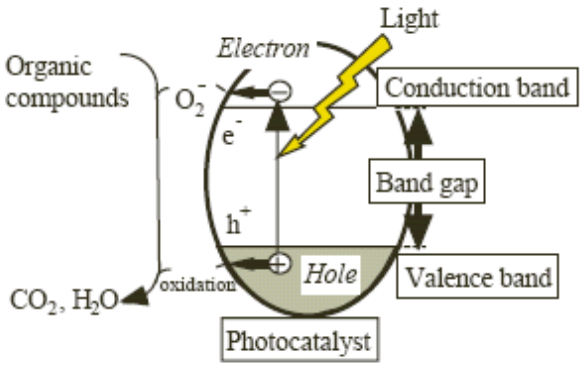

Fig. 2.5: Mechanism of Photocatalysis

2.9 APPLICATIONS OF TITANIUM DI-OXIDE

2.9.1 Self-cleaning function

The finding of the photo-induced hydrophilicity has markedly widened the application range of TiO_2 –coated materials (**A.Fujishima et al., 1999**). That is, the stains adsorbed on the TiO_2 surface can easily be washed by water, because water soaks between stain and the highly hydrophilic TiO_2 surface. In other words, this has removed the limitation of the cleaning function of the TiO_2 photocatalysis, that is, the function is limited by the number of photons. Even though the number of photons is not sufficient to decompose the adsorbed stains, the surface is maintained clean when water is supplied. Thus TiO_2 –coated materials used outside where they are exposed to rain fall shows a very effective self –cleaning function, i.e., stains are decomposed partially by the conventional photocatalytic reaction as well as washed by rain water. Titanium dioxide can be coated on many building materials. These films exhibit a self cleaning effect due to the strong oxidizing properties

2.9.2 Anti-fogging glass

Generally if moist air comes in contact with glass, small droplets of water are formed, and the glass becomes fogged. On titanium dioxide coated glass, the water forms a continuous flat sheet, so that there is no fogging. TiO_2 coated tiles in a hospital environment showed the surface bacteria on the wall surfaces were reduced to zero, plus airborne bacteria counts were reduced.

(a) (b) (c)

Fig. 2.6: Applications of Titanium Dioxide

(a) TiO_2 coated tent material

(b) TiO_2 coated glass

(c) TiO_2 coated tiles in a hospital environment.

2.9.3 Photocatalytic Anti Bacterial Effect

Photocatalytic decomposition can be applicable to micro-organisms. Escherichia coli (E.Coli) cells completely disappear on TiO_2 after about one week under a UV irradiation of $1mW/cm^2$.The photocatalytic deactivation of microorganism requires a much longer time under in door conditions than under outdoor ones. However, the anti-bacterial function of a TiO_2 photocatalyst is markedly enhanced even with weak UV light, using a fluorescent lamp and the aid of either silver or copper(**Sunada et al.,2003**), which is harmless to the human body. When the copper /TiO_2 film is irradiated with very weak UV light, the survival rate begins to decrease.

2.10 INTRODUCTION TO THE SOL – GEL TECHNOLOGY

The sol-gel processing has low temperature chemical method used for production of inorganic oxide materials. Such a process may be used to yield a form of single and multi-component oxides as crystalline or amorphous form (**Brinker and Scherer, 1990**). It is also used to give bulk materials but is suitable for thin film coatings production. The method of Sol – Gel helps oxide to be deposited on a substrate at much lower temperatures than traditional ceramic, (**Twite and Bierwagon, 1998**).There are many advantages involved in Sol – Gel during conventional methods concerning oxide (**Saveninije, 1998**) materials which have the possibility of changing the film features extensively through altering the composition of the solution as well as in a relatively low process cost (**Manea et al., 2007**), (**Carp et al., 2004**). In addition Sol-Gel overcomes the difficulties of producing a high quality dielectric semiconductor interface, and obtaining a stoichiometric ratio of elements and molecular homogeneity in multicomponent oxide film As for example, (**Fujishima and Honda, 1972**), the Titanium Dioxide (TiO_2) belongs to an important material class because of its various uses in wide applications. (**Oregan and Gratzal., 1991**, **Kubota et al., 2001**)

For example in solar cells as an electron-hole generator,TiO_2 thin film have been receiving much attention in the past as their chemical stability high refractive index and high dielectric constant allow their use as components in optoelectronic devices and sensor (**Rancourt, 1987**, **Fleisher et al., 1999**, **Battiston et al., 1994**). There are

many deposition techniques have been used to prepare them, such as chemical vapor deposition, evaporation, reactive D.C. or diode or magnetron sputtering (**Lobl et al., 1994**), (**Martin et al., 1994**), ion beam techniques (**Fernandez et al., 1994**), and sol-gel processes. The sol-gel processing are particularly efficient in producing thin, transparent, multi-component oxide layers of many compositions on various substrates, including glass (**Brinker and Harrington , 1981**).TiO_2 crystallizes in three types Anatase, Rutile, and Brookite (**Landoft and Bornstein, 1984**), Rutile is being the most stable of the three types (**Henrich, 1985**). To the author's knowledge, brookite has not appeared so far in thin film form and rutile has been extensively studied both theoretically and experimentally. Importance of Anatase in solar cell technology has been recently increasing (**Graetzel, 1991**), which differs in its electronic properties from those of rutile (**Furro et al., 1994**).

This distinctness is in agreement with the study of the electronic and optical properties of thin anatase thin film (**Tang et al., 1994**). TiO_2 is an excellent material which shows most promising prospect in environmental purification, photoelctrochemical solar energy conversion and optical coating application (**Fujishima et al., 2000**).This is due to several properties such as remarkable activity, chemical stability, non-toxicity (**Raseshwar and Ibanez, 1995**), highly oxidative photogenerated holes, high energy conversion, highly transparency and high refractive index (**Tryl et al., 2000**). Due to its high dielectric constant, thin films of TiO_2 have also been studied for application as a gate insulator for Metal Oxide Semiconductor (MOS) device applications, with reduced leakage current (**Paily et al.,2002**). This is an inherently n-type semiconducting material due to stoichiometric oxygen deficiency in the film structure, with a wide band gap typically 3.1eV and a high index of refraction of about n=2.6. TiO_2 in anatase is an n-type semiconductor (**Gugliemi et al., 1992, Forro et al., 1994)**.

2.11 STEPS IN PRODUCING Si WAFERS

Si mainly occurs in the form of oxide of Si, SiO_2. It is found in the form of quartz, sand and silicates. It is normally produced from raw quartzite. The naturally occurring quartzite contains a wide range of impurities including Al, B, P, Cu, Ca, Mg, Fr, Ti, Mn, Mg, etc. These impurities should be removed to an acceptable level from the Si before it becomes suitable for use in either electronic or solar cell applications. The acceptable range of impurities is generally in the part per billion (ppb) range for the

electronic applications, and it is in the part per million (ppm) range for the solar cell applications. Si has atomic density of $5x10^{22}$ atoms/cm^3. Thus, a ppb level of impurity means $5x10^{13}$ impurity atoms/cm^3 in Si and a ppm level of impurity means $5x10^{16}$ impurity atoms/cm^3 in Si.

Various steps are involved in converting a quartzite material to a high purity crystal wafer where electronic devices can be fabricated. These steps are summarized in Fig. 2.7. The first step is to produce the so-called Metallurgical Grade Si (MGS) from quartzite. The MGS is about 98% pure. The next step is to further purify the MGS to ppb impurity level. Density of Si atoms in its lattice is about $5x10^{22}$ atoms/cm^3. Thus, impurity level of ppb means impurity level in the range of $5x10^{13}$ atoms/cm^3. This, in terms of percentage, is equivalent to 99.9999999% or is referred to as nine 9s impurity level. This Si is known as Electronic Grade Si (EGS). The MGS Si is purified in the form of EGS Si. It is done by converting the MGS into halides of Si, usually chlorosilances. These gases have low boiling point due to which they can be easily purified by distillation to ppb level. The pure gases are then converted to pure solid Si. At this stage, Si is in the polycrystalline form (grains are of less than mm size). It is then converted to the high purity monocrystalline (infinite grain size) or multicrystalline (grain size in the range of cm) form by melting the EGS polycrystalline Si followed by a controlled solidification. These high purity mono or multicrystalline solids are called ingots. The monocrystalline ingots are cylindrical in shape, and the multi crystalline ingots are cubical in shape. The last step is to cut Si wafers (circular or square) from the ingots. This process is called wafer dicing.

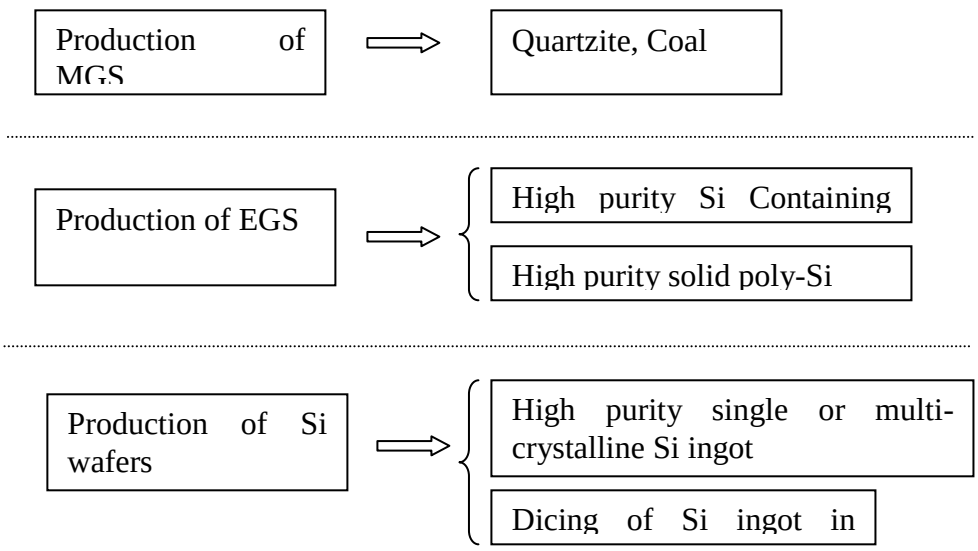

Fig. 2.7: Steps in production of Si wafers from raw Si (Quartzite)

2.12 MULTICRYSTALLINE Si INGOTS

The multicrystalline Si ingots are particularly developed for solar cell applications. As the name suggests, there are several crystals of different orientations in an ingot. The crystals are separated by grain boundaries. Due to this reason, the overall material is quite defective as compared to the mono crystalline material produced using CZ and FZ processes. But it has several advantages as well. The capital cost of producing multicrystalline Si is less as compared to CZ and FZ processes. The throughput is much higher, and it provides higher tolerance to poor feedstock quality. In the late 1990s, the contribution of multicrystalline wafer in the worldwide PV module production was about 25% and the contribution of monocrystalline wafer-based module was about 65%. The situation is reversed now. Almost 70% of the PV modules are produced in the multicrystalline Si wafer and about 25% in the monocrystalline Si wafers. Moreover, due to grain boundaries, the solar cell efficiencies are typically 1% to 2% lower in multicrystalline Si wafers as compared to the monocrystalline wafers. But multicrystalline wafers are of square shape. They allow higher packing density of cells in the module.

Due to this at the module level, efficiency of mono and multicrystalline Si PV modules is nearly the same. The multicrystalline Si ingots are produced using cheaper block costing method as shown in Fig. 2.8. In this process, EGS is melted and poured into a square-shaped SiO- SiN-coated graphite crucible. After this, the heat is removed from the bottom of the crucible. The controlled directional solidification of the crucible results in multicrystalline Si block with grain size from mm to cm range. In this block casting process, due to large Si to crucible contact area, more impurities get incorporated in Si. These impurities, up to some extent, are controlled during the solar cell manufacturing by processes like impurity gettering and hydrogen passivation. The size of the multicrystalline crucible can be quite large. It is normally of the order of 60 cm x 60 cm x 20 cm, and the weight of the crucible could be several hundred kilograms. This big block of multicrystalline Si ingot is first cut in small blocks, with cross-sectional area equal to the required wafer area (up to 15 cm x 15 cm). The multicrystalline Si produced in this way is only used in solar PV industry.

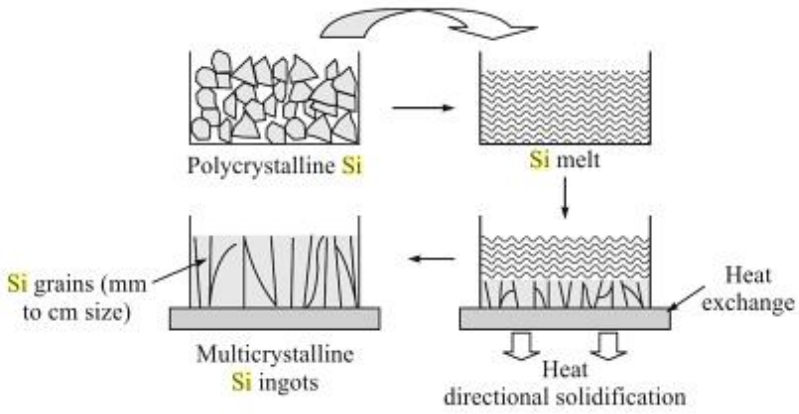

Fig. 2.8: Process for production of multicrystalline Si ingots

2.13 SOLAR CELL CHARACTERISTICS

Solar cells are characterized and compared with each other with four parameters: Short circuit current I_{sc}, open circuit voltage V_{oc}, Fill Factor FF and efficiency η. These parameters can be represented using Fig. 2.9.

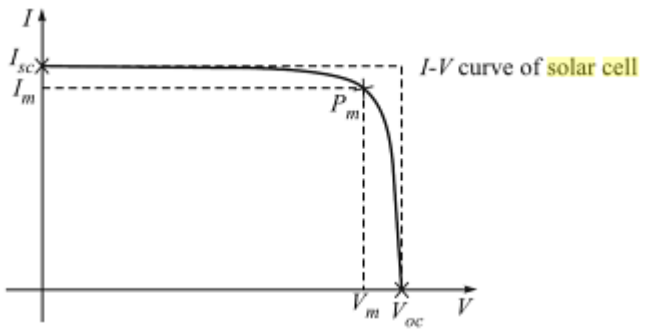

Fig. 2.9: Typical plot of a solar cell I-V curve and its parameters

2.13.1. Short circuit current(I_{sc}) :

This is the maximum current that flows in a solar cell when its terminals at P-side and N-side are shorted with each other, i.e., V=0 (Fig. 2.9).When we put V=0 in Eq 2.9, we will get I_{sc}=-I_L. Thus, short circuit current is nothing but the light –generated current. The short circuit current is usually represented in terms of current density and current per unit area, in terms of mA/cm^2

$$I_{Total} = I_o \left(e^{qv/kT} - 1\right) - I_L \qquad \ldots\ldots\ldots\ldots\ldots\ldots \quad \text{Eq (2.7)}$$

2.13.2 Open circuit Voltage V_{oc} :

As the name suggests, it is the maximum voltage generated across the terminals of a solar cell when they are kept open, i.e., I=0 (Fig. 2.6). Putting this condition in the Eq 2.7, the following expression for open circuit voltage is obtained:

$$V_{oc} = \frac{kT}{q} ln\left[\frac{I_L}{I_o} + 1\right] \quad \text{..... Eq (2.8)}$$

Thus, open circuit voltage depends on the light-generated current and reverse saturation current. The V_{oc} is given in terms of mV or V.

2.13.3 Fill factor FF:

It is the ratio of maximum power $P_m = V_m \times I_m$ (Fig. 2.9) that can be extracted from a solar cell to the ideal power $P_o = V_{oc} \times I_{sc}$, Thus,

$$(FF) = \frac{V_m I_m}{V_{oc} I_{sc}} \quad \text{..... Eq (2.9)}$$

The FF represents the squareness of the solar cell I-V curve. It is represented in terms of percentage.

2.13.4 Efficiency η:

It is defined as the ratio of the power output to power input. The power output is the maximum power point P_m of a solar cell, and input power is the power of solar radiation P_{rad}. According to the international standard for characterization of solar cells, P_{rad} is equal to 100mW/cm^2 or 1000W/m^2.

$$\eta = \frac{P_m}{P_{rad}} \quad \text{..... Eq (2.10)}$$

Using $P_m = V_m \times I_m$ and Eq 2.11 the Eq 2.12 can be rewritten as

$$\eta = \frac{V_m I_m}{P_{rad}} = \frac{V_{oc} I_{sc} FF}{P_{rad}} \quad \text{..... Eq (2.11)}$$

2.14 ANALYTICAL TECHNIQUES

After the solar cells are fabricated, or even during the fabrication process, the cells need to be constantly monitored for their performance. This helps in segregating the solar cells into various levels. This segregation could be done on the basis of efficiency, peak power or on the basis of I_{sc}. The characterization techniques that are used could range from the tools used for online monitoring of the solar cells while in mass production or in the laboratory when some specific properties are to be obtained. The most important tool used for characterization is the solar simulator which can provide the voltage- current behavior of the cell, which in turn gives information about the various electrical parameters as well as the efficiency of the cell.

2.14.1 Solar simulator : I-V measurement

Solar simulator plots the current-voltage relationship (I-V curve) for the solar cell. The information obtained from the I-V curve is useful in evaluating the solar cell performance in terms of its efficiency, maximum current and voltage or peak power. A setup of solar simulator is given in Fig. 2.10. The solar simulator makes use of an artificial light source whose illumination spectrum matches with that of the sun. Arc lamps (for instance, xenon or mercury arc lamps) are preferably used as the light source as their spectrum nearly matches with that of the sun at AM 1.5.

The light, when incident on the solar cells, generates current and voltage that are measured with the help of the data acquisition systems (DAS). An internal sweep circuit applies either current or voltage and the measurement circuit measures the other quantity (voltage or current, respectively). In this way, the current-voltage or I-V curve of the cell is obtained. The information gathered from the I-V curve gives the I_{sc}, V_{oc}, FF, Peak Power, I_{mp}, V_{mp} series resistance and efficiency. The typical I-V curve, power curve and other solar cell parameters obtained from solar simulator are shown in Fig. 2.11. All these parameters are useful in determining the solar cell performance.

The solar simulators are manufactured to provide standard test conditions (STC) for solar cells. The simulator works at irradiation levels of 1000 W/m^2 and at AM 1.5 spectrums. In order to match the spectrum, some filters are also used. A proper temperature control system needs to be set up which can maintain the solar cell temperature at about 25 ^{o}C as shown in Fig. 2.10. The rear side of the cell is placed on a metal chuck, which is cooled down by flowing water.

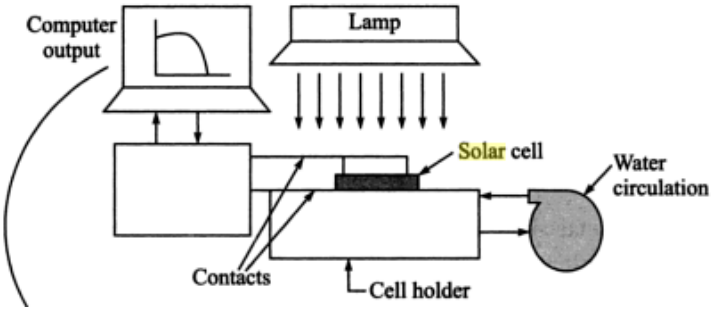

Fig. 2.10: Setup of solar simulator for I-V characterization of solar cell

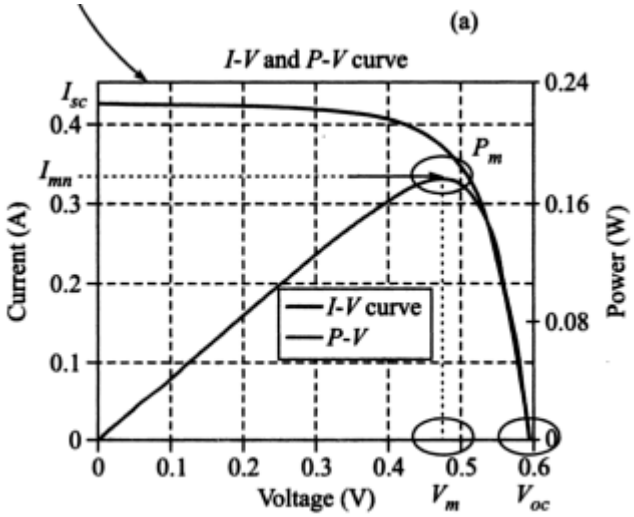

Fig. 2.11: Typical I-V curve and other parameters obtained from solar simulator

2.14.2 UV –Visible Spectroscopy

The instrument used in ultraviolet-visible spectroscopy is called as UV/visible spectrophotometer. It measures the intensity of light passing through a sample (I), and compares it to the intensity of light before it passes through the sample (I_o). The ratio (I/I_o) is called the transmittance, and is usually expressed as a percentage (%T). The absorbance, A is based on the transmittance

$$A = -\log(\%T/100\%) \quad \ldots\ldots\ldots\ldots\ldots\ldots\ldots\ldots \quad 2.12$$

The UV-Visible spectrophotometer can also be configured to measure reflectance. In this case, the spectrophotometer measures the intensity of light reflected from a sample (I), and compares it to the intensity of light reflected from a reference material (I_o). The ratio I/I_o is called the reflectance, and is usually expressed as a percentage (%R).

The basic parts of a spectrophotometer are a light source, a holder for the sample, a diffraction grating in a monochromator or a prism to separate the different wavelengths of light, and a detector. The radiation source is often a Tungsten filament (300-2500 nm), a deuterium arc lamp, which is continuous over the ultraviolet region (190-400 nm), Xenon arc lamp, which is continuous from 160-2,000 nm; or more recently, light emitting diodes (LED) for the visible wavelengths. The detector is typically a photomultiplier tube, a photodiode, a photodiode array or a charge-coupled device (CCD). Single photodiode detectors and photomultiplier tubes are used with

Scanning monochromator, which filters the light so that only light of a single wavelength reaches the detector at one time. The scanning monochromator moves the diffraction grating to "step-through" each wavelength so that its intensity may be measured as a function of wavelength. Fixed monochromators are used with CCDs and photodiode arrays. As both of these devices consist of many detectors grouped into one or two dimensional arrays, they are able to collect light of different wavelengths on different pixels or groups of pixels simultaneously.

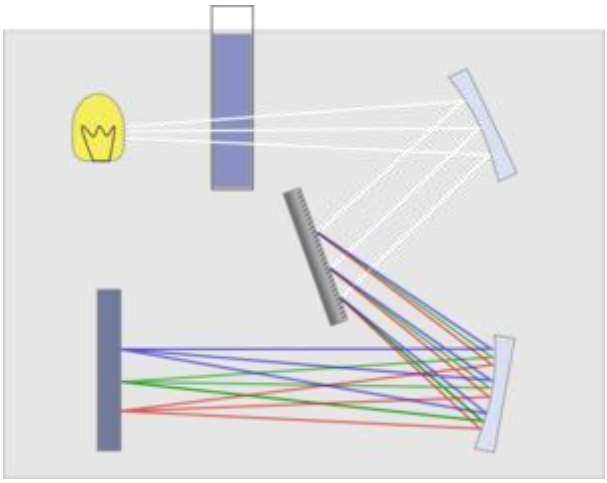

Fig. 2.12: Diagram of a single-beam UV/Vis spectrophotometer

2.15 INTRODUCTION TO DESIGN OF EXPERIMENTS

Design of experiments (DOE) refers to experimental methods used to quantify indeterminate measurements of factors and interactions between factors statistically through observance of forced changes made methodically as directed by mathematically systematic tables.

2.15.1 Full factorial design

A full factorial design contains all possible combinations of a set of factors (**Astha Kukreja, 2011**). This is the most conservative design approach, but it is also the most costly in experimental resources. The Full Factorial Design supports both continuous factors and categorical factors with up to nine levels. In full factorial design, the experiment is performed at every combination of the factor levels. The sample size is the product of the number of levels of the factors.

2.15.2 Main effect plot

The importance of main effect plot is that it shows the behavior of the system when one parameter is varied by keeping another parameter constant (**Astha Kukreja, 2011**). A main effect occurs when the mean response changes across the levels of a factor and it can be used to compare the relative strength of the effects across each factor.

2.15.3 Interaction Plot

The interaction plot gives average output for each level of the factor with the level of the second factor held constant (**Astha Kukreja, 2011**). These plots are used to interpret significant interactions between the process parameters. Interaction is present when the response at a factor level depends upon the levels of other factors. Since they can magnify or diminish the main effects of the parameters, evaluating interactions is extremely important.

2.16 SUMMARY

In this chapter, a literature review of the relevant journals was made on mechanism of electroless copper coating, parameters influencing the electroless copper coating process and several other aspects of solar cell technology. In addition, a review of previous studies on the coating on solar cell, drawbacks of multi crystalline solar cell, methods to overcome the draw backs were discussed. This forms the basis for defining the objective of the present investigation and also in identifying the experimental methods to be adopted in this research. Literature review was made on the properties of titanium dioxide, its application on various areas and the mechanism of photocatalysis. The solar cell parameters and the characterization techniques to evaluate the efficiency of solar cell were also discussed. At the end of this chapter, the introduction about the design of experiments was given and the full factorial method used for the analysis was discussed along with the main effect plot and the interaction plot. The experimental methods used in this work are explained in detail in the following chapter.

CHAPTER 3 : EXPERIMENTAL DETAILS

3.1 PROBLEM DEFINITION

The existing multicrystalline solar cell possesses

1. Smooth surface of silicon which leads to high reflective losses
2. Deposition of dirt and other organic particles on the solar cell
3. Erosion and corrosion due to rain and other environmental changes.
4. Processing cost of solar cell

3.2 PROPOSED SOLUTION

Proposed solution to overcome the above problem is,

- By creating roughness on silicon surface by encapsulating silicon surface with copper.
- Corrosion and antibacterial properties of the solar cell will be improved by copper coating on grid surface.
- TiO_2 coating on the copper coated surface enhances the photocatalytic property (self cleaning surface).

3.3 COATING TECHNIQUES USED

1. Electroless coating –To Coat Copper and Copper with nano additive on solar cells
2. Spin coating – To Coat TiO_2 on Copper coated solar cell and Copper with nano additives coated solar cell.

3.4 BASIC GOVERNING EQUATION

When the monochromatic light of wavelength λ is incident on the front surface, the photocurrent and the spectral response, that is, the number of carriers collected per incident photon at each wave length can be given (**Sze, 2008**) by

$$J_L = q\int_0^{\lambda m} F(\lambda)[1 - R(\lambda)]SR(\lambda)d\lambda \quad \ldots\ldots\ldots \text{Eq (3.1)}$$

The generation rate of electron-hole pairs at a distance x from the semiconductor surface is given by $G(\lambda,x) = \alpha(\lambda)\, F(\lambda)[1-R(\lambda)]\exp[-\alpha(\lambda)x]$ …… Eq (3.2)

α(λ) = Absorption coefficient

F(λ) = Number of incident photons/cm ^{2}/s per unit band width

R(λ) = Fraction of these photons reflected from the surface.

SR(λ) = Spectral Response .

From equation1 to get large number of carriers collected per incident photon one has to minimize R(λ) and maximize SR(λ). In this research an attempt was made to reduce the reflection such that the carrier collection rate will be increased which leads to increase in open circuit current and thus better efficiency of the cell.

3.5 MANUFACTURING OF MULTICRYSTALLINE SOLAR CELL

3.5.1 Wafer dicing: ID and wire sawing

The Si ingots need to be diced in order to obtain Si wafers. Two types of techniques are most common: Inner Diameter (ID) sawing and wire sawing. These are shown schematically in Fig. 3.1 and Fig. 3.2.The cylindrical ingots are subjected to the grinding processes before wafer dicing. The ingots produced from the CZ and FZ processes are a little larger in diameter. In the grinding process, the diameter of the ingot is reduced to a pre-determined size. Also, before dicing, the tapered or conical ends and tails of the ingots are cut away. This material is of EGS quality and is recycled. Both of these kinds of material loss do not occur in multicrystalline Si ingots.

The ID sawing uses a metal blade whose cutting edge is located at the interior of the blade as shown in Fig. 3.1. The saw blade is a thin (about 325μm) stainless steel sheet with diamond bonded on the inner rim.

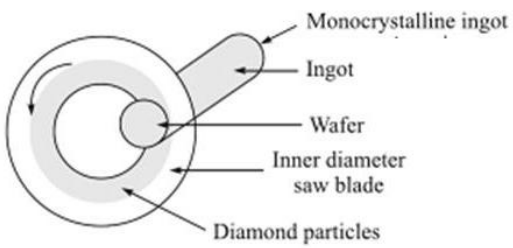

Fig. 3.1: Inner Diameter Sawing

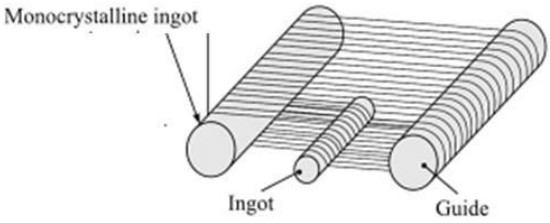

Fig. 3.2: Wire Sawing

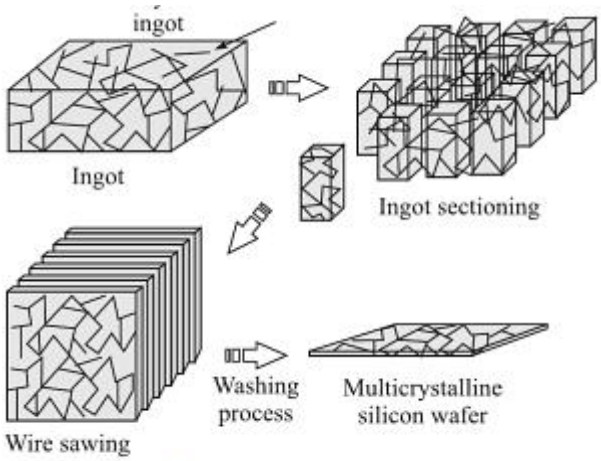

Fig. 3.3: Dicing of Multicrystalline Square Wafers

3.6 ELECTROLESS COPPER COATING PROCESS

3.6.1 Preparation of the Substrates

The substrates used in this study were multi-crystalline solar photovoltaic cell of 0.45 Volts capacity having dimensions of 156mm×156mm, which were turned into dimension of 78 × 12 mm for experimental purpose. After that, finally the samples were surface finished and used.

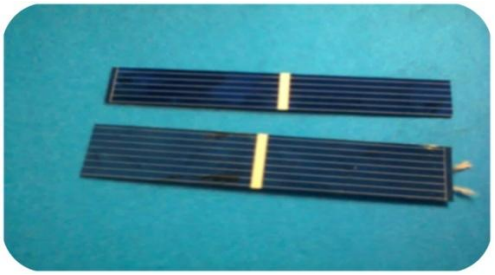

Fig. 3.4: Solar Cell Samples Cut Into Required Dimensions

3.6.2 Cleaning of the Substrates

Prior to the coating, it must be ensured that the substrate is free from any impurities. So cleaning is very important to achieve efficient coating. Cleaning can be carried out with acetone then followed by rinsing in distilled water and then dipping in methanol for 2 minutes.

Fig. 3.5: Chemicals required for cleaning

3.6.3 Activation / Catalyzation of the Substrate

Tin sensitization followed by palladium activation is an important route to the formation of the catalyst on a variety of substrates (**Eea, 2004**). Activation (**Hanna, 2003**) was carried out by three steps: 1. Etching by 10% nitric acid and 10% hydrofluoric acid, 2. Sensitisation by 10 g/l of stannous chloride mixed with 50ml/l of hydrochloric acid, 3. Catalysation by 0.5g/l of palladium chloride mixed with 10ml/l of hydrochloric acid. Here activation is carried out for 2 minutes and immersed in the electroless bath for 1 hour.

Fig. 3.6: Beakers showing the chemicals required for activation of the substrate

3.6.4 Electroless Copper Coating Bath and Operating Conditions

The electroless copper bath (**Elansezhian, 2009 and Paunovic, 1968**) consists of 5 g/l copper sulphate ($CuSO_4.5H_2O$), 12 g/l ethylene diamine tetraacetic acid (EDTA), 1.2 g/l sodium dodecyl sulphate (SDS) and 5 ml/l formaldehyde (HCHO). The pH level was adjusted to 9 (**Hanna, 2003**) by the addition sodium hydroxide solution obtained from NaOH pallets (**Elansezhian, 2009**).

Table 3.1: Compositions of plating bath used for electroless copper coatings

Electroless copper bath compositions			**Quantity (g/l)**	
			Bath A	**Bath B**
Copper source	Copper sulphate	$CuSO_4.5H_2O$	5g/l	5g/l
Reducing agent	Formaldehyde	HCHO	5 ml/l	5 ml/l
Complexing agent	Ethylene diamine tetraacetic acid (EDTA)	$C_{10}H_{16}N_2O_8$	12g/l	12g/l
Anionic surfactant	Sodium do-decyl sulphate(SDS)	$NaC_{12}H_{25}SO_4$	–	0 – 1.5
		Temperature	85^0C ($\pm1^0C$)	85^0C ($\pm1^0C$)
		pH	9 – 10	9 – 10

Fig. 3.7: Electronic precision balance

Fig. 3.8: Magnetic stirrer with conical flask

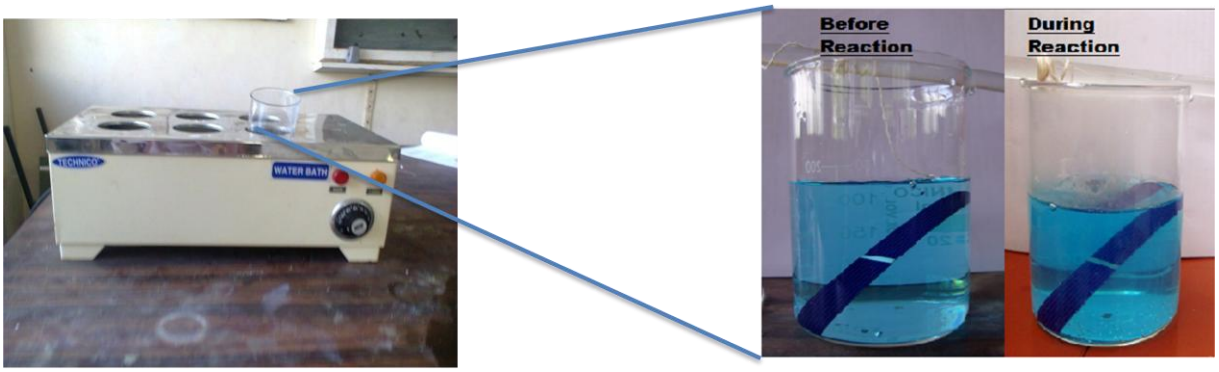

Fig. 3.9: Electroless coating equipment

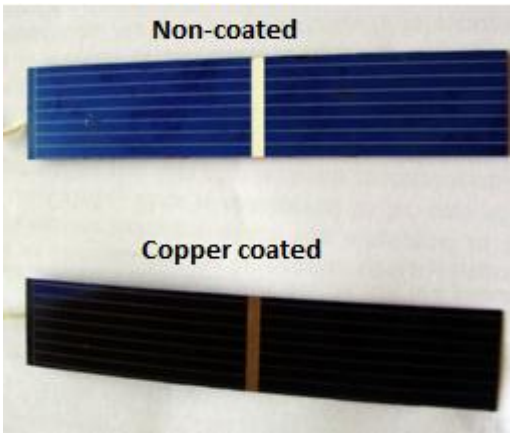

Fig. 3.10: Non coated and copper coated Solar cell samples

Here various process parameters such as pH, temperature, surfactant concentration, activation time of the substrate and the immersion time of the sample were optimized to the value of pH=8-9, temperature of 85^{o}C with surfactant (SDS) concentration of 1.2 g/l. The sample was activated for 2 minutes and immersed in the bath for 1 hour.

Conventional silicon texturing, that is, the use of pyramidal structures of crystal planes at the surface of solar cells, is less effective in providing anti - reflection and light

trapping for multicrystalline silicon than for single crystal silicon due to the range of crystal orientations (**Jeremy Barbe et al., 2011**). Even though the entrapped copper particles reduces the reflective losses they are less effective in providing anti - reflection. Hence an attempt was made to spin coat the TiO_2 on copper coated solar cell to enhance the anti-reflection property.

3.7 SPIN COATING PROCESS

The sol-gel was prepared using Titanium-iso propoxide - 6.3ml (SOURCE), Ethanol - 50ml (SOLVENT) and Acetic acid - 5ml (COMPLEXING AGENT). Ethanol was mixed with a magnetic stirrer for around 50 minutes and then 5ml of acetic acid was added and allowed to mix for 10 minutes. Titanium-iso prop oxide was then added to the mixture and allowed to mix for 20 minutes to form the sol-gel solution as shown in Fig. 3.11. This formed gel was used in spin coating of TiO_2.

TIP is a metal alkoxide, where metal alkoxides have the general formula M (OR) n, where M=metal, R=alkyl group and n is the valence of the metal atom.

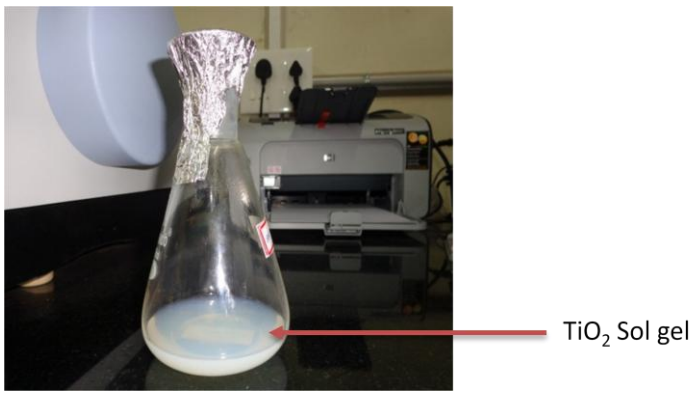

Fig. 3.11: TiO_2 Sol-gel solution

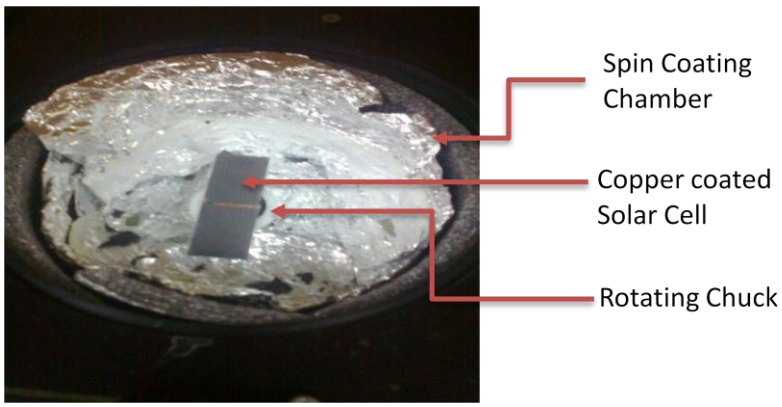

Fig. 3.12: Sample Fixed in Chuck of Spin Coating Equipment

For preliminary experiments, Samples were coated at different rpm ranges from 1000 rpm to 5000 rpm at the interval of 500 rpm. Spinning time was varied from 20 sec to 120 sec with the interval of 20 secs. The coated samples were heated to various temperatures such as 50 ^{o}C, 100 ^{o}C, 150 ^{o}C and 200 ^{o}C. Design of experiments was conducted using full factorial method with 3 parameters and 2 levels which gives the combination of 2^3 factorial design.

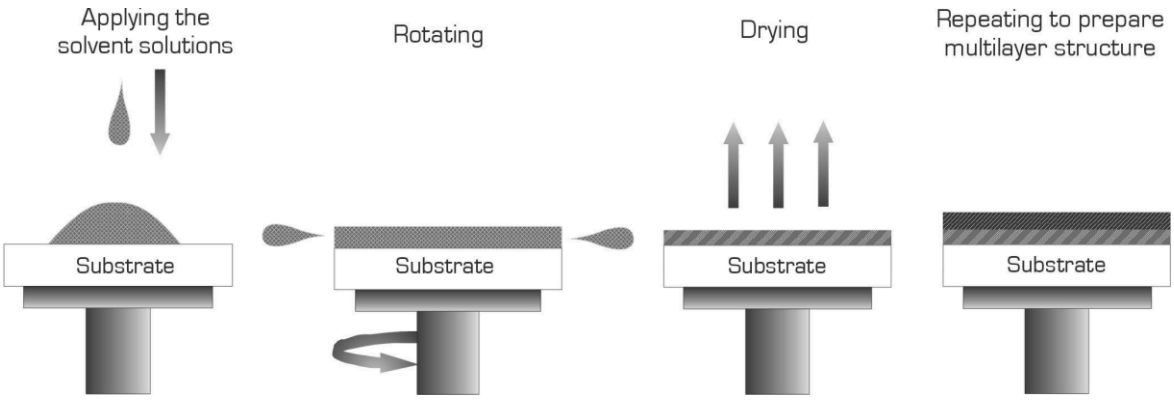

Fig. 3.13: Procedure for Spin coating process

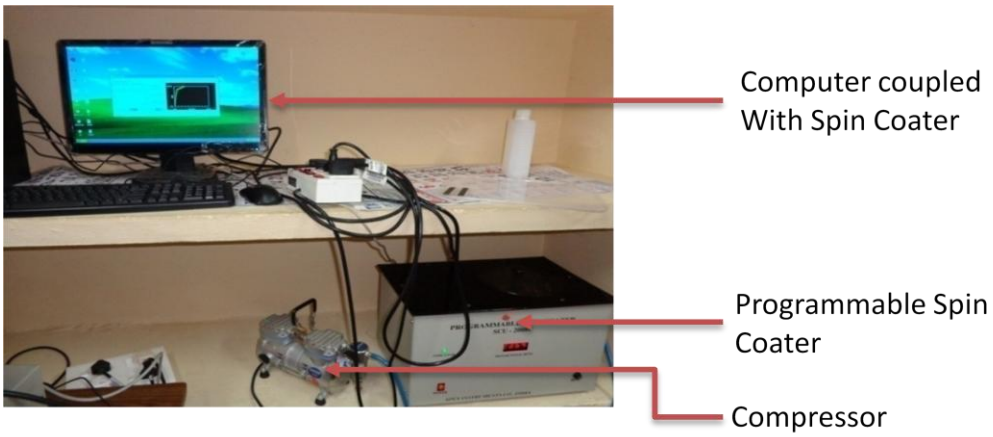

Fig. 3.14: Spin Coating Equipment

3.8 MEASUREMENT OF PH

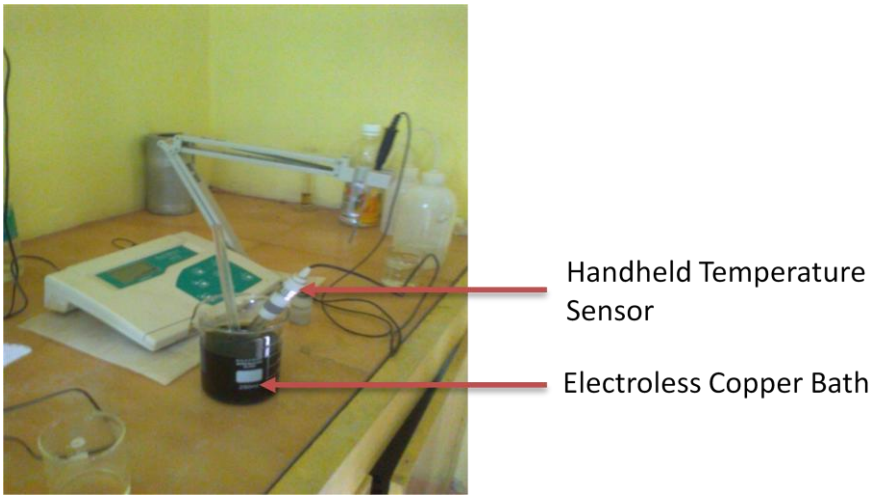

Fig. 3.15: Measurement of pH using cyberscan pH 510

The pH was measured using Cyberscan pH 510, Eutech instruments. It can measure the pH, with the range of 0.00 to 14.00 and with the resolution of 0.01&± 0.01 pH. It can also measure the temperature from 0 to 100 ^{o}C with 3 points accuracy. The 250 ml bath was prepared with the chemical composition as mentioned in the section 4.1.5. The pH of the bath was adjusted by the addition of sodium hydroxide pellets.

3.9 COATING THICKNESS MEASUREMENT

The coating thickness was measured using the device positector 6000. It works on the principle of magnetic effect. This instrument uses the force of attraction between the substrate and a piece of magnet and calibrates the same against the thickness of the coating. When the probe is place on the coating, there would be a beep and the measurement would be displayed. In case of solar cell the electroless copper coating was continuous on the grid surface and the copper was coated on the activated silicon surface which was not continuous. The size and the pattern of the copper particles deposited on the silicon surface were shown in Chapter 5. The thickness of the electroless copper coating on grid surface was verified using cross section analysis by SEM as shown in Chapter 5.

Fig. 3.16: Coating thickness gauge

3.10 SURFACE ROUGHNESS MEASUREMENTS

The surface roughness of the substrate samples before and after electroless copper coating was measured by means of a Mitutoyo portable surface roughness tester. It was decided to use the Ra^2 to describe the surface roughness. All the reported data represents the average of at least ten surface roughness measurements.

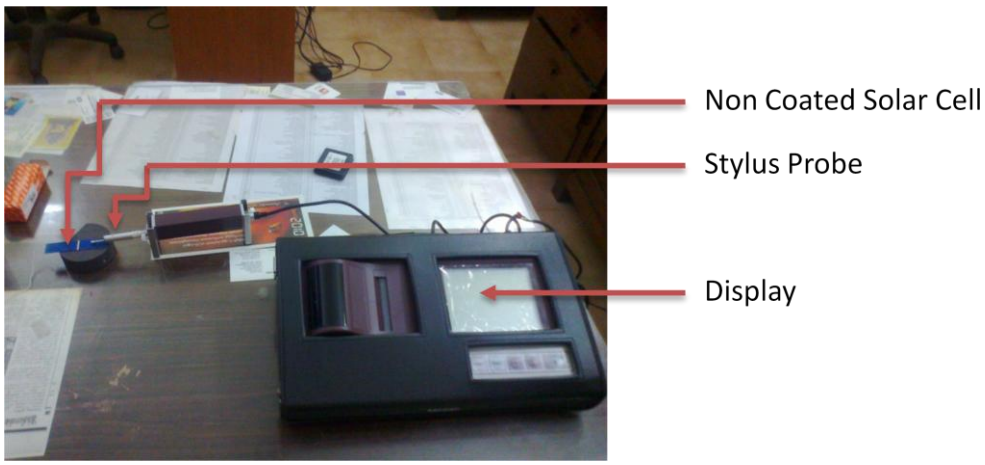

Fig. 3.17: Surface roughness measurement of non-coated solar cell

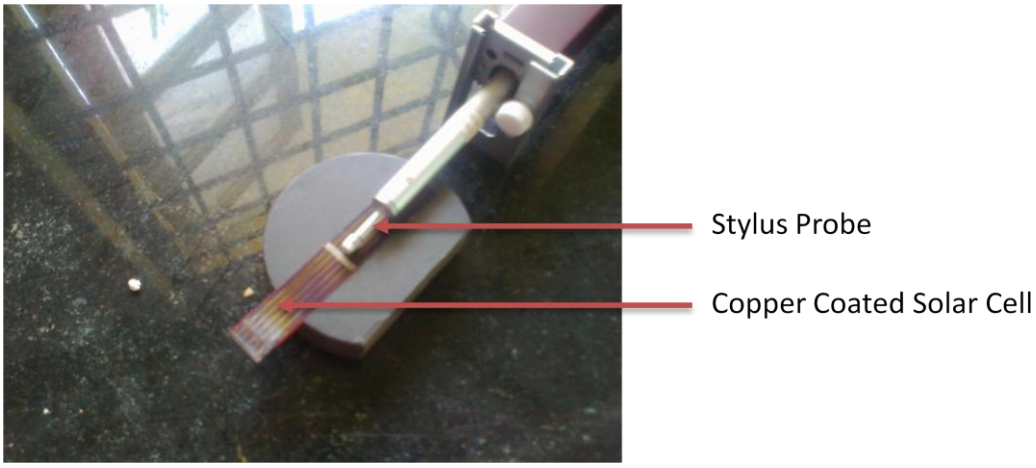

Fig. 3.18: Surface roughness measurement of copper coated solar cell

3.11 ESTIMATION OF CONTACT ANGLE

Contact angles were measured using the pendant drop shape method with a GBX Digidrop contact angle analyzer and the contact angle meter is shown in Fig. 3.19. The images were captured with a CCD video camera with image resolution of 768 × 576 pixels. The frame speed employed was 25 images per second. Samples from the electrolyte bath before and after reaction were used for the measurements. The contact angles presented in this study were measured before and after the coating reaction was over and also with and without addition of surfactants. The schematic representation of contact angle measurement is shown in Fig. 3.20. An electrolyte drop of 5 µl was made to fall from a micro syringe unit on EN deposited specimen. The drop image was captured and stored by the video camera and an image analysis system calculated both the left and right contact angles from the shape of the drop with an accuracy of ±0.1°. All measurements were made at controlled ambient temperature of 20° C and relative humidity (74%).

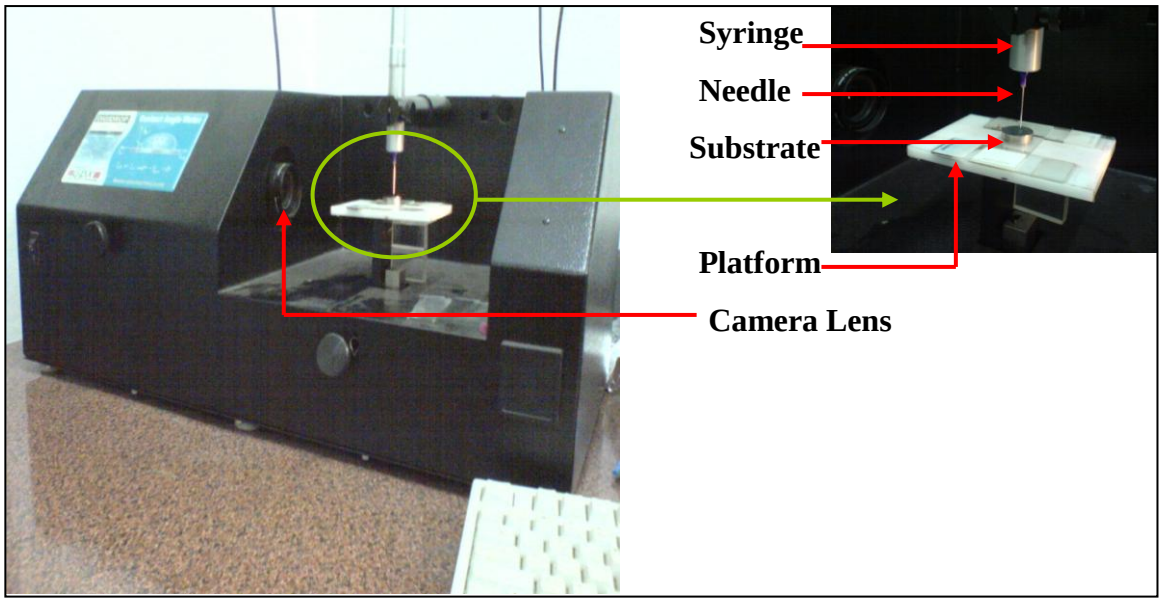

Fig. 3.19: Contact angle meter

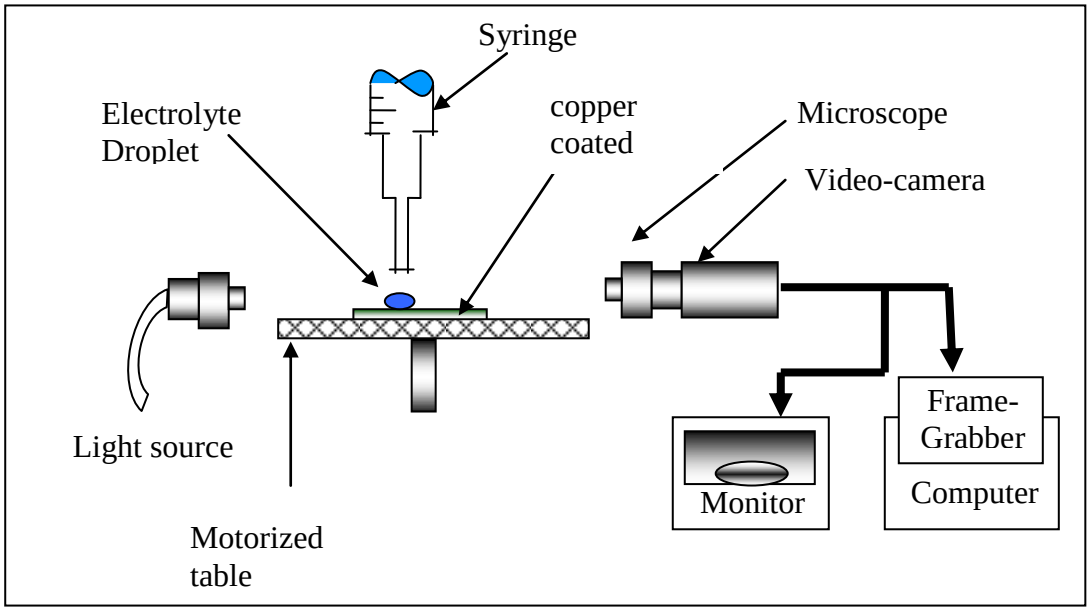

Fig. 3.20: Schematic line drawing of Contact angle measurement set – up

3.12 PENDANT DROP SHAPE METHOD

The pendant drop shape analysis is a convenient method to measure contact angles (**Woodward, 2001**). The drop looks like a pendant and hence this method is named as pendant drop shape analysis. A sample drop of fluid having pendant shape is shown in Fig. 3.21. The principal assumptions made in the analysis are:

1. The drop is symmetric about a central vertical axis which means it is irrelevant from which direction the drop is viewed.

2. The drop is not in motion in the sense that viscosity or inertia is playing a role in determining its shape which means that interfacial tension and gravity are the only forces shaping the drop.

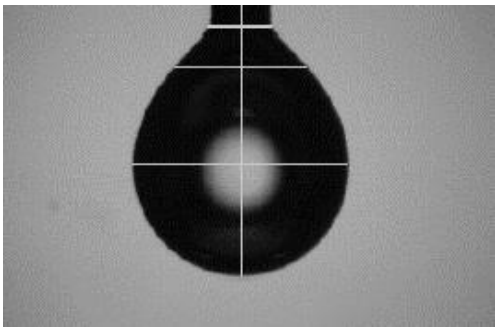

Fig. 3.21: Image of the drop having pendant shape

The contact angles are measured by fitting a mathematical expression to the shape of the drop and then calculating the slope of the tangent to the drop at the electrolyte-substrate-vapor (liquid-solid-vapor) interface line. The image of electrolyte dropped from the syringe is shown in Fig. 3.22 and the contact angle is measured on the left and right side of the drop and the average of two angles are taken as the contact angle.

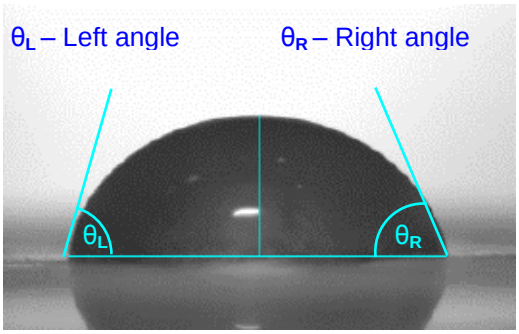

Fig. 3.22: Final image of drop used for analysis of contact

3.13 ESTIMATION OF SURFACE TENSION

Surface tension measurements were carried out using Nima Dynamic Surface Tensiometer 9005 and the instrument is shown in Fig. 3.23. This tensiometer measured the surface tension (ST) of liquids with the Wilhelmy plate method (**Cipriano et al., 2005**). This is a fully computer operated instrument for measuring

dynamic advancing and receding surface tension. It consists of a 5g balance, motorized platform for computer controlled immersions, a stirrer and a temperature sensor. The whole unit was enclosed in housing for optimum temperature control. Test sample liquid of 5 ml was filled in the test vessel. Samples from the electrolyte bath before and after reaction were used. Measurements were taken for samples with and without addition of surfactants. Wilhelmy plate of 10.5 mm wide and 0.25 mm thick was used for taking measurements. The schematic line drawing of surface tension measurement is shown in Fig. 3.24.

Fig. 3.23: Surface Tensiometer Setup

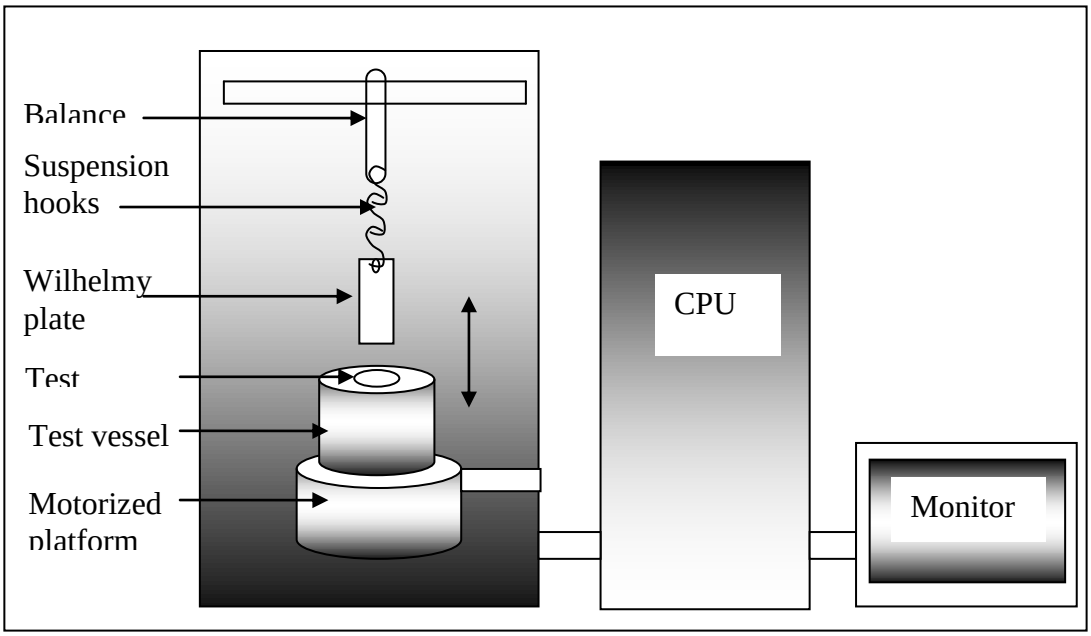

Fig. 3.24: Schematic line drawing of Surface Tensiometer Setup

The plate was attached to the balance and was lowered to the liquid surface, which was detected automatically, immersed and withdrawn again until the maximum pull on the plate was found. The surface tension was displayed both graphically and digitally. The surface tension was displayed with an accuracy of ±0.1mN/m. All measurements were made at air conditioned room temperature (20°C).

3.14 SCANNING ELECTRON MICROSCOPE (SEM)

Surface morphology and the cross section of the sample were studied using SEM (Hitachi S-3400N) analysis as shown in Fig. 3.25 and the elemental composition of the sample was identified using Energy-dispersive X-ray spectroscopy (EDAX).

Fig. 3.25: Scanning Electron Microscope

Hitachi S-3400N is a variable pressure scanning electron microscope. It has a tungsten filament emitter with resolution ~5 nm at 30 KV (10 nm at 3 KV); it allows the study of wet, oily, non-conductive and/or uncoated samples by variable pressure mode; the low vacuum range is from 6 Pa to 270 Pa. Compositional and topographic images can be obtained by the high sensitive 4 segments BSE detector. It also equipped with EDX and EBSP detectors for elemental and crystallographic information mapping, respectively.

3.15 X-RAY DIFFRACTOGRAM (XRD)

The X-ray diffraction method is a powerful technique widely used for studying the microstructure, phase identification, and compound analysis of materials.

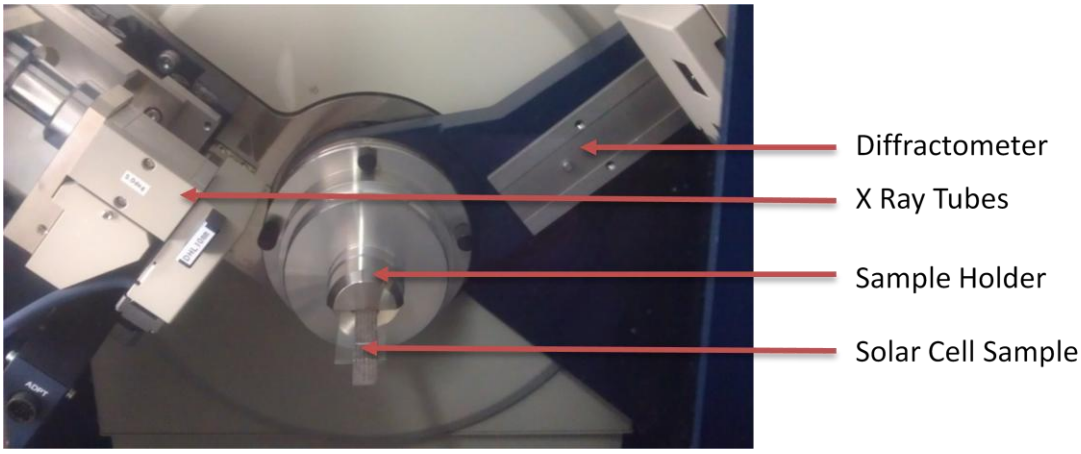

Fig. 3.26: RIGAKU ULTIMA IV X-ray Diffractometer with solar cell

The structure and compound analysis of electroless copper coatings, as-plated and heat-treated, were investigated using a RIGAKU ULTIMA IV X-ray Diffractometer with monochromatic Cu K_{α} radiation as shown in Fig. 3.26. The Ultima IV X-ray Diffractometer is an advanced general purpose X-ray diffraction (XRD) instrument for materials science, semiconductor, and nanotechnology research and development as well as quality assurance for the manufacturing environment. The design features a new high speed detector for 100X faster measurements, unrivaled application flexibility provided by patented Cross Beam Optics (CBO), and a 50% smaller size than a conventional XRD system.

The innovative design of a fully optioned Rigaku Ultima IV can span applications that would have required up to four separate conventional XRD instruments in the past. A modular "build-up" platform allows users to add additional capabilities as new application requirements arise, including support for high resolution diffraction, thin film measurement, micro diffraction, and handling of very small samples.

3.16 MEASUREMENT OF I_{SC} AND V_{OC}

The open circuit voltage and short circuit current were measured using multimeter (exitech) with decade box arrangements (Fig. 3.27) under environmental condition as shown in Fig. 3.28. The short-circuit current is the current through the solar cell when

the voltage across the solar cell is zero (i.e., when the solar cell is short circuited). The open-circuit voltage, V_{OC}, is the maximum voltage available from a solar cell, and this occurs at zero current.

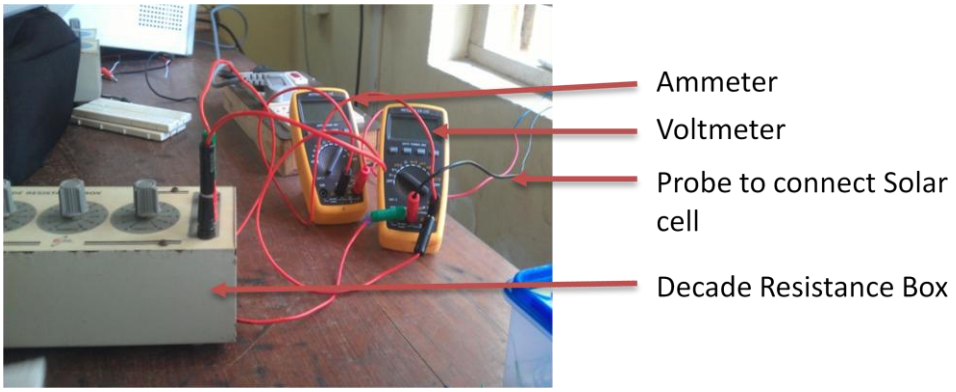

Fig. 3.27: Measurement of I_{SC} and V_{OC} with decade box arrangements

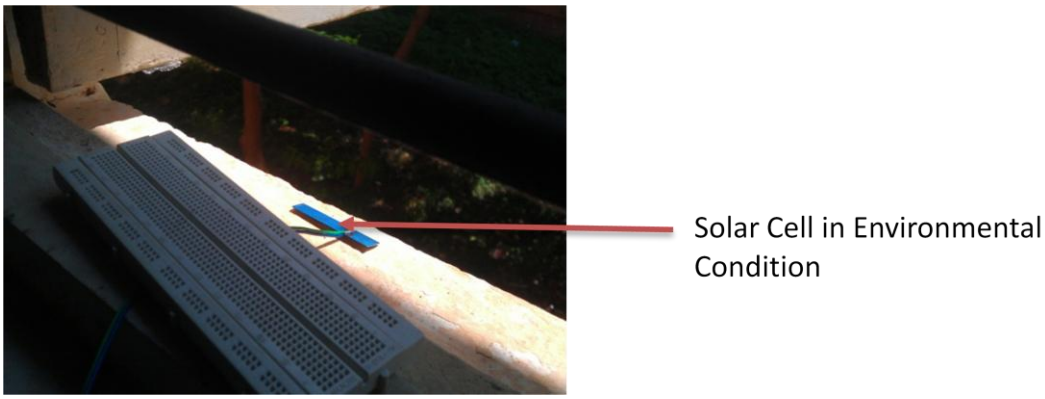

Fig. 3.28: Solar cell exposed to environmental conditions

In the circuit diagram as shown in Fig. 3.29, the decade box was connected to the voltage terminal and the solar cell was connected to replace the circuit resistance. On starting the measurement the voltage was made zero and the short circuit current was noted and the voltage was slowly increased by increasing the resistance in the decade box. The resistance was increased until the current become zero, so that the open circuit voltage was obtained.

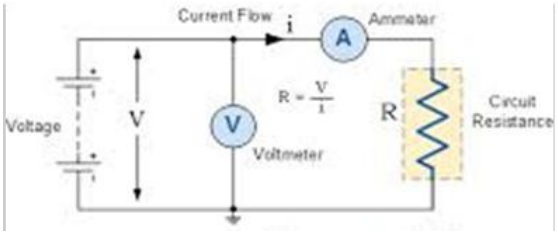

Fig. 3.29: Circuit diagram for voltage and current measurement

3.17 I-V MEASUREMENT

The I-V characteristics were measured using a solar simulator (class AAA solar simulator-ORIEL SYSTEMS) as shown in Fig. 3.30. Oriel Sol3A simulators are certified to IEC 60904-9 Edition 2 (2007), JIS C 8912, and ASTM E 927-05 standards for Spectral Match, Non-Uniformity of Irradiance, and Temporal Instability of Irradiance. The Oriel Sol3A simulators all use a single lamp design to meet not one or two, but all three performance criteria without compromising the 1 Sun output power, providing true Class AAA performance. Sol3A also integrates a partial sun attenuating device to allow easy variation of the output from .2 - 1.0suns with the simple turn of a knob. The method of measurement and the working of sun simulator was discussed in the literature review.

Fig. 3.30: Oriel Sol3A sun simulator used for I-V measurement

3.18 UV-VISIBLE SPECTROSCOPY

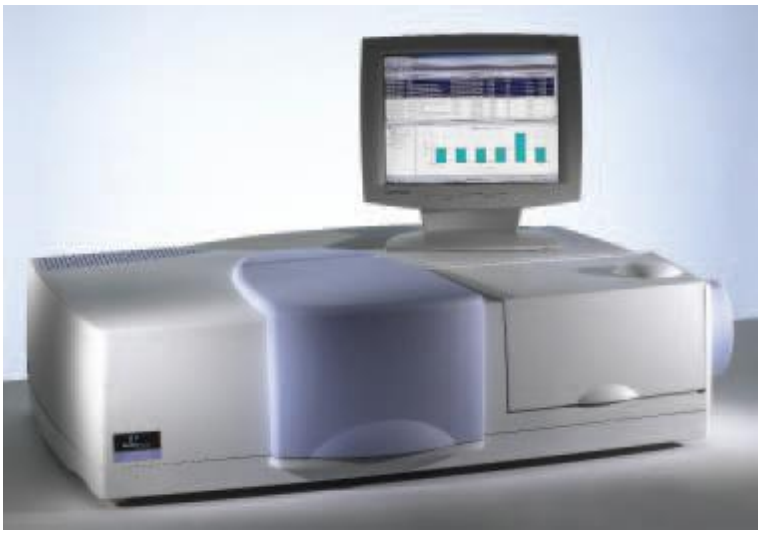

Fig. 3.31: Perkin Elmer lambda 650 S UV/VIS spectrometer

The Perkin Elmer 150 mm integrating sphere optical design is shown in Fig. 3.31. The transmittance sample holder at the entrance of the sphere enables the measurement of light scattering solutions or solids more efficiently than in a standard focusing UV/Vis spectrometer with a conventional detector arrangement. In the latter configuration, light will be lost before it reaches the detector, resulting in significant photometric errors and uncontrolled variation between samples.

The integrating sphere, however, collects all the light which has passed through the sample. For reflectance measurements, samples are mounted in the rear sample mount. Either total reflectance or diffuse reflectance only can be measured by placing either a light trap or Spectral on TM plate at the specular reflectance angle (Fig. 3.32). Measurement on irregularly-shaped solids such as solar cells, textiles, prisms and lenses is also possible using the center-mount option in which the sample is suspended in the middle of the sphere. The center-mount port, complete with positioning wheel for reproducible sampling, is shown being lifted out of the sphere in Fig. 3.32. The transmittance and reference ports are also shown. The reflectance port is located under the light blue cover on the right-hand side of the accessory. Even very large samples, for example sheets of glass, can be brought up to the reflectance port for analysis. Additionally, for small samples or to sample small areas on larger samples, a small spot kit is available to focus or center-ports of the sphere.

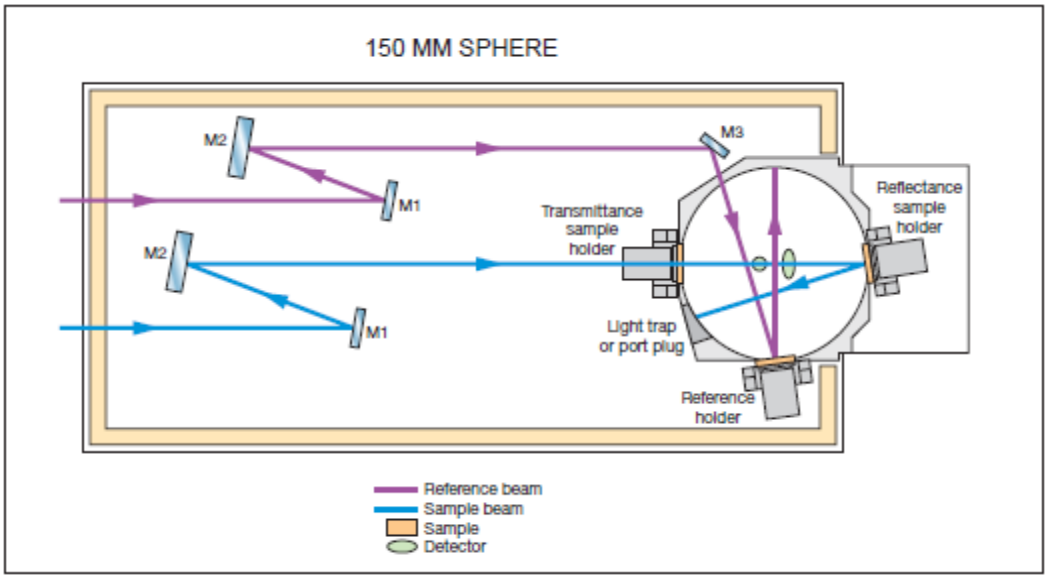

Fig. 3.32: Optical design of 150 mm integrating sphere

UV/Vis spectroscopy is a convenient method of characterizing the transmission loss of silicon photocells. Since the samples are highly scattering, an integrating sphere must be used. Using the center-mount facility, the reflectance of the solar cell can be measured at various angles to mimic the passage of the sun across the sky. The thickness of any coating over the silicon cell can be calculated if necessary.

3.19 SUMMARY

The details of various equipments used in this work and experimental procedures involved in carrying out the present investigations are explained in this chapter. In the next chapter, the results and discussions of the electroless copper coating process and the spin coating of TiO_2 on copper coated solar cell is described with the characterization of solar cell.

CHAPTER 4 : EXPERIMENTAL RESULTS AND DISCUSSIONS

4.1 PRELIMINARY EXPERIMENTS FOR ELECTROLESS PROCESS

4.1.1 Preliminary Experiments by varying pH of the Bath

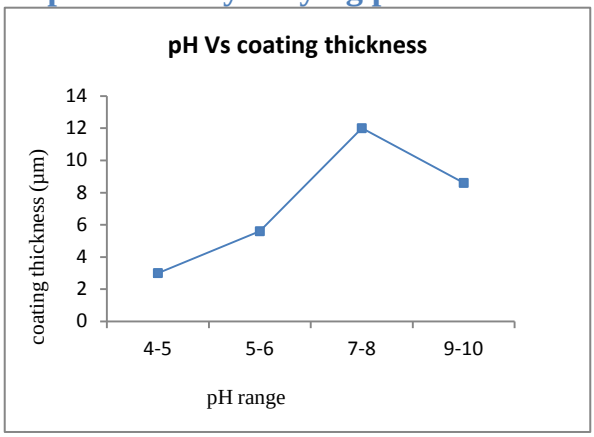

Fig. 4.1: Coating thickness of electroless coated by varying pH

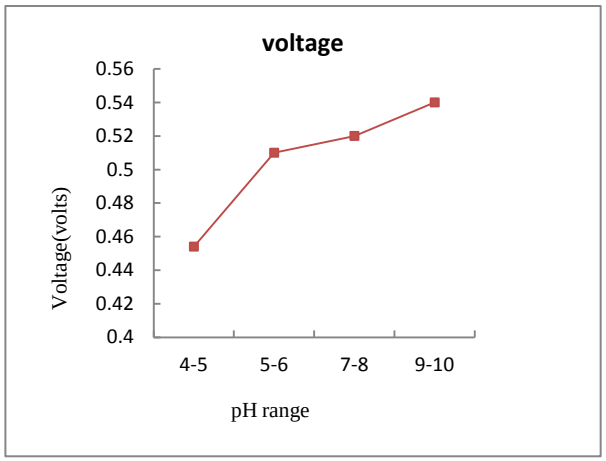

Fig. 4.2: Voltage of electroless coated copper by varying pH

The pH was varied at 4 different values such as 4-5, 5-6, 8-9, 9-10 . From the Fig. 4.1and Fig. 4.2 the result shows, when pH was 8-9 the coating thickness was maximum of 12 µm and it was minimum of 3 µm, when pH was at 4-5. These results follow a similar trend as reported by earlier researchers (**Hanna, F. et al., 2003**).

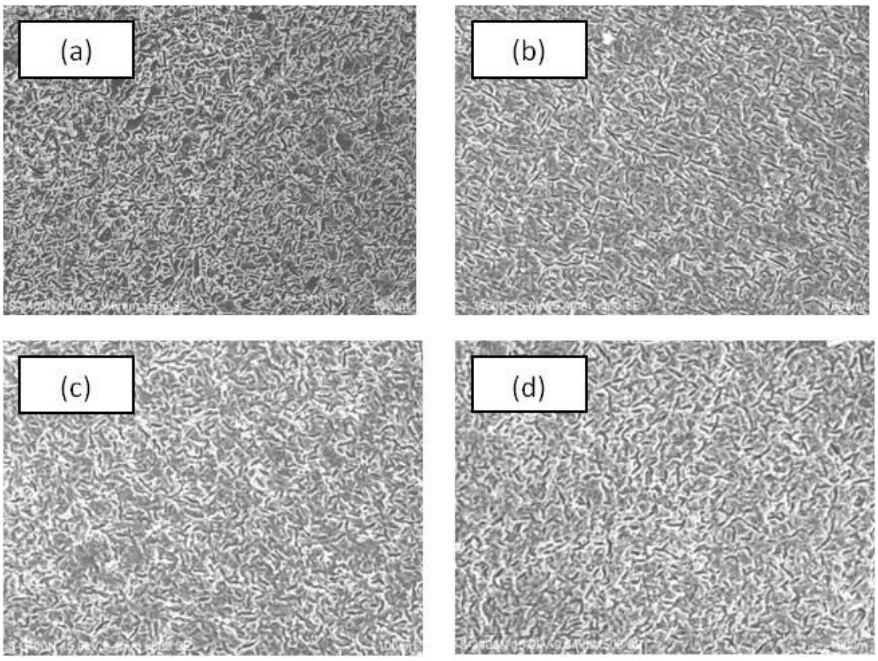

Fig. 4.3: SEM micrograph of electroless copper samples with (500X) magnification by varying pH (a) 4-5 (b) 5-6 (c) 8-9 (d) 9-10

Fig. 4.3 shows the SEM micrograph of electroless copper sample with 500X by varying pH. Here when pH was 4-5 the coating was not proper and it is uneven. When the pH increases, the coating is formed but the surface is not smooth and the grain size is coarse. When the pH was 9-10 the surface was smooth and the grain size is also fine.

4.1.2 Preliminary Experiments by Varying Temperature of the Bath

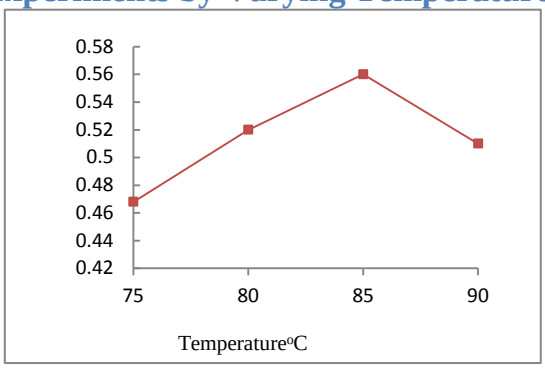

Fig. 4.4: Voltage of electroless copper coated sample by varying temperature

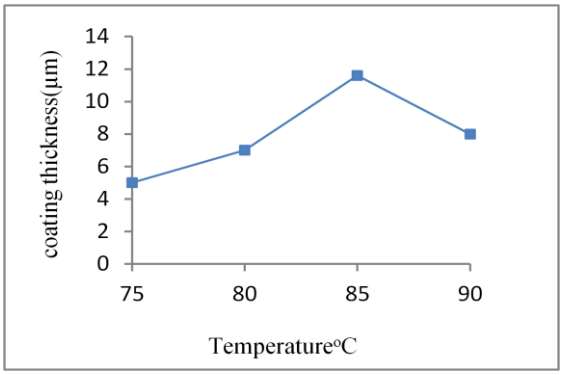

Fig. 4.5: Coating thickness of electroless copper coated sample by varying temperature

The temperature was varied at different values such as 75°C, 80 °C, 85 °C, and 90 °C. From Fig. 4.4 and Fig. 4.5, the result shows that when the coating thickness increases, the temperature increases up to 85°C (12µm) and further increase in temperature destabilizes the electroless bath. These results follow a similar trend as reported by earlier researchers (**Hanna, F. et al., 2003**).

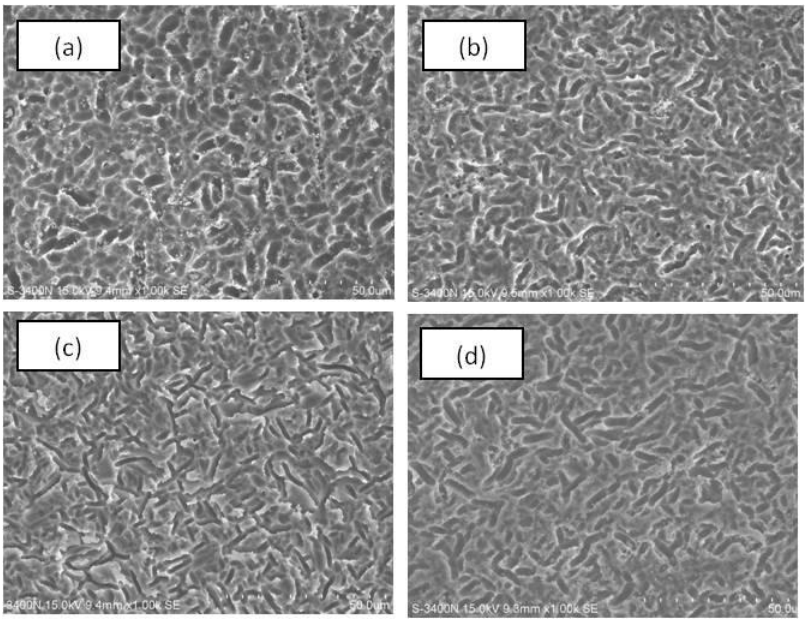

Fig. 4.6: SEM micrograph of electroless copper coated solar PV cell with magnification 1000X at temperatures (a) 75°C (b) 80°C (c) 85°C (d) 90°C

4.1.3 Preliminary Experiments by Varying Surfactant Concentration.

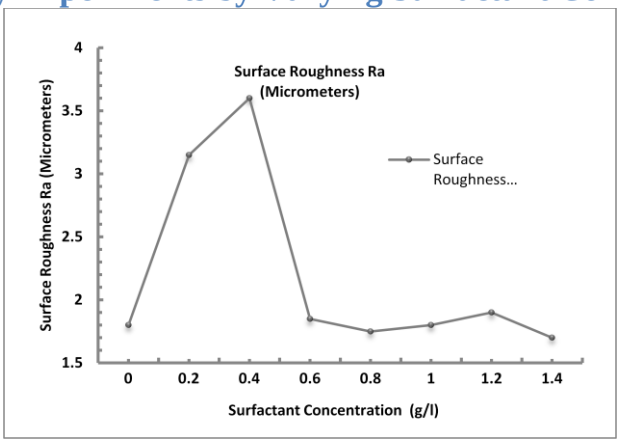

Fig. 4.7: Effect of surfactant on surface roughness

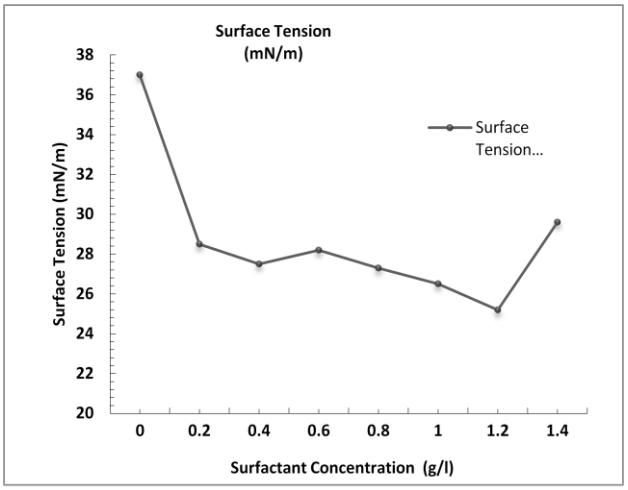

Fig. 4.8: Effect of surfactant on surface tension

The surfactant sodium do-decyl sulfate was used and its concentration was varied from 0-1.4g/l. Coating thickness, voltage, surface roughness, contact angle and surface tension were measured for the samples with different surfactant concentrations. The result shows that the surface roughness increases up to 0.4g/l of surfactant concentration and then it decreases due to the better wettability property of the surfactant.

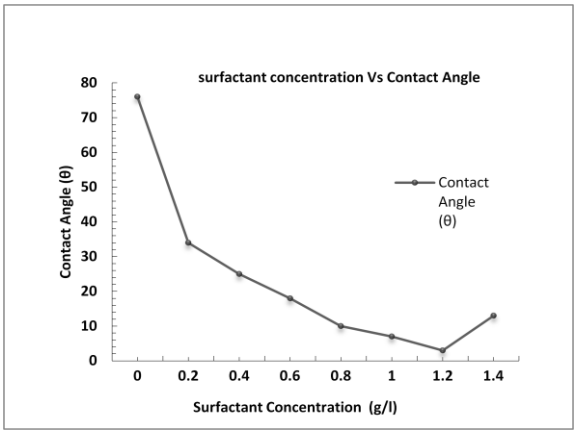

Fig. 4.9: Effect of surfactant on contact angle

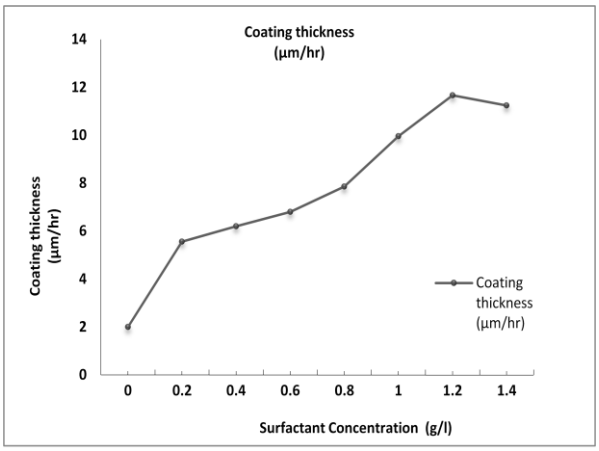

Fig. 4.10: Effect of surfactant on coating thickness

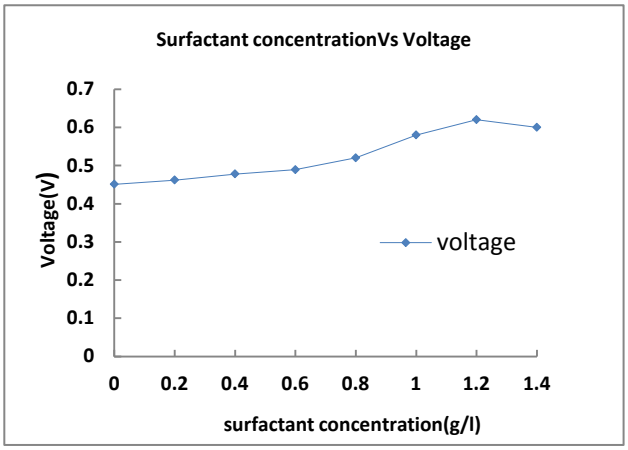

Fig. 4.11: Effect of surfactant on coating thickness

From Fig. 4.10, the coating thickness increases up to the surfactant concentration of 1.2 g/l and then decreases. A surfactant is a chemical which reduces the surface tension which can be seen in Fig. 4.8. As the surfactant concentration increases, the contact angle decreases, as shown in Fig. 4.9, which is due to the decrease in surface tension and it is minimum at 1.2 g/l since it attain its critical micelle concentration at

that point. As the coating thickness increases the voltage all increases up to11 µm and then the voltage decreases. The maximum voltage 0.62V was obtained at 11.67 µm based from the Fig. 4.11. Since, the deposition rate increases with increase in surfactant concentration, the coating thickness also increases with increase in surfactant concentration. The contact angle decreased with an increase in surfactant concentration resulting in better improved wettability of Electroless Cu deposits on the substrate. The surface tension decreased with an increase in surfactant concentration resulting in better spreading of copper deposits on the substrate. Janczuk et al., (1994) studied the surface free energy of fluorite in the presence of SDS and reported that as the concentration of surfactant increases, the SDS molecules at the solid/solution interface are adsorbed forming a stable monolayer. If this is the case, this could be a basis of an explanation for the delay in the initiation of the reaction as observed in the present study and hence less coating thickness. In the presence of SDS surfactant the amount of copper deposited on the substrate surface steadily increase with increase in surfactant concentration.

4.1.3.1 SEM Micrograph at Different Surfactant Concentration

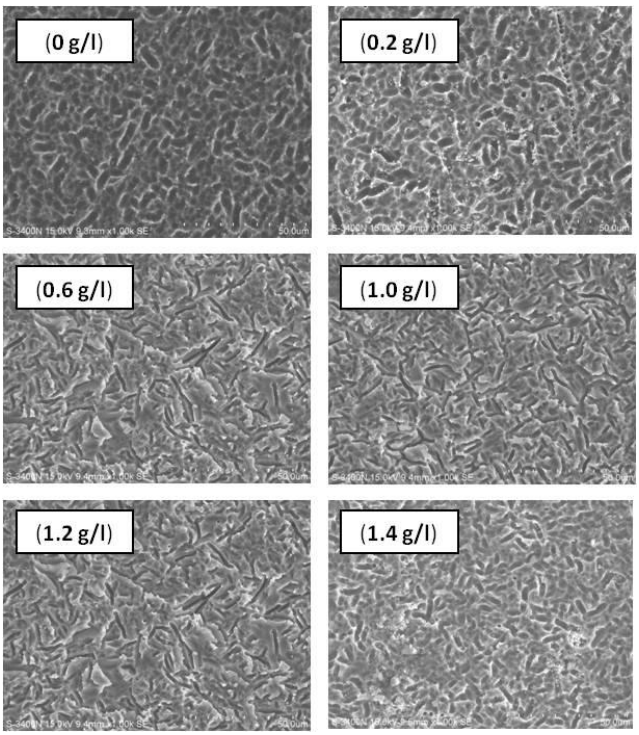

Fig. 4.12: SEM micrograph of electroless copper coated solar PV cell with magnification 1000X at different surfactant concentration

The morphology of the deposits was analyzed by employing scanning electron microscope (SEM). The SEM micrographs of electroless copper deposits without surfactant and with surfactants SDS are presented in Figs. 4.12. As the concentration of SDS surfactant increases to 1.2 g/l, smooth surface is formed and surface morphology has changed from non-smooth nodular appearance to a smooth surface.

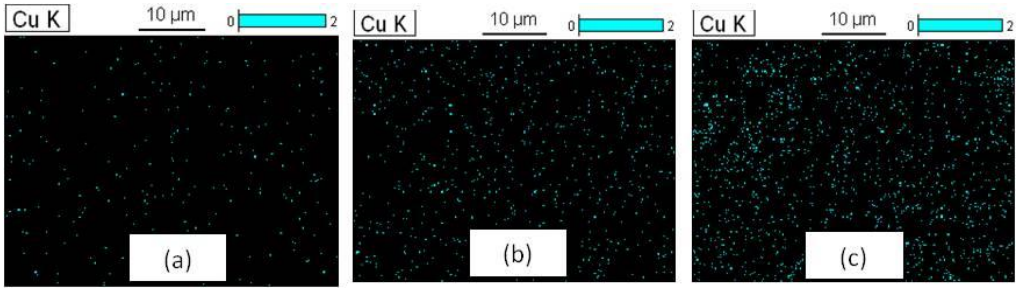

Fig. 4.13: Mapping of copper coated silicon surface with surfactant SDS (a) Without surfactant (b) 0.75 g/l (c) 1.2g/l

Fig. 4.13(a) shows the mapping of copper coated silicon surface without surfactant addition to the electroless copper bath. It is interesting to note that in the case of electroless copper deposit without surfactant, the dispersion of Cu particles seem to be less (Fig. 4.13(a)) when compared to deposit with surfactant. With addition of surfactant the amount of Cu particle deposition is more. The reason is the Cu particles produced inside the electrolyte is deposited on the activated substrate surface and surfactant addition does not allow the Cu particles to escape to the top surface and get deposited on the region other than the substrate surface. Evidence is provided in Fig. 4.13(b) and Fig. 4.13(c). As the surfactant concentration increases from 0.15 g/l, the amount of cu particles deposited also increases and there in steep increase in 0.75 g/l of SDS surfactant and the deposition rate becomes constant after 1.2 g/l of SDS since the critical micelle concentration is attained. Below the CMC, the addition of surfactant to an aqueous solution causes an increase in the number of charge carriers ((aq) Na^+ and (aq) $^-OSO_3Cl_2H_{25}$) and consequently, an increase in the conductivity. Above the CMC, further addition of surfactant increases the micelle concentration while the monomer concentration remains approximately constant (at the CMC level). Since a micelle is much larger than a SDS monomer it diffuses more slowly through solution and so is a less efficient charge carrier.

4.1.4 Measurement of Various Properties for Different Activation Times.

The activation time was varied from 1min to 5 mins from table 4.1 and from Fig. 4.14, the voltage and current density was maximum at 2 minutes of activation time and hence it is considered as optimum time of activation. From Fig. 4.15 as activation increases the coating thickness increases up to 2 mins and then decreases and as the coating thickness increases the surface roughness decreases.

Table 4.1: Experiments by Varying Activation Time

Sl.No	Activation Time(minutes)	Voltage(Volts)	Current Density (mA/cm^2)	Surface Roughness (Ra)	Coating Thickness (µm)
1	1 min	0.438	8.547	0.41	8.67
2	2 min	0.529	12.821	0.4	9.86
3	3 min	0.515	11.396	0.46	7.89
4	4 min	0.509	7.479	0.51	4.95
5	5 min	0.387	3.561	0.55	2.87

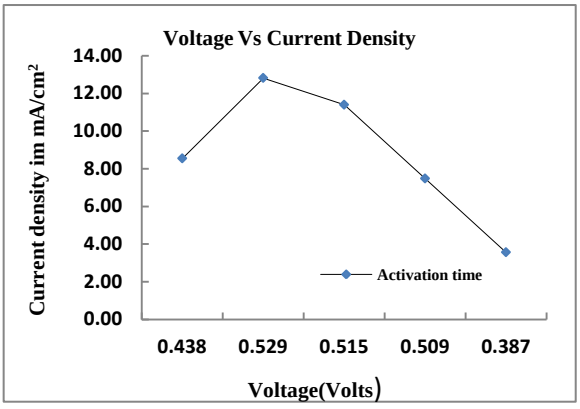

Fig. 4.14: Voltage and Current Density by Varying Activation Time

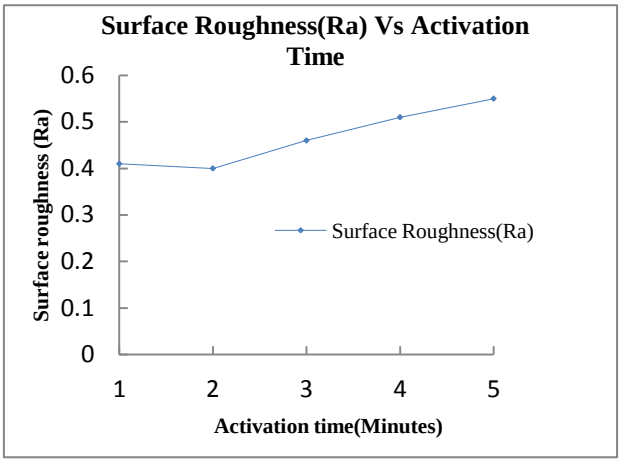

Fig. 4.15: Surface Roughness for Various Activation Time

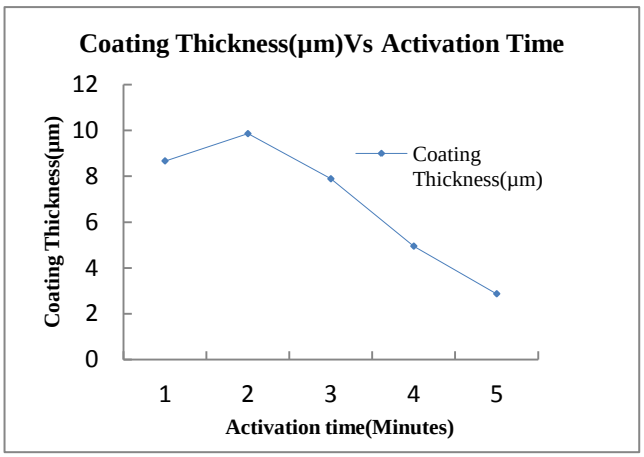

Fig. 4.16: Coating Thickness for Various Activation Time

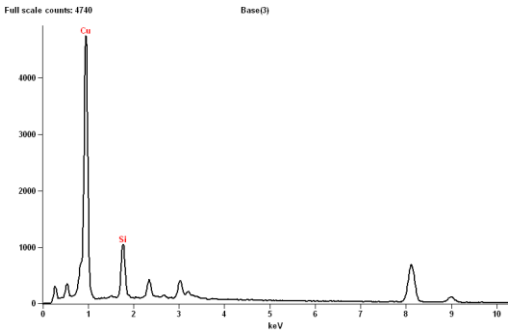

Element Line	Atom %	Formula
Si K	41.13	Si
Cu K	58.87	Cu
Cu L	---	
Total	100.00	

Fig. 4.17: EDAX spectrum of solar cell with activation time of 2 minutes

4.1.4.1 SEM Micrograph for Different Activation Time

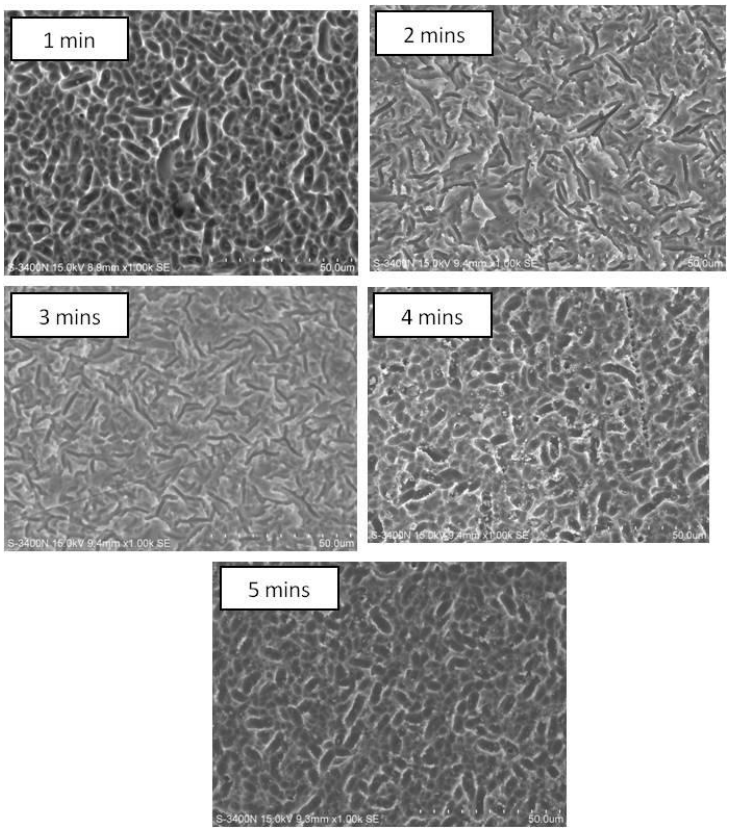

Fig. 4.18: SEM Micrograph of Electroless Copper Coated Solar PV Cell with Magnification 1000X by Varying Activation Time

4.1.5 Measurement of Various Properties for Different Immersion Times.

Table 4.2: Experiments by Varying Immersion Time

Sl.No	Process Parameter	Voltage(V)	Current Density (mA/cm^2)	Surface Roughness (Ra)	Coating Thickness (µm)
1	15 min	0.492	7.479	2.17	1.87
2	30 min	0.518	12.108	0.68	2.85
3	45 min	0.511	12.821	0.42	4.12
4	1 hour	0.536	20.655	0.4	5.97
5	1 hour 15 min	0.527	11.040	0.43	5.67
6	1 hour 30 min	0.526	17.450	0.48	7.86
7	1 hour 45 min	0.493	6.054	0.38	6.89
8	2 hours	0.436	4.808	0.51	9.65

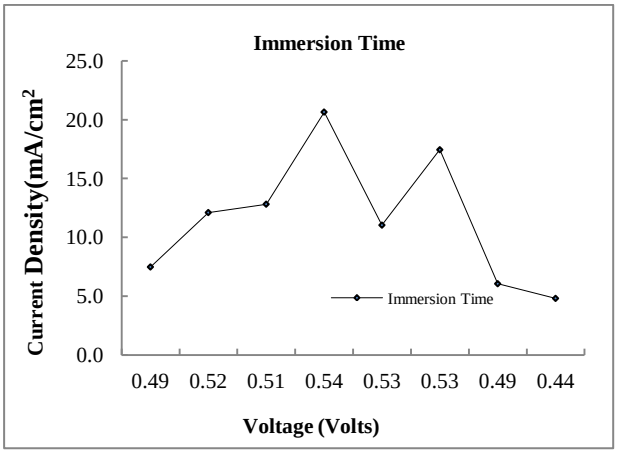

Fig. 4.19: Voltage and Current Density by varying immersion Time

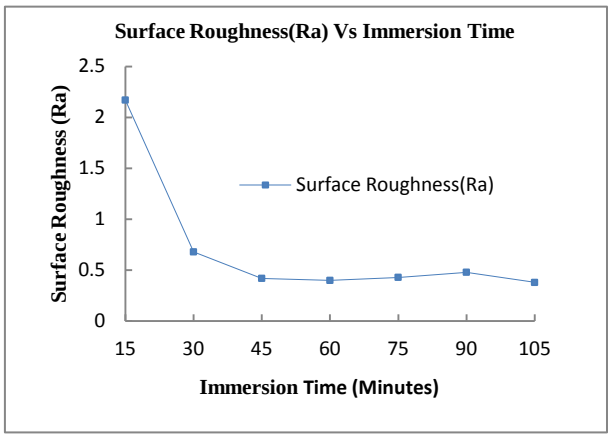

Fig. 4.20: Surface Roughness for Various Immersion Times

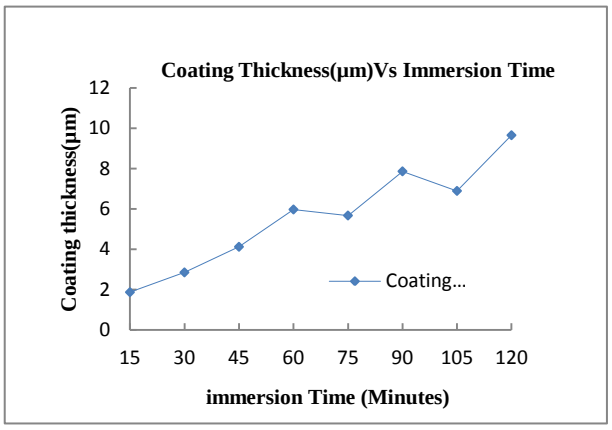

Fig. 4.21: Coating Thickness for Various Immersion Times

From Table 4.2, the immersion time was varied with time gap of 15 mins for 2 hours and from Fig. 4.18, the voltage and current density were maximum at 1 hour of immersion time and from Fig. 4.20, the coating thickness increases as the immersion time increases and there is gradual increase in coating thickness up to 1 hour of immersion and there is variation of coating thickness after 1 hour. From Table 4.2, as coating thickness increases the surface roughness decreases. The surface roughness was at a minimum of 0.4 from Fig. 4.20, corresponding to a coating thickness of 5.67 µm for 1 hour immersion time, which can be considered as the optimum immersion time for copper coating on solar cells.

4.2 ELECTROLESS COPPER COATING ON MULTICRYSTALLINE SOLAR CELL

Fig. 4.22 shows the SEM image of dense copper particles on the grid lines. The Fig. 4.23 and the EDAX analysis table confirm the presence of more amount of copper on the grid lines. Results of EDAX analysis at the silicon surface in the table in Fig. 4.24 confirms the less amount of copper dispersed on the silicon surface which is not masked by the copper line.

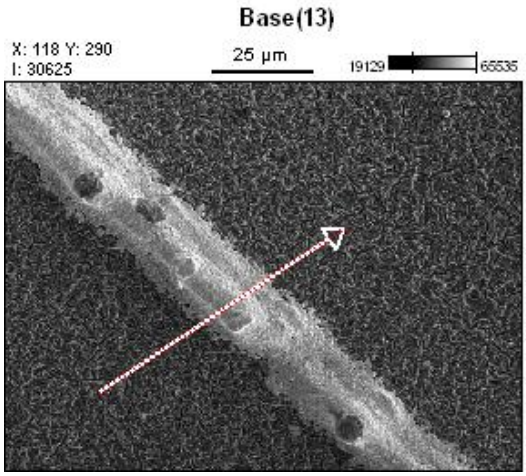

Fig. 4.22: SEM image of copper coated solar cell across the grid

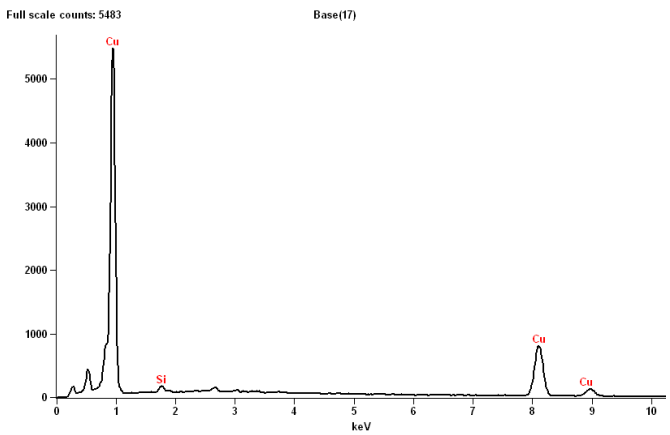

Element Line	Atom %
Si K	5.90
Cu K	94.10

Fig. 4.23: EDAX spectrum of copper coated on grid surface

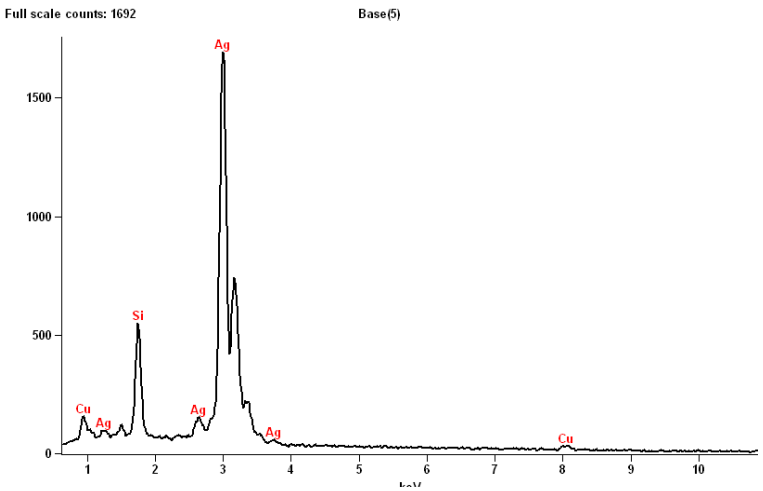

Element Line	Atom %
Si K	25.95
Cu K	3.48
Ag L	70.57

Fig. 4.24: EDAX spectrum at the silicon surface

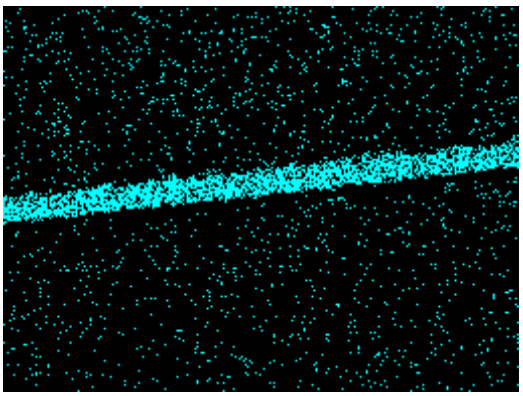

Fig. 4.25: Mapping of deposition of cu particles on silicon surface and the grid

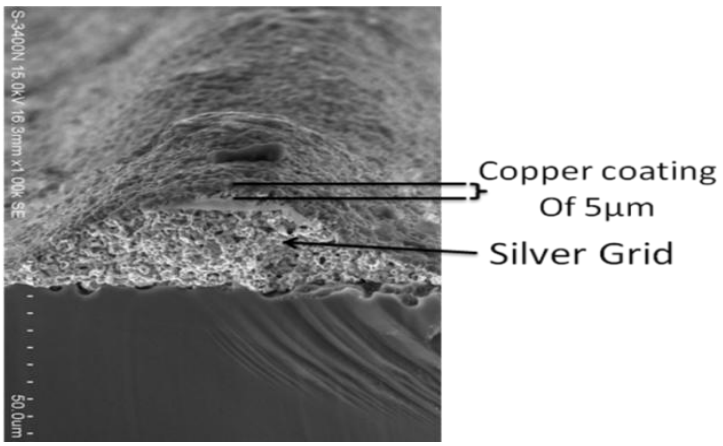

Fig. 4.26: Cross section SEM image of copper coated on grid lines

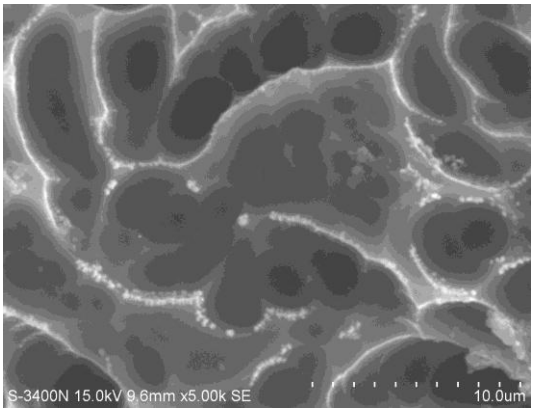

Fig. 4.27: SEM image of copper coated solar cell showing the copper nano particles at 5000X

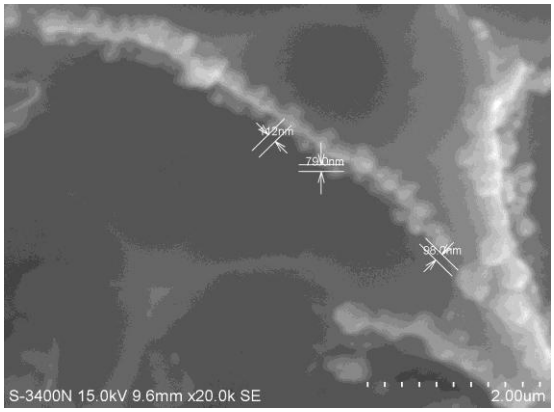

Fig. 4.28: SEM image showing the size of copper nano particles on silicon surface at20,000X

Fig. 4.25 shows the mapping of the copper coated silicon wafer showing the dense layer of copper on the grid lines and uniform dispersion of copper particles on the silicon surface. The roughness of the bare multi crystalline silicon wafer equal to 0.68 µm increases to 0.81 µm (**Ali Bahrami et al., 2013)** when the copper particles having sizes of 80nm to 120 nm were dispersed on the silicon surface as shown in Fig. 4.28. These copper particles dispersed on the surface will act as a anti reflection coating which makes multiple reflections within the particles and reduces the scattering of light on the silicon surface. The copper deposited on the grid lines has good adhesion property and uniformity due to the effect of surfactant SDS and the copper was coated to 5 µm thickness on the grid lines as shown in the Fig. 4.26. This coating of copper improves the anti bacterial properties and corrosion strength of the cell when it is exposed to atmospheric conditions. Since the conduction property of copper is very near to silver, it should be possible to replace the silver grid by copper in the future.

4.3 PRELIMINARY EXPERIMENTS FOR SPIN COATING PROCESS

4.3.1 Preliminary Experiments by Varying Spinning Speed

Table 4.3: Measurement of Various Properties by Varying Spinning Speed

Sl.No	SPINNING SPEEDS (RPM)	SURFACE ROUGHNESS(µm)	COATING THICKNESS(µm)	VOLTAGE(VOLTS)
1	1500	0.97	1.12	0.56
2	2000	0.94	1.35	0.6
3	2500	0.84	2.23	0.59
4	3000	0.81	2.87	0.56
5	3500	0.74	3.12	0.51
6	4000	0.68	3.45	0.48
7	4500	0.45	3.44	0.46
8	5000	0.42	3.41	0.45

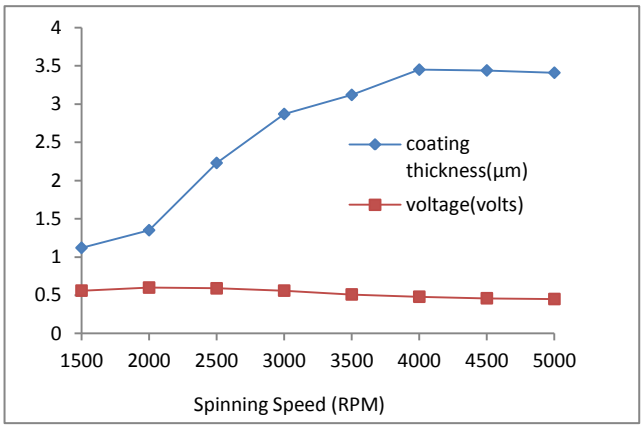

Fig. 4.29: Variation of coating thickness and voltage with spinning speed

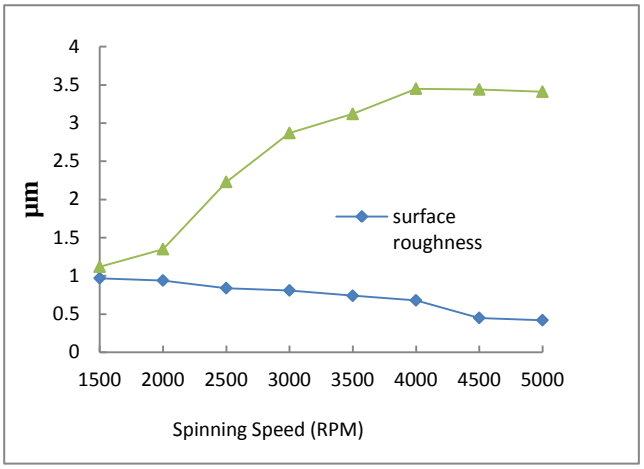

Fig. 4.30: Variation of coating thickness and surface roughness with spinning speed

Table 4.3 shows the measurement of various properties by varying spinning speed. From Table 4.3, the coating thickness increases with increases in spinning speed and there is no steep increase in the thickness after 4000 rpm and the maximum voltage of 0.62 Volts was obtained at 4000 rpm with the coating thickness of 3.45 µm. The thickness of the TiO_2 layers is an important parameter for optimizing the cell efficiencies. Thick layers (>10 µm) show high light absorption, but have also higher recombination losses compared to thin layers (<5µm) due to larger distances to the current collecting electrodes (**Yongxiang Li et al., 1999**). Hence the control levels were fixed with the high level value of 4000 rpm and low level value of 2000 rpm.

4.3.2 Preliminary Experiments by Varying Spinning Time

From the Fig. 4.31, as the spinning time increases the coating thickness increases and it becomes constant after 100 seconds of time, since no solgel will be available for further coating to increase the thickness and the surface roughness decreases with spinning time due to the uniform spreading of the solgel on the surface of the solar cell. The open circuit voltage decreased with increase in coating thickness (**Guan-Jun Yang et al., 2011**).

Table 4.4: Measurement of Various Properties by Varying Spinning Time

SL. NO	SPINNING TIME(SEC)	COATING THICKNESS (µm)	V_{OC}(VOLTS)	SURFACE ROUGHNESS (µm)
1	20	1.35	0.58	0.63
2	40	1.52	0.56	0.74
3	60	2.15	0.52	0.51
4	80	3.23	0.49	0.39
5	100	3.45	0.46	0.34
6	120	3.46	0.46	0.29

The maximum open circuit voltage was obtained at less coating thickness and the voltage was trying to decrease after 100 seconds as shown in Fig. 4.32. This is due to the fact that the increase in coating thickness leads to increase in total internal surface area which can absorb more photons and contribute to an increased in short circuit current density, but however the further increases in coating thickness may lead to less electron generation due to inefficient absorption of irradiation and cause more recombination sites which leads to decrease in short circuit current density. Hence the control levels were fixed with the low level of 20 seconds and high level of 100 seconds.

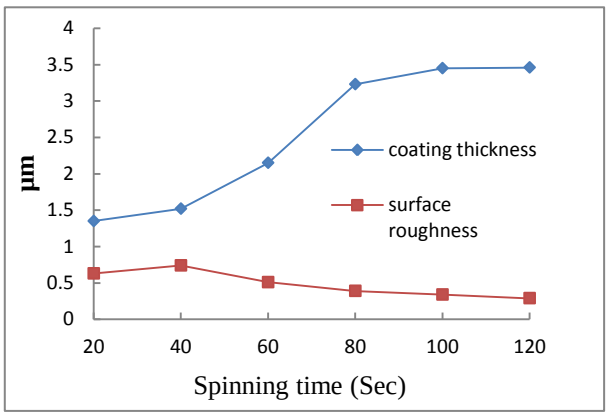

Fig. 4.31: Variation of coating thickness and surface roughness with spinning time

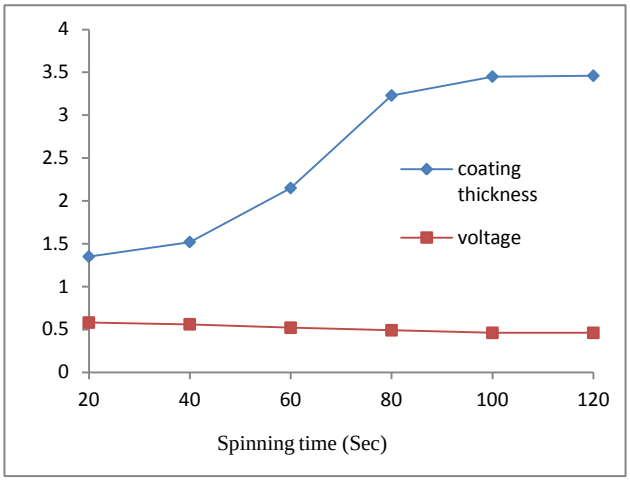

Fig. 4.32: Variation of coating thickness and voltage with spinning time

4.3.3 Preliminary Experiments by Varying Temperature

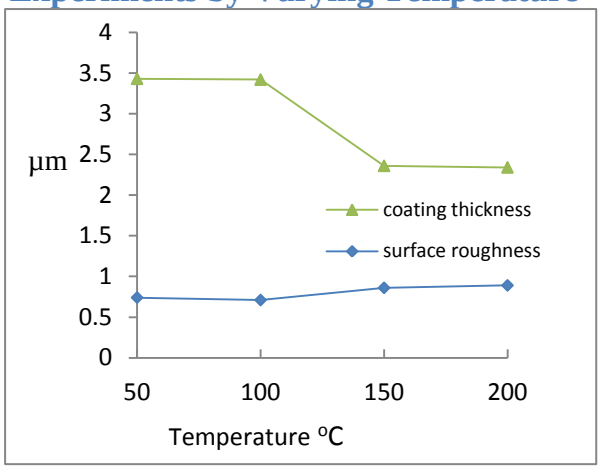

Fig. 4.33: Variation of coating thickness and surface roughness with temperature

Table 4.5: Measurement of Various Properties by Temperature

SL.NO	TEMPERATURE (°C)	COATING THICKNESS(µm)	Voc (VOLTS)	SURFACE ROUGHNESS(µm)
1	50	3.43	0.49	0.74
2	100	3.42	0.486	0.71
3	150	2.36	0.54	0.86
4	200	2.34	0.51	0.89

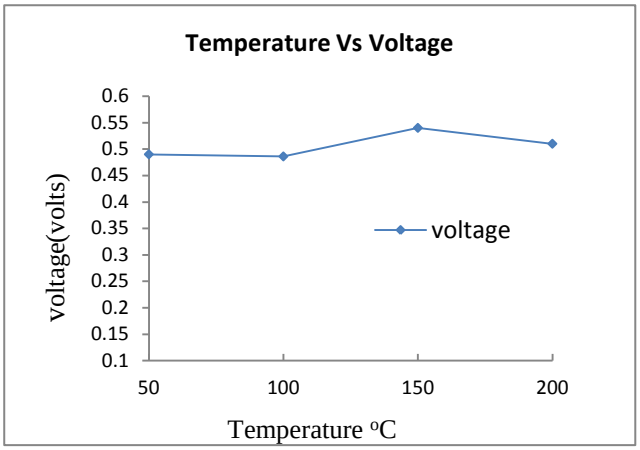

Fig. 4.34: Variation of voltage with temperature

The thickness of TiO_2 films with annealing temperatures like 60°C, 100 °C, 200 °C, 300 °C and 350 °C has been Estimated and reported by **K. Narasimha Rao et al**. Table 4.5 shows the experimental results of various parameters by varying the annealing temperature. As the temperature increases the coating thickness decreases due to the evaporation of the solvent in TiO_2 coating with increase in temperature which follows the same pattern as reported by **K. Narasimha Rao et al**. When the heating temperature increases to 150 °C and 200 °C the thickness of the film becomes almost constant and this is due to the complete evaporation of the solvent.

4.4 SPIN COATING OF TIO_2 ON COPPER COATED SOLAR CELL

The surface morphology and the cross section of the sample were studied using SEM (Hitachi S-3400N) analysis and the elemental composition of the sample was identified using Energy-dispersive X-ray spectroscopy (EDAX).

A popular method in solar cell technology is to minimize electron-hole recombination by depositing metal on the semiconductor surface (**Sahrul Saehana et al.,**) The excited electrons are trapped at the metal surface, increasing charge carrier lifetimes and to decrease recombination of electron-hole pairs and increase quantum efficiency of the photocatalytic process, the solar cell was coated with TiO_2 thin films using an interconnected metal (Cu) for electron transport. From the Fig. 4.35, the SEM micrograph shows the copper particle dispersed on the silicon surface which reduces the reflection by making multi reflection within the copper particles and the TiO_2 coating on the copper textured solar cell which act as anti-reflection coating. The bulk Cu is in contact with the TiO_2 particles and the Cu distribution is not uniform and that the deposit consists of isolated small grains of Cu in contact with TiO_2 particles. The

EDAX table of Fig. 4.36 confirms the presence of Cu and Ti, Si and O on the solar cell surface. Fig. 4.36 displays Cu peaks, indicating that the TiO_2 films were successfully coated with Cu to the extent of 0.87%. From Fig. 4.38 (a) and Fig. 4.38 (b), the mapping shows the uniform distribution of copper particles on bare silicon surface and the formation of TiO_2 layer on the silicon surface.

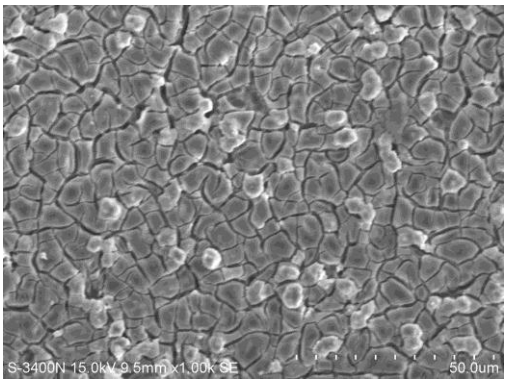

Fig. 4.35: SEM micrograph of spin coated TiO_2oncopper coated solar cell

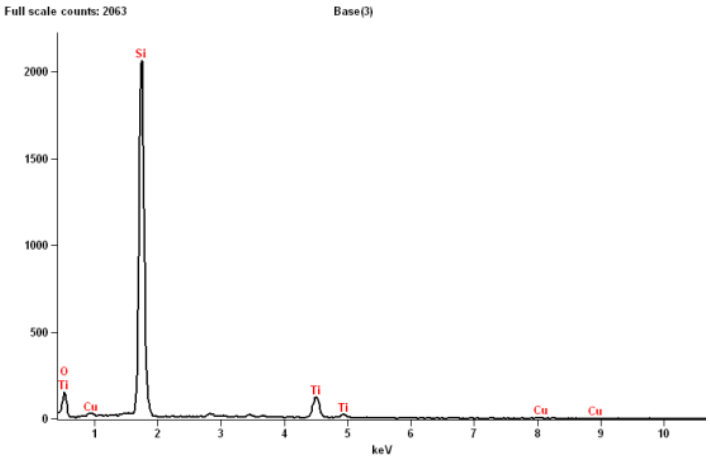

Element Line	Atom %
O K	38.71
Si K	52.30
Ti K	8.12
Cu L	0.87

Fig. 4.36: EDAX spectrum at the surface of spin coated TiO_2 on copper coated solar cell

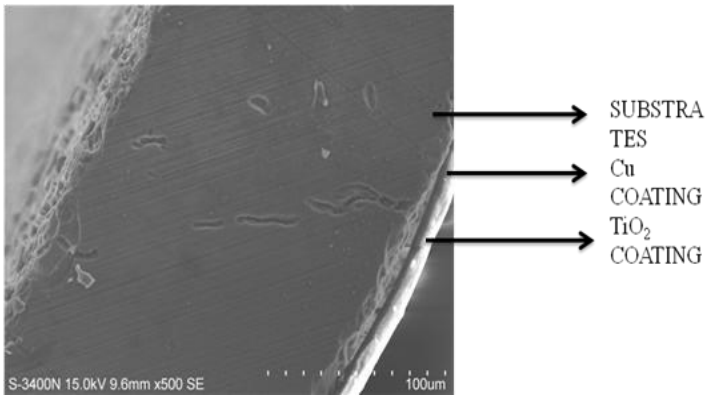

Fig. 4.37: SEM micrograph showing the cross section of spin coated TiO_2 on Copper Textured solar cell

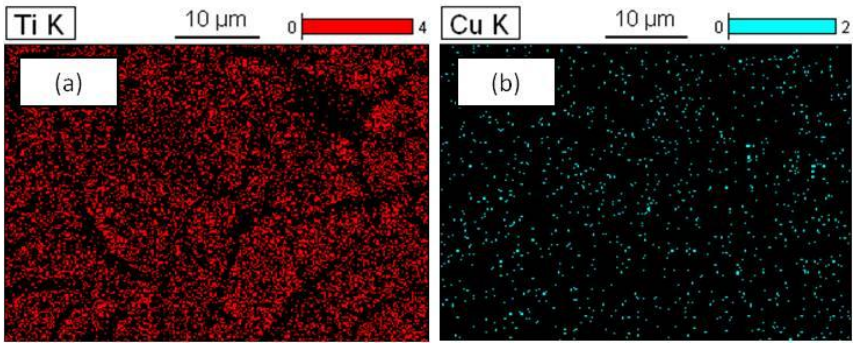

Fig. 4.38: Mapping of Spin Coated TiO_2 on Copper Coated Solar Cell (a) Distribution of Ti (b) Distribution of Cu

4.5 X-RAY DIFFRACTION ANALYSIS

The XRD analysis was made using (RIGAKU ULTIMA IV) X-ray Diffractometer and Fig. 4.39 shows the XRD pattern of copper coated multicrystalline solar cell showing SiO_2 corresponding to JCPDS 01-082-1576 and the presence of copper in the form of Cu_8O (200) (JCPDS-78-1588) and Cu_8O (036) (JCPDS –78-1588) corresponding to the peak at 2θ value of 32.7370 and 77.552 respectively. As the future work the presence of oxide can be reduced by selecting proper plating solution which will further improve the efficiency.

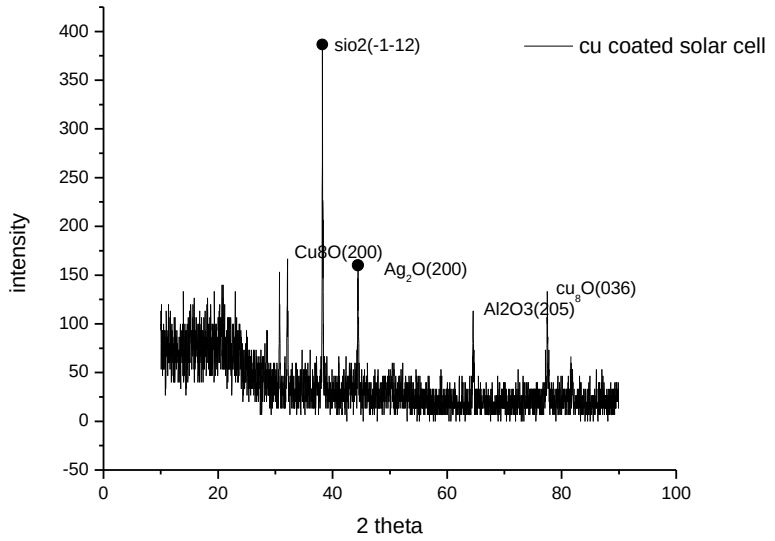

Fig. 4.39: XRD pattern of Copper Coated PV Cell

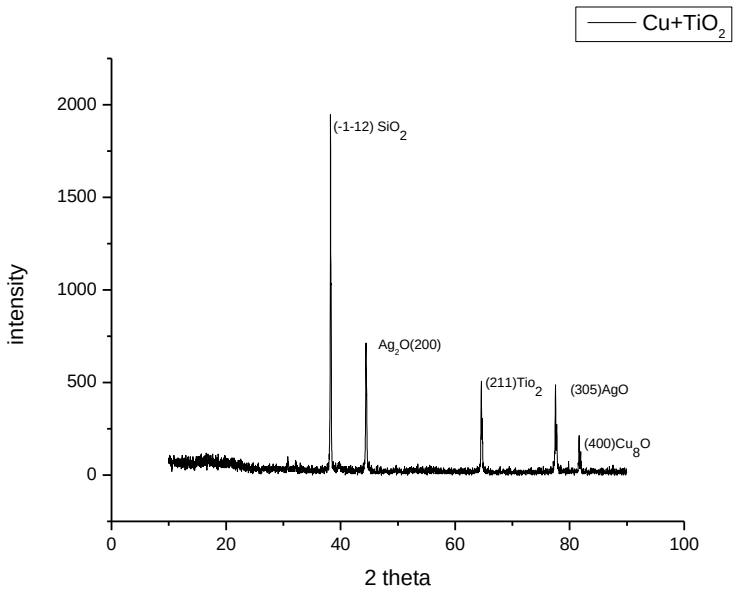

Fig. 4.40: XRD pattern of Spin coated TiO_2 on Copper Coated PV Cell

Fig. 4.40 shows the XRD pattern of spin coated TiO_2 on copper coated solar cell showing the presence of TiO_2 (211) in rutile form and the presence of copper in the form of Cu_8O(400) (JCPDS –78-1588) corresponding to the peak at 2θ of 64.569 and 81.66 degrees, respectively.

4.6 UV-VISIBLE SPECTROSCOPY ANALYSIS

The multicrystalline silicon solar cell suffers from a high natural reflectivity at the surface which reduces the short circuit current and thus the efficiency of the

device. Therefore, the reduction of optical losses consisting in reflection of the part of incident light from the front surface of the cell is extremely important for efficient solar device (**SM.Sze, 2008**).

The absorbance and reflectance characteristics of the samples were studied using UV-VIS spectrometer (Perkin Elmer lambda 650 S UV/VIS spectrometer) and from Fig. 4.41, the absorbance of non coated solar cell was about 1.1% in the wavelength of 287nm and after coating of copper the absorbance of the cell was increased to 1.5 % and the curve was shifted to visible region to the wavelength of 423nm and there was almost constant absorption throughout the visible region. 200-400 nm is the UV range and 400nm-800nm is the visible range. Fig. 4.42 shows that the reflectance of the cell was decreased from 46% to 35 % for the copper coated solar cells in the reflection mode such that less photons were reflected back due to multiple reflection with the copper nano particles.

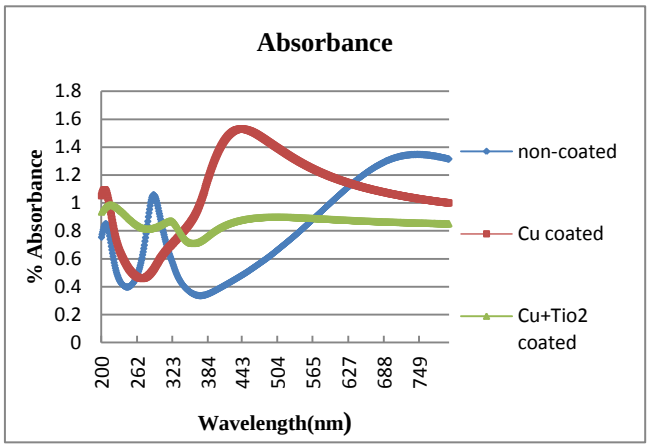

Fig. 4.41: UV-Vis Absorbance spectra for non- coated, Copper coated and TiO_2 solar cell

The absorbance of the TiO_2 coated cell is almost closer to the reference cell and there is presence of two peaks in the UV region that leads to maximum absorption in that range. The reflectance is reduced to 20% when compared to 46% reflectance of the reference cell due to the anti reflective property of TiO_2 coating.

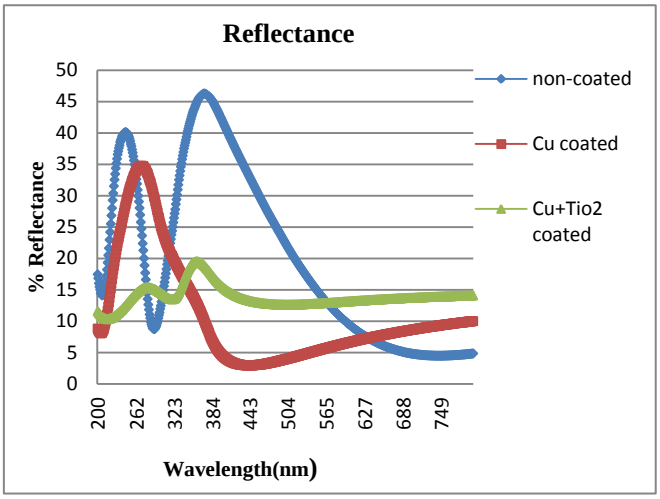

Fig. 4.42: UV-Vis Reflectance spectra for non- coated, Copper coated and TiO_2 solar cell

4.7 I-V CHARACTERISTICS

The light I-V characteristics of multicrystalline solar cells without coating (reference cell), with copper coating and TiO_2 coating on copper coated solar cell were measured and the experimental results are summarized in Table 4.6, and the corresponding I-V curve is shown in Fig. 4.43, Fig. 4.44 and Fig. 4.45 .The most important electrical parameter for the solar cell industry is the efficiency η given by Eq.4.2 because it incorporates the open circuit voltage (V_{oc}), short circuit current (I_{sc}) and fill factor as given by Eq .4.1

V_{oc} = Open circuit voltage (Volts)

I_{sc} = Short circuit current (mA)

J_{sc} = short circuit current density = $\frac{Isc}{Area\ of\ cell}$ (mA/cm^2)

Area of cell = 7.8 cm ×1.2 cm = 9.36 cm^2

Fill factor (FF) = $\frac{\text{Pmax}}{\text{Jsc Voc}}$ ..... Eq (4.1)

P_{max} = maximum power produced by cell (watts).

$P_{max} = J_{mp} \times V_{mp}$

J_{mp} = Current density at P_{max} = $\frac{\text{Imp}}{Area\ of\ cell}$ (mA/cm^2)

V_{mp} = Voltage at P_{max} (volts).

Efficiency (η) = $\frac{\text{Pmax}}{Pin} = \frac{Pmax}{E \times Ac}$ .....Eq (4.2)

E = irradiance of the incident light (1000W/m^2)

Ac = surface area of the solar cell in m^2

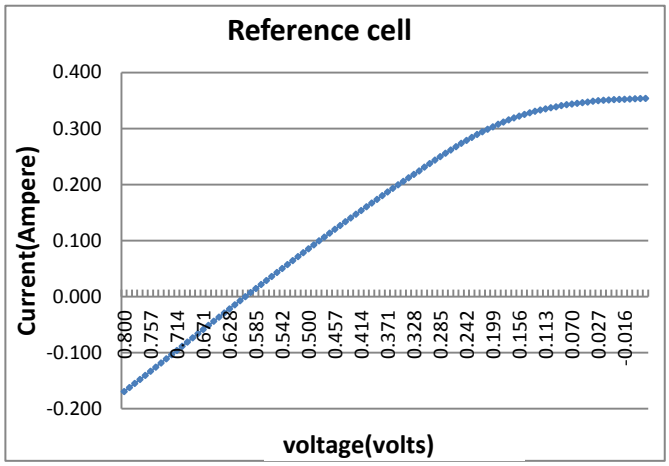

Fig. 4.43: I-V characteristics of reference cell

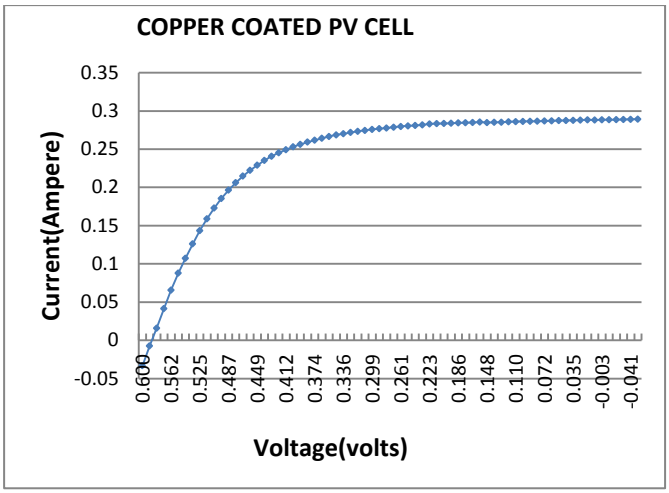

Fig. 4.44: I-V characteristics of copper coated solar cell

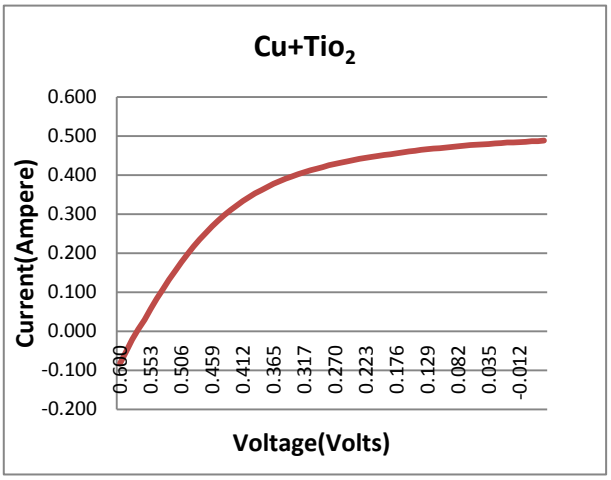

Fig. 4.45: I-V characteristics of spin coated TiO_2 on copper coated solar cell

Table 4.6: Electrical Properties of Copper Coated Solar Cell and Reference Cell

Electrical properties	V_{oc} (Volts)	I_{sc} (Amps)	I_{max} (Amps)	V_{max} (Volts)	P_{max} (mW)	Fill Factor (%)	Efficiency
Reference cell	0.60	0.350	0.229	0.313	71.71	33.96	7.661
Copper coated	0.587	0.288	0.238	0.433	103.58	61.15	11.06
TiO_2 + Cu coated	0.572	0.483	0.358	0.387	138.78	50.11	14.82

From the Table 4.6, even though the electrical properties such V_{oc} and I_{sc} were slightly less than the reference cell, the I_{max} and V_{max} value of the solar cell coated with copper has increased to 0.238 Ampere and 0.433 Volts respectively. The fill factor of the copper coated solar cell is 61.15 % compared to 33.96% of the reference cell which leads to increase of 4% efficiency. The open circuit current of TiO_2 coated sample increased to 0.483 Ampere which leads to the increase in fill factor of 50.11% and the efficiency of 14.82% (**Hocinel, D., 2012**).

4.8 SUMMARY

In this chapter the results were discussed based on the preliminary experiments conducted to fix the various process parameters in electroless copper coating and spin coating of TiO_2 of copper coated solar cell. The parameters were fixed and the electroless and spin coating process were carried out using optimized values of parameters. The characterization of the solar cell was also carried out using XRD, IV-characteristics and UV-Visible spectroscopy. The procedure for conducting DOE and the effects of various parameters and its interactions are explained in the next chapter.

CHAPTER 5 : DESIGN OF EXPERIMENTS

5.1 DESIGN OF EXPERIMENTS FOR ELECTROLESS COPPER COATING ON SOLAR CELLS

In the electroless coating of copper on silicon wafer, process parameters such as pH, temperature and surfactant concentration were varied and corresponding coating thickness on the grid surface, voltage, current density and the surface roughness were measured. Design of experiments (DOE) was conducted using full factorial method to optimize these process parameters and the analysis was made using Analysis of Variance method (ANOVA). The preliminary experiments were conducted by varying the level of pH at four different intervals such as 4-5, 5-6, 8-9, 9-10 and temperature was varied at different values such as 75 ºC, 80 ºC, 85 ºC, 90 ºC. The surfactant SDS was used and its concentration was varied from 0-1.4g/l. Coating thickness, voltage, surface roughness, surface tension and contact angle were measured for the samples with different surfactant concentrations. The experiments were conducted to fix the activation and immersion time of the sample and the activation time was fixed at 2 minutes and the immersion time at one hour. The control parameters and their levels were fixed for three factors such as pH, temperature and surfactant concentration and the Design matrix was framed with 3 factors and 2 levels (2^3 Factorial Design). Minitab software was used for the analysis and the mathematical equations were framed relating different process parameters.

5.1.1 Control Parameters and Their Levels

Preliminary experiments were carried out to fix the control parameters as shown in Table 6.1. At Low pH (4-5), the rate of deposition is low and the life of bath is high. At high pH value (9-10), the rate of deposition is high and the life of bath is low. Hence, pH interval of 8-9 is considered as optimum. At low temperature (75 ºC), the viscosity of bath is higher, so coating is not properly formed on the substrate. At high temperature (90ºC), the bath decomposes and affects the coating on the substrate. Hence, the proper reaction takes place at 85 ºC. When the surfactant is 0 g/l, proper coating does not take place. When the surfactant concentration is increased to 1.4g/l, the electroless bath becomes unstable. So the proper uniform coating takes place at 1.2 g/l.

Table 5.1: Control Parameters

Parameters	High value	Low value
pH	10	4
Temperature	90 ºC	75 ºC
Surfactant concentration	1.2 g/l	0 g/l

5.1.2 Design Matrix

Table 5.2: Design Matrix for Electroless Copper Coating Process

Sl.No	**Run label**	**PH [a]**	**Temperature ºC[b]**	**Surfactant concentration(g/l) [c]**
1	I	-[4]	-[75]	-[0]
2	a	+[10]	-[75]	-[0]
3	b	-[4]	+[90]	-[0]
4	c	-[4]	-[75]	+[1.2]
5	bc	-[4]	+[90]	+[1.2]
6	ac	+[10]	-[75]	+[1.2]
7	ab	+[10]	+[90]	-[0]
8	abc	+[10]	+[90]	+[1.2]

Table 5.2 represents the number of experiments conducted. Here + represents the high value of parameters and – represents the low value of parameters. Based on full factorial design, eight experiments have been conducted.

5.1.3 Measurement of Various Properties for Electroless Copper Coated Solar cells at Different Run Labels.

Table 5.3: Properties at Different DOE Run Labels

Run order	DOE conditions	Surface roughness(Ra) in(µm)	Coating thickness(µm)	Current (Amps)	Voltage (volts)	Power=V×I (Watts)
1	pH=4,T=65,sds=1.2	0.41	11.2	0.092	0.48	0.045
2	pH=10,T=85,sds=1.2	0.25	14.2	0.105	0.613	0.065
3	pH=10,T=85,sds=0	0.95	6.3	0.081	0.47	0.038
4	pH=4,T=65,sds=0	0.93	7.8	0.072	0.463	0.033
5	pH=10,T=65,sds=0	0.51	10.56	0.103	0.493	0.051
6	pH=4,T=85,sds=0	0.53	9.85	0.104	0.53	0.056
7	pH=10,T=65,sds=1.2	0.31	13.60	0.104	0.576	0.060
8	pH=4,T=85,sds=1.2	0.37	12.32	0.100	0.49	0.049

5.1.4 Analysis of Electroless Copper Coating Process Using ANOVA

5.1.4.1 Main Effects Plot for Various Output Responses

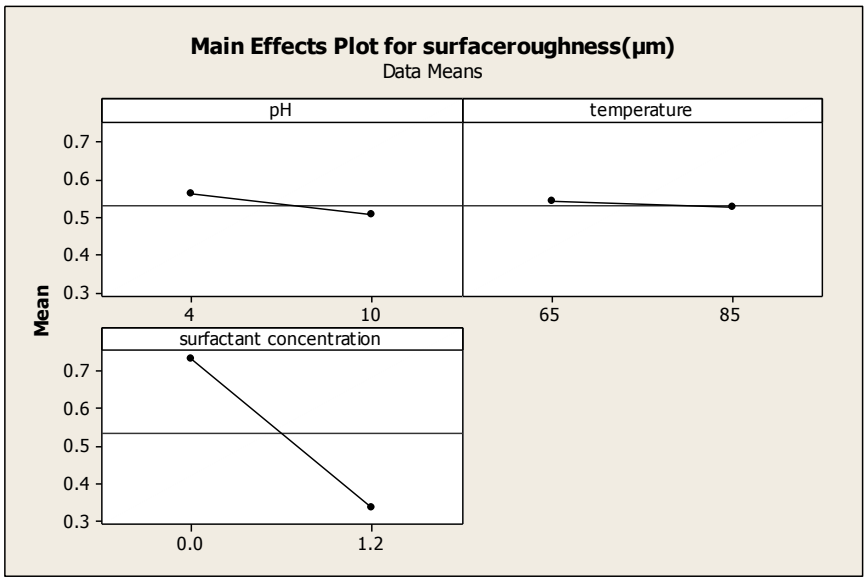

Fig. 5.1: Main Effect Plot for Surface Roughness

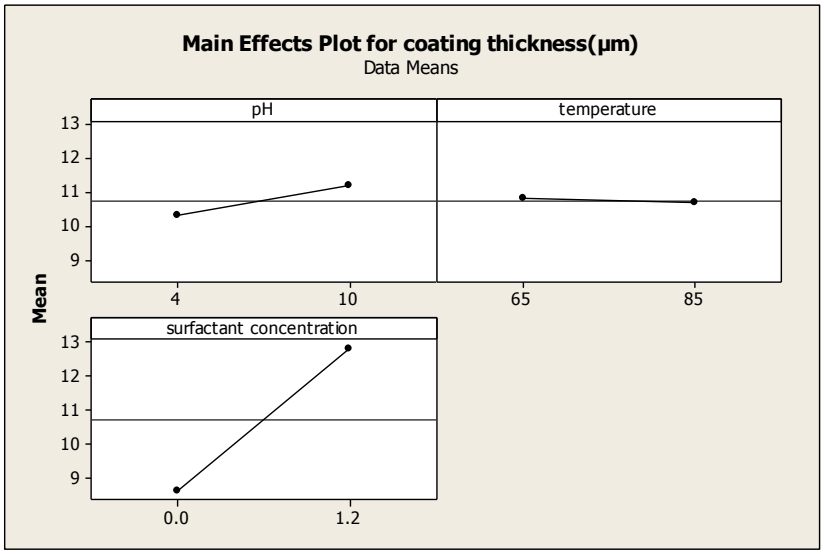

Fig. 5.2: Main Effect Plot for Coating Thickness

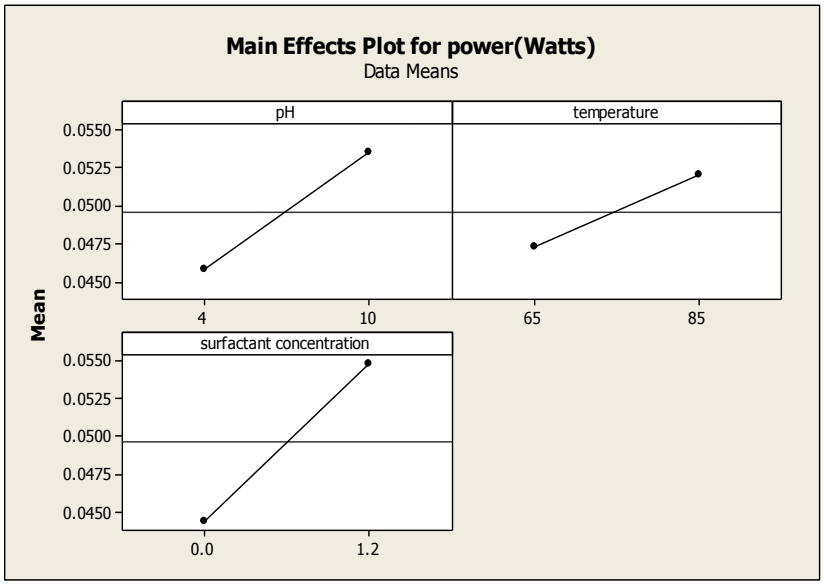

Fig. 5.3: Main Effect Plot For output power

This main effect graph plots the mean value of the high and low of each factor. The main effect plot of surface roughness in Fig. 5.1 shows that surfactant has major influence on the surface roughness while the horizontal line of pH and temperature show that it has least effect on surface roughness. Since the surfactant contributes to the wettability of the metal ions, an increase in its concentration increases the coating thickness as shown in Fig. 5.2 and leads to uniform deposition and hence the surface roughness is minimum at higher concentration of surfactant. The main effect plot of power (Fig. 5.3) shows that pH and surfactant concentration have major influence on power production and the temperature also has some amount of influences. The table

generated by Minitab software for the Analysis of Variance (ANOVA) and the equations framed relating various process parameters are presented in the appendix.

5.1.4.2 Interaction Plot for Various Output Responses

The interaction between the factors can be visualized with an interaction plot. The interaction plot graphs the means of replicates, organized based on high and low of the factors. The interaction plot of surface roughness in Fig. 6.4 shows that temperature and pH has major interaction and other parameters have least interaction.

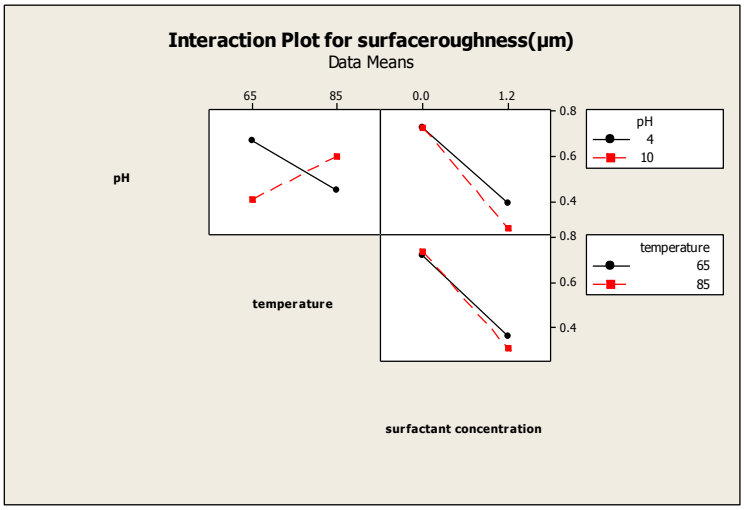

Fig. 5.4: Interaction plot for surface roughness

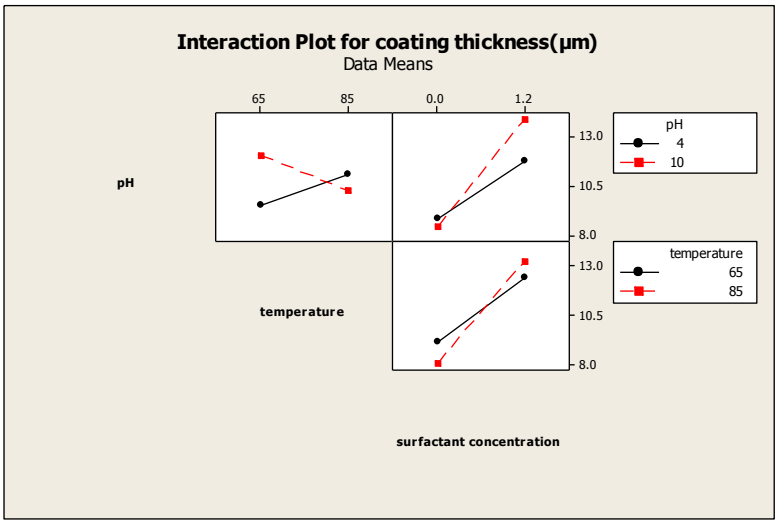

Fig. 5.5: Interaction plot for coating thickness

The interaction plot of coating thickness, as shown from Fig. 5.5, shows that temperature and surfactant concentration have major interaction at its average value and the pH and temperature will have the interaction at the higher mean values.

In the interaction plot for power as shown in Fig. 5.6, the lines in temperature versus surfactant concentration are parallel, indicating a lack of interaction between the these factors and hence it suggests that mutual interaction between these factors have negligible effect on the power. The pH and temperature has interaction at higher values and the pH and surfactant concentration has its interaction at its lower values.

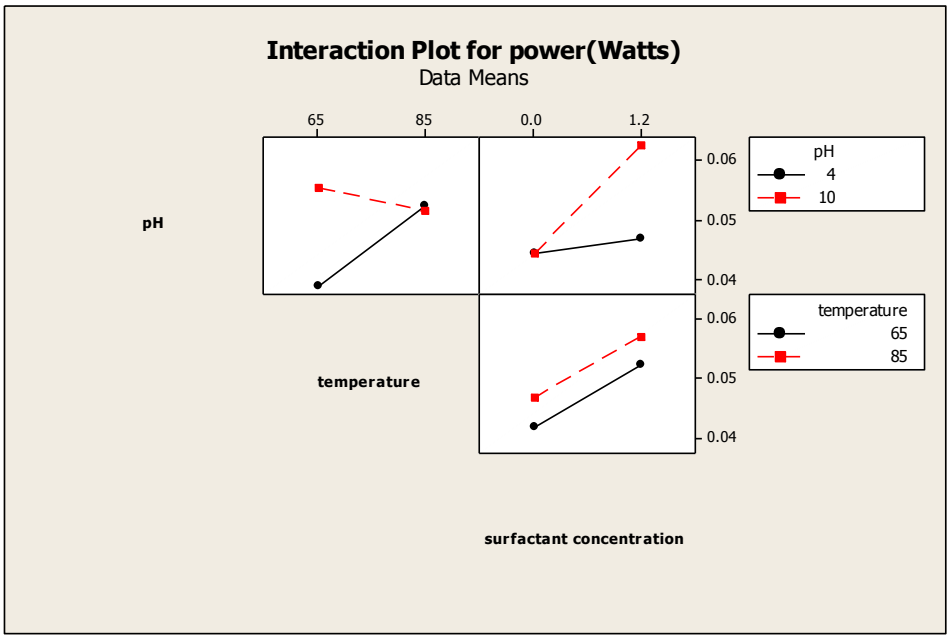

Fig. 5.6: Interaction plot for output power

5.2 DESIGN OF EXPERIMENTS FOR SPIN COATING OF TiO_2 ON COPPER COATED SOLAR CELLS

Preliminary experiments were conducted by coating the samples at different rpm ranging from 1000 rpm to 5000 rpm at the interval of 500 rpm with the spinning time ranging from 20 sec -120 sec with the interval of 20 sec. The samples were heated to different temperatures from 50^{o}C to 200^{o}C, since the coating thickness depends on the evaporation of the solvent at high temperature. The control parameters and their levels were fixed for these three factors and the Design matrix was framed with 3 factors and 2 levels (2^3 Factorial Design). The analysis was made using Analysis of Variance method (ANOVA). Minitab software was used for the analysis and the mathematical equations were framed relating different process parameters.

5.2.1Control Parameters and Their Levels

The influence of the various deposition parameters like spinning speed, spinning time and annealing temperature on the thickness of the TiO_2 films and the variation of film thickness with time in ambient atmosphere was also studied and reported by **K. Narasimha Rao et al**. Preliminary experiments were conducted and the control parameters were fixed as shown in the Table 5.4. In preliminary experiments, samples were coated at different rpm ranging from 1000 rpm to 5000 rpm at an interval of 500 rpm. Spinning time was varied from 20 seconds to 120 seconds with an interval of 20 seconds. The coated samples were heated to various temperatures such as 50^{o}C, 100^{o}C, 150^{o}C and 200^{o}C.

Table 5.4: Control Parameters

Parameters	Low level	High level
Spinning speed	2000rpm	4000rpm
Temperature	100 ^{o}C	150 ^{o}C
Coating Time	20 sec	100 sec

5.2.2 Design Matrix

Design of experiments were conducted using full factorial method with 3 parameters such as spinning speed, spinning time and annealing temperature and 2 levels which gives the combination of 2^3 factorial design. Here + represents the high value of parameters and – represents the low value of parameters. Based on full factorial design, eight experiments have been conducted as represented in Table 5.5 and the measurements of various parameters were shown in Table 5.6.

To analyze the data from a design of experiment, evaluating the statistical significance by computing one way ANOVA, or for more than one factor N-way ANOVA is essential (**Rati Saluja et al**., **2012**). The analysis was made using Analysis of Variance method (ANOVA) and the Minitab software was used for the analysis and the mathematical equations were framed relating different process parameters and are presented in the appendix.

Table 5.5: Design Matrix for Spin Coating Process

Sl.No	Run label	Spinning speed in RPM [a]	Spinning time in sec [b]	Temperature ºC [c]
1	I	- [2000]	- [20sec]	-[100]
2	bc	-[2000]	+[100]	+[150]
3	c	-[2000]	-[20]	+[150]
4	abc	+[4000]	+[100]	+[150]
5	ab	+[4000]	+[100]	-[100]
6	a	+[4000]	-[20]	-[100]
7	b	-[2000]	+[100]	-[100]
8	ac	+[4000]	-[20]	+[150]

5.2.3 Measurement of Various Output Responses for Different Run Labels

Table 5.6: Various Output Responses for Different Run Labels

Run label	Coating Thickness(µm)	Surf Roughness	Voltage(Volts)	Current(Amps)	Power=V×I
1	4.37	0.4	0.486	0.090	0.0438
2	3.58	0.75	0.503	0.093	0.0469
3	3.39	0.43	0.613	0.105	0.0641
4	2.19	0.93	0.443	0.086	0.0382
5	3.02	0.88	0.446	0.088	0.0391
6	2.89	0.89	0.562	0.097	0.0543
7	5.14	0.34	0.458	0.084	0.0383
8	3.65	0.66	0.476	0.093	0.0442

5.2.4 Analysis of Spin Coating Of TiO_2 on Copper Coated Solar Cell Using ANOVA

5.2.4.1 Main Effect Plot

The importance of main effect plot is that it shows the behavior of the system when one parameter is varied by keeping another parameter constant (**Astha Kukreja, 2011**).

Fig. 5.7: Main Effect Plot For output power

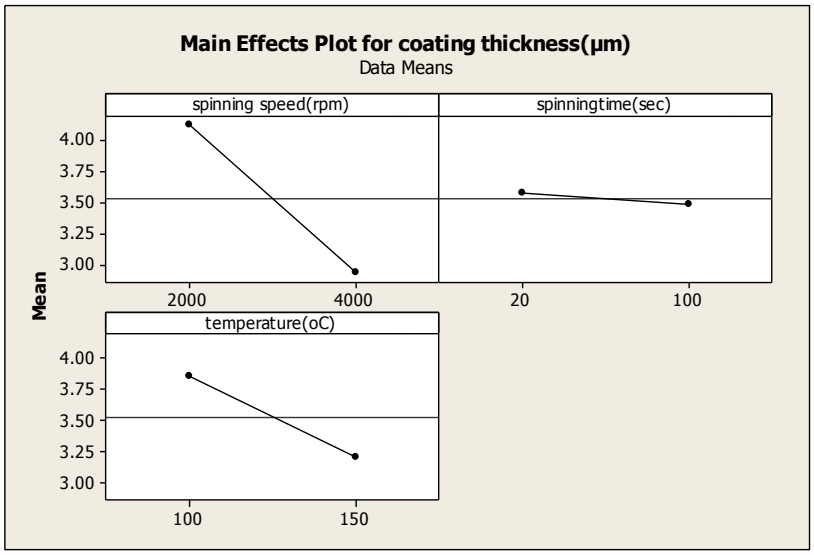

Fig. 5.8: Main Effect Plot for Coating Thickness

A main effect occurs when the mean response changes across the levels of a factor and it can be used to compare the relative strength of the effects across each factor. It can be inferred from the plot (Fig. 5.7) that the spinning speed and the spinning time have negative effects while the temperature has positive effect on the output power. It can also be concluded that spinning time has profound effect on the output followed by spinning speed and temperature.

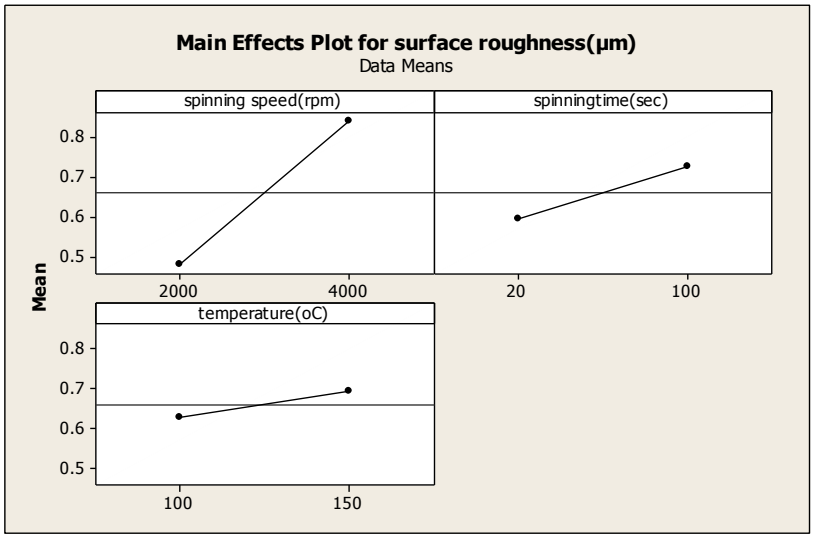

Fig. 5.9: Main Effect Plot for Surface Roughness

It can be inferred from the plot (Fig. 5.8) that the spinning speed and the temperature have negative effects while the spinning time has least effect on coating thickness

which is indicated by the horizontal line of the plot. It can also be concluded that spinning speed has major effect on the coating thickness but on the negative side. From the Fig. 5.9 all the factors have the positive effect on surface roughness which is just the opposite trend of coating thickness, since increase in coating thickness will reduce the surface roughness.

5.2.4.2 Interaction Plot

The interaction plot gives average output for each level of the factor with the level of the second factor held constant (**Astha Kukreja, 2011**). These plots are used to interpret significant interactions between the process parameters. Interaction is present when the response at a factor level depends upon the levels of other factors. Since they can magnify or diminish the main effects of the parameters, evaluating interactions is extremely important. In the interaction plot for power as shown in Fig. 5.10, the lines in spinning speed versus spinning time and the lines in spinning time versus temperature are approximately parallel. This indicates a lack of interaction between these factors and hence this suggests that mutual interaction between these factors have negligible effect on the power. Since the P-value (as shown in appendix) of the effect spinning speed (rpm)*temperature (^{o}C) is less than the chosen value of α=0.05 for the analysis, it has significant effect on the output power.

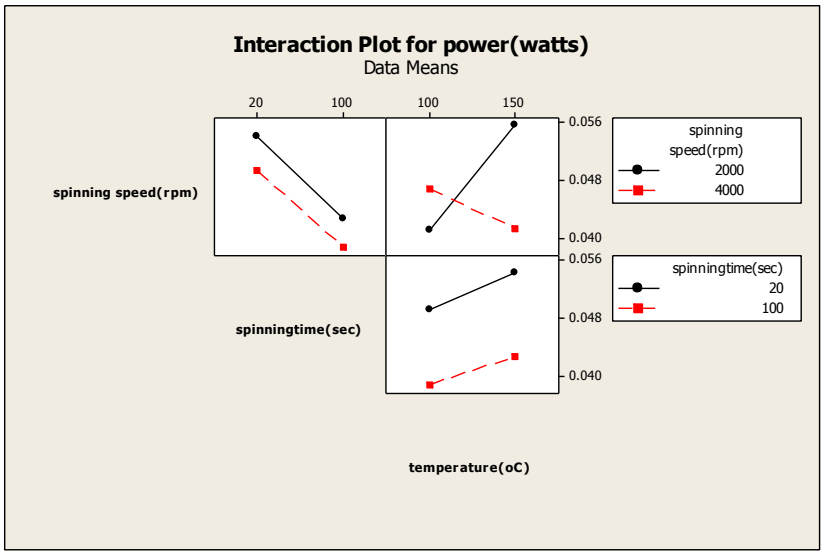

Fig. 5.10: Interaction plot for output power

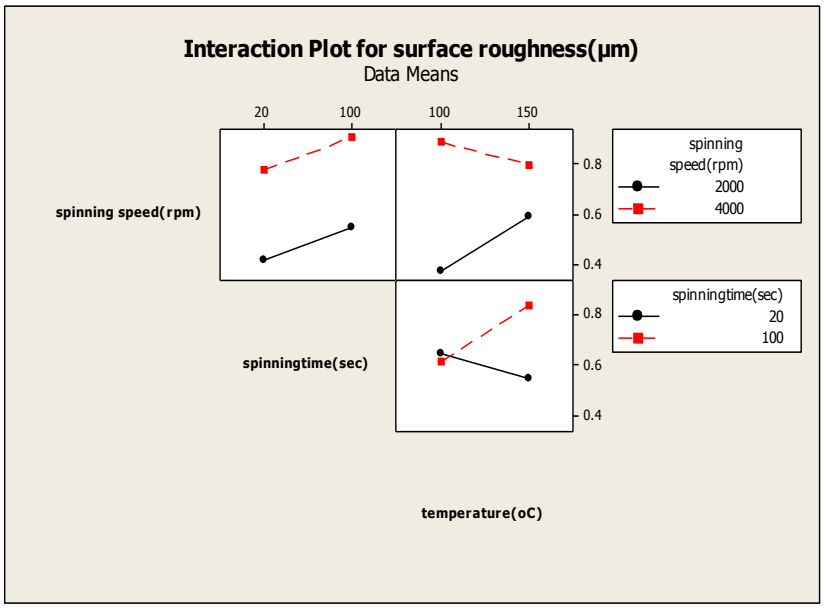

Fig. 5.11: Interaction plot for surface roughness

Fig. 5.11 shows the interaction plot for surface roughness in which the spinning time and the temperature have maximum interactions since these parameters influence the coating thickness and the grain size of the particles. In the interaction plot of coating thickness Fig. 5.12 there exists antagonistic interaction between the spinning speed and temperature and also in the interaction between spinning speed and spinning time as the lines of the graph cross each other.

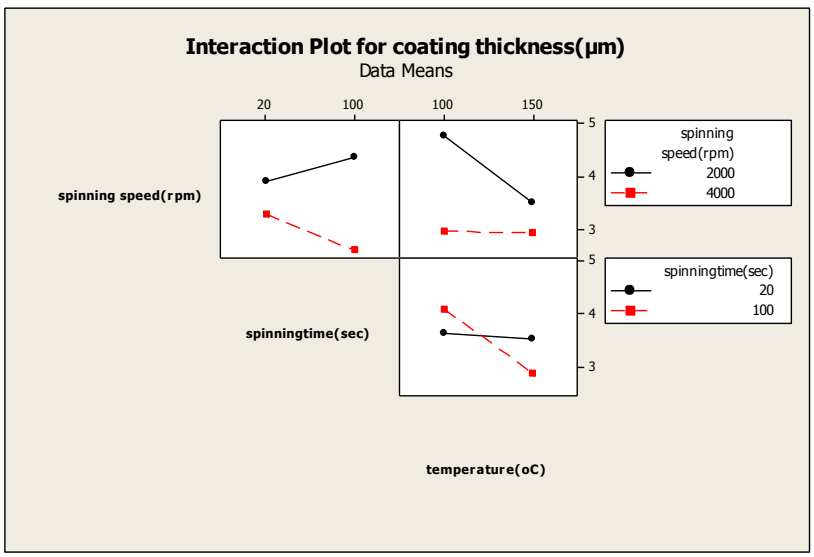

Fig. 5.12: Interaction plot for coating thickness

Similarly, the interaction plot of spinning time and temperature shows that there is synergistic interaction between them. Although the lines on the plot do not cross each other, the lack of parallelism of lines exhibit significant interaction. The greater the departure of the lines from the parallel state, the higher the degree of interaction (**Astha Kukreja, 2011**).

5.3 SUMMARY

This chapter discuss about the design of experiments using full factorial method and the analysis of process parameters using ANOVA (Analysis of Variance) method. The ANOVA was carried out using Minitab software and the results were discussed using main effect plot and interaction plot. The equations were framed relating different process parameters and were presented in appendix. The comparative study with the addition of different nano additives to the electroless copper bath was presented in next chapter.

CHAPTER 6 : COMPARATIVE STUDIES

6.1 COMPARITIVE STUDY WITH THE ADDITION OF NANO ADITIVES TO THE ELECTROLESS COPPER BATH

As a third module, in this research a comparative study was made with the addition of nano additives to the electroless copper bath. The nano additives such as ZnO, CuO and Al_2O_3 were added at various percentages in the electroless copper bath and the samples were coated with the above nano additives. Studies were made on the influence of nano additives on solar cells with respect to improvement of coating thickness, surface roughness, voltage and power generated. Comparisons were made between (i) copper coated samples, (ii) Cu + TiO_2 coated samples, (iii) Cu + Nano CuO, (iv) Cu + Nano ZnO, (v) Cu + Nano Al_2O_3, (vi) Cu + Nano CuO + TiO_2 coated samples, (vii) Cu + Nano ZnO + TiO_2 coated samples, (viii) Cu + Nano Al_2O_3 + TiO_2 coated samples and (ix) non-coated sample. The comparative study was made using SEM, EDAX and UV-VIS spectroscopy.

6.1.1 Measurement of Various Properties of Copper Coated Solar Cell With Addition of Nano Additives

Table 6.1: Various Parameters by the Addition of CuO Nano Additives

Percentage of Nano CuO	Surface roughness(µm)	Open circuit voltage (V_{oc})	Coating thickness (µm)
0.10%	0.79	0.51	11.7
0.50%	0.52	0.48	14.1
1%	0.41	0.497	17.2
2%	0.45	0.472	19.1

Table 6.2: Various Parameters by the Addition of Al_2O_3 Nano Additives

Percentage of Nano Al_2O_3	Surface roughness(µm)	Open circuit voltage (V_{oc})	Coating thickness (µm)
0.10%	0.86	0.548	2.4
0.50%	0.63	0.485	3.6
1%	0.44	0.46	4.3
2%	0.79	0.402	7.2

Table 6.3: Various Parameters by the Addition of ZnO Nano Additives

Percentage of Nano ZnO	Surface roughness(µm)	Open circuit voltage (V_{oc})	Coating thickness (µm)
0.10%	0.74	0.404	3.8
0.50%	0.76	0.465	8.1
1%	0.38	0.482	11.4
2%	0.49	0.554	12

From Table 6.1 and Fig. 6.1 and Fig. 6.3 the addition of CuO % shows increase in coating thickness on the grid surface and the maximum voltage was obtained at the coating thickness of 11.7 µm which was obtained at the addition of CuO to the lower percentage of 0.10%. The voltage of the sample was less at higher percentage of CuO due to the synergistic effects of the electron back-transport reaction and the resistive losses.

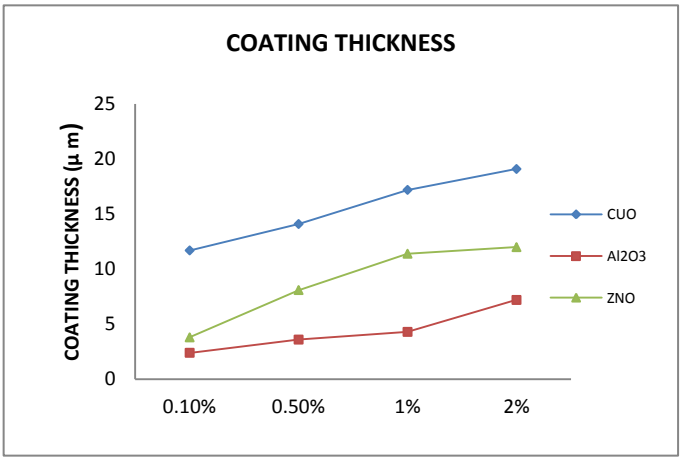

Fig. 6.1: Variation of coating thickness with percentage variation of nano additives

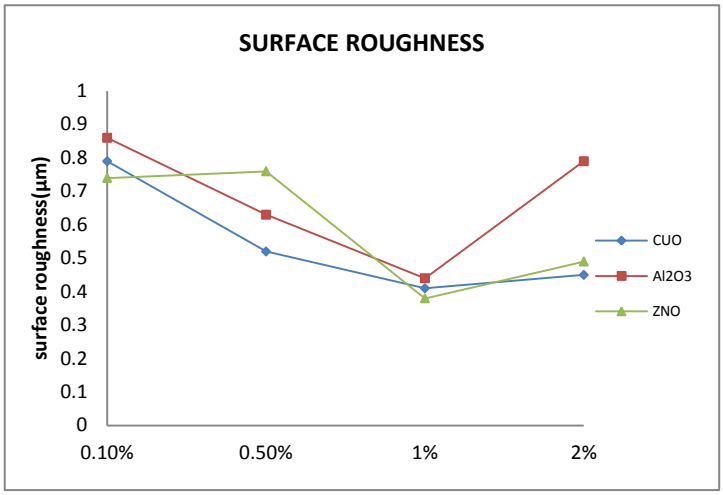

Fig. 6.2: Variation of surface roughness with percentage variation of nano additives

From Table 6.2, the addition of Al_2O_3 shows better voltage generation at the addition of nano additive to the lower percentage of 0.1 and from Table 6.3, the addition of ZnO nano additive shows better performance at its addition to the higher level of 2% showing the voltage of 0.554 volts and less surface roughness of 0.49 µm. This is due to the photo luminescence property of zinc oxide at higher percentage.

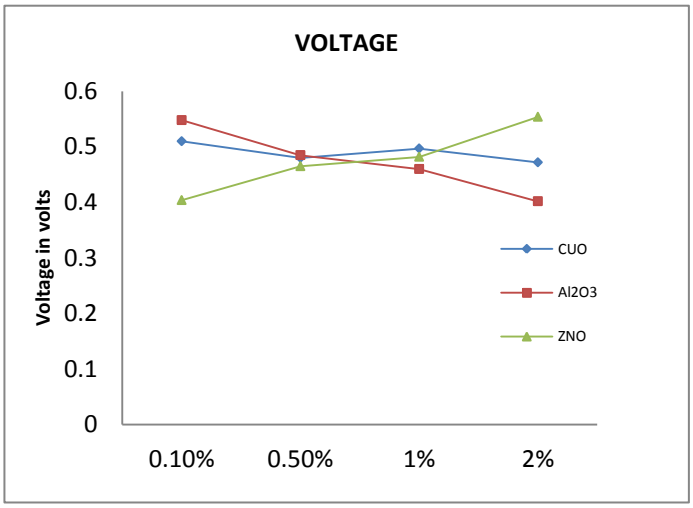

Fig. 6.3: Variation of open circuit voltage with percentage variation of nano additives

6.1.2 SEM Images of Copper Coated Solar Cell With the Addition of Nano Additives

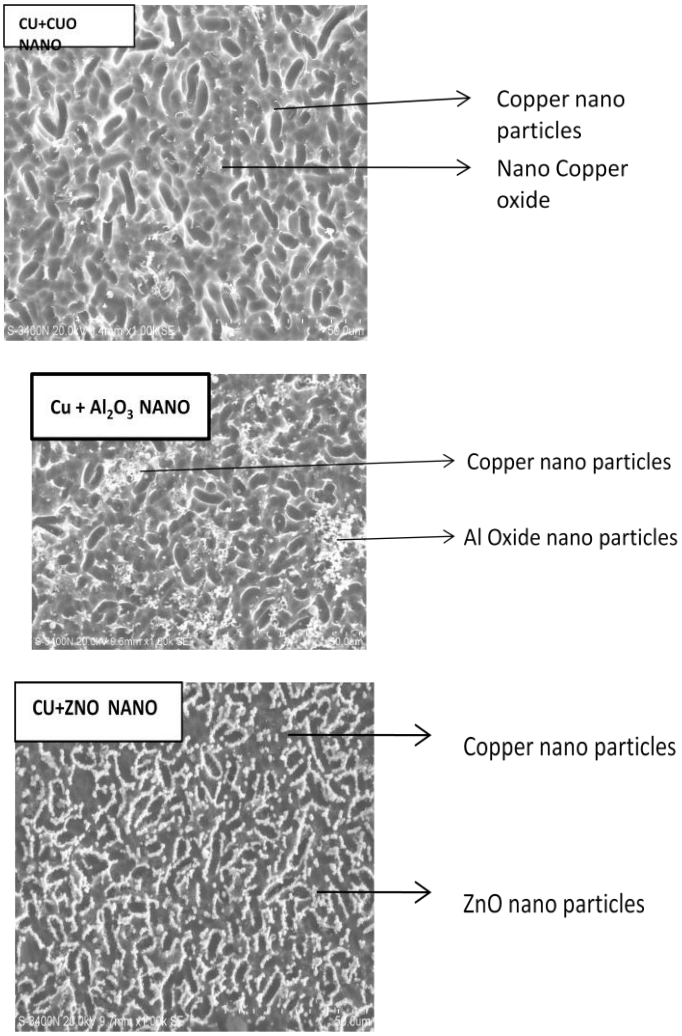

Fig. 6.4: SEM images of electroless copper coated solar cells with the addition of nano additives with 1000x magnification

6.1.3 Energy-Dispersive X-Ray Analysis Results of Copper Coated Solar Cell With the Addition of Nano Additives

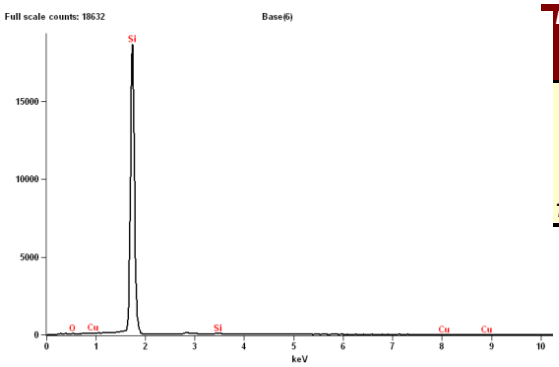

Element Line	Atom %	Formula
O K	0.63	O
Si K	98.98	Si
Cu K	0.39	Cu
Total	100.00	

Fig. 6.5: EDAX of copper coated solar cell with copper oxide nano additive

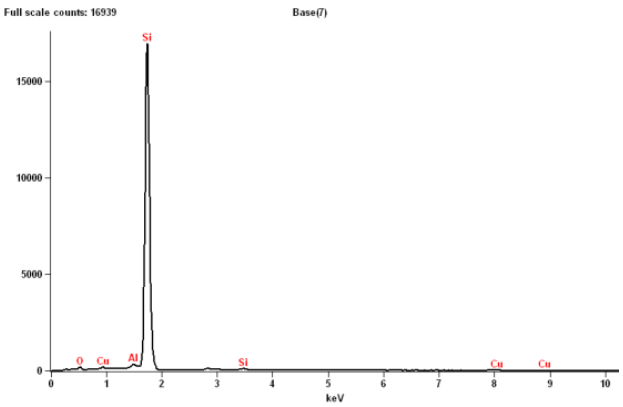

Element Line	Net Counts	Atom %	Formula
O K	580	4.98	O
Al K	1800	0.99	Al
Si K	164867	93.87	Si
Cu K	53	0.17	Cu
Cu L	866	---	
Total		100.00	

Fig. 6.6: EDAX of copper coated solar cell with Aluminium oxide nano additive

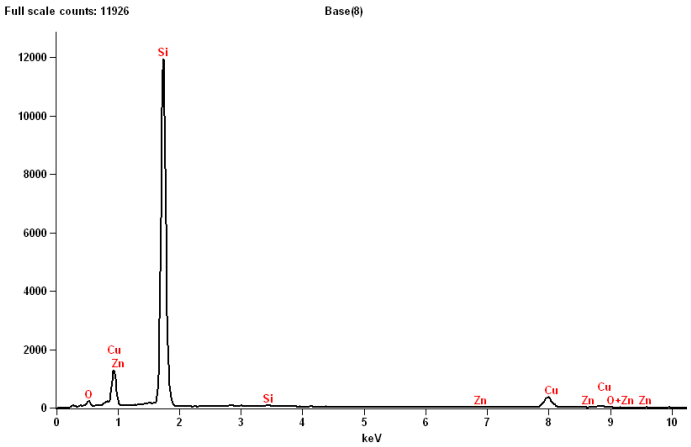

Element Line	Net Counts	Atom %	Formula
O K	1327	8.25	O
Si K	114525	73.93	Si
Cu K	6698	17.52	Cu
Zn L	270	0.31	Zn
Total		100.00	

Fig. 6.7: EDAX of copper coated solar cell with Zinc oxide nano additive

6.1.4 Comparison of UV-Visible Spectroscopy of Copper Coated Solar Cell with Addition of Nano Additives

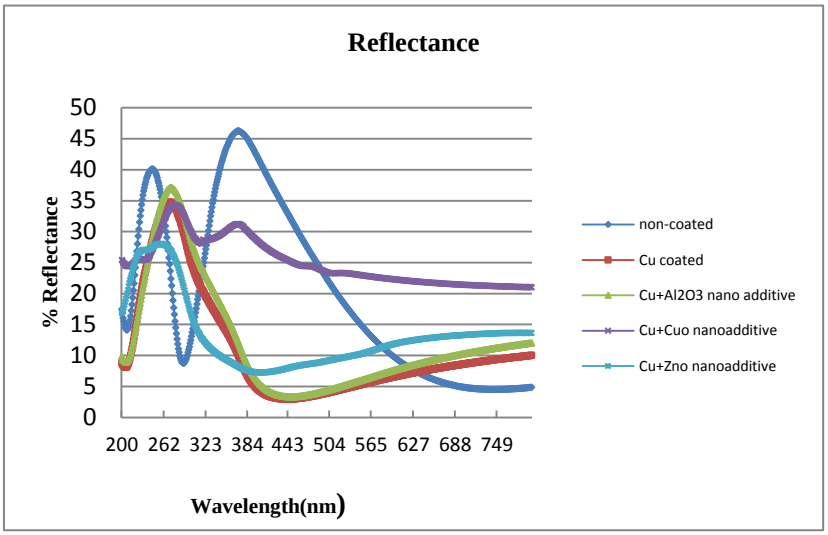

Fig. 6.8: UV –Visible reflectance spectra of copper coated Solar cell with nano additives

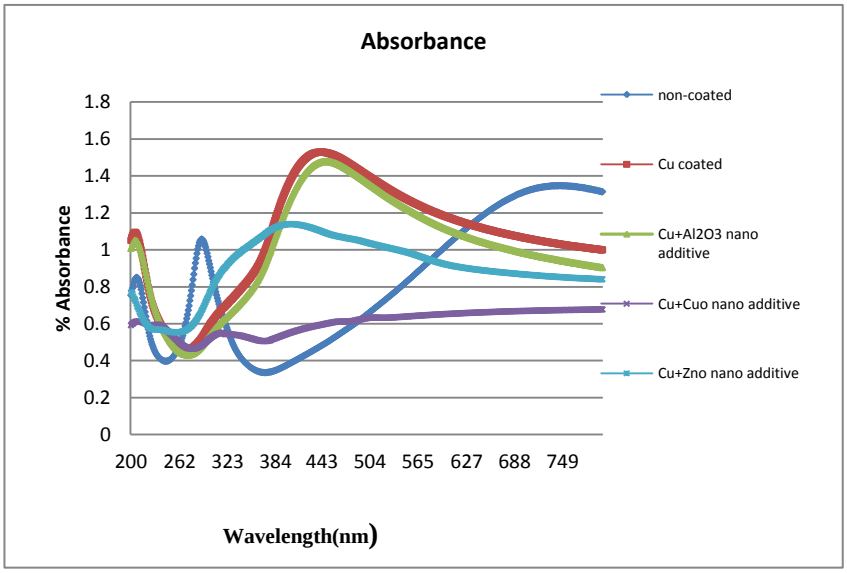

Fig. 6.9: UV-Visible Absorbance spectra of copper coated solar cell with nano additives

From Fig. 6.8, the reflectance of copper coated solar cell with the addition of zinc oxide nano additives shows better reduction in reflectance to 27% when compared to the reference cell. The copper coated solar cell with Al_2O_3 shows better absorbance next to Cu coated cell. The rank next to aluminium oxide is zinc oxide and the addition of CuO to copper shows less absorbance since the addition of CuO shows increase in coating thickness which will mask the surface.

6.2 COMPARITIVE STUDY WITH THE SPIN COATED TiO_2 ON COPPER COATED SOLAR CELL WITH NANO ADDITIVES

6.2.1 SEM and EDAX analysis

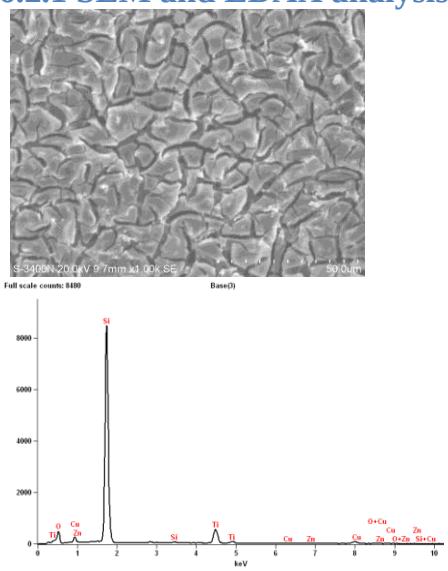

Element Line	Net Counts	Atom %	Formula
O K	3159	29.76	O
Si K	81632	57.11	Si
Ti K	7480	8.80	Ti
Cu K	1259	4.09	Cu
Zn L	208	0.24	Zn
Total		100.00	

Fig. 6.10: SEM image and EDAX of TiO_2 coated on copper coated solar cell with zinc oxide nano additive

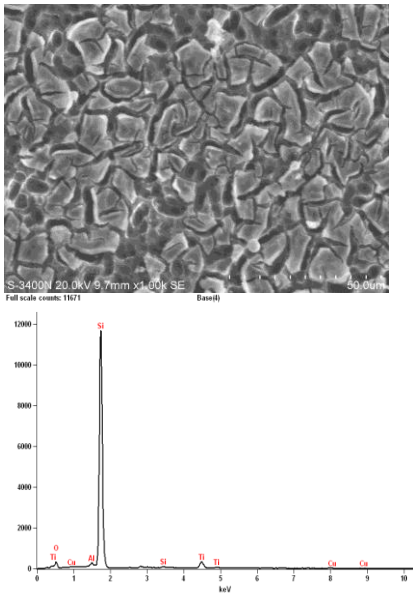

Element Line	Net Counts	Atom %	Formula
O K	2050	19.87	O
Al K	1815	1.19	Al
Si K	113444	73.26	Si
Ti K	4397	5.38	Ti
Cu K	93	0.31	Cu
Total		100.00	

Fig. 6.11: SEM image and EDAX of TiO_2 coated on copper coated solar cell with aluminium oxide nano additive

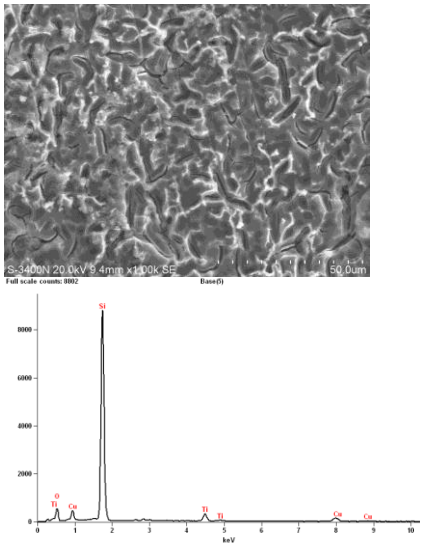

Element Line	Net Counts	Atom %	Formula
O K	3826	28.85	O
Si K	85201	58.24	Si
Ti K	3955	4.32	Ti
Cu K	2862	8.59	Cu
Total		100.00	

Fig. 6.12: SEM image and EDAX of TiO_2 coated on copper coated solar cell with zinc oxide nano additive

6.2.2 UV-Visible Spectroscopy analysis

The samples coated with copper with the addition of zinc oxide nano additives to the electroless copper bath with TiO_2 coating shows better absorbance of 1.1% and the reduction in the maximum reflectance to 13% from Fig. 6.13, when compared to other results derived from the addition of nano additives aluminium oxide and copper oxide.

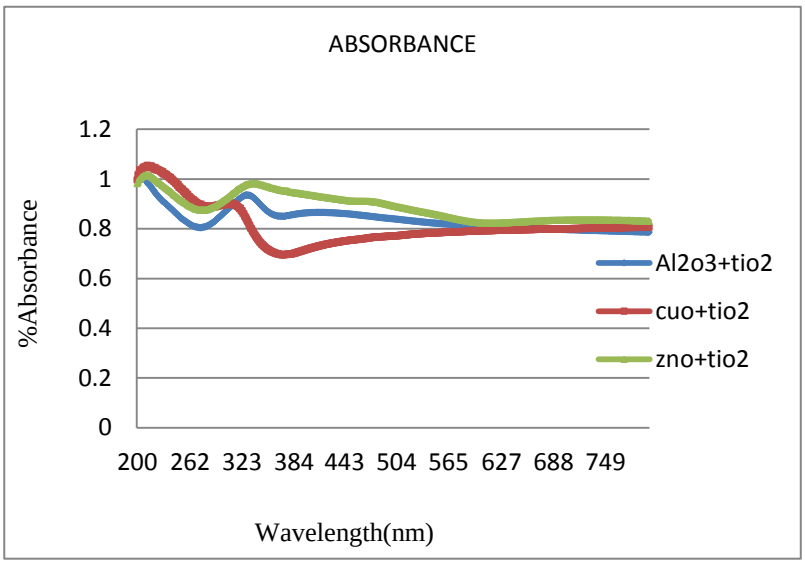

Fig. 6.13: UV-Visible Absorbance spectra of spin coated TiO_2 on copper coated solar cell with nano additives

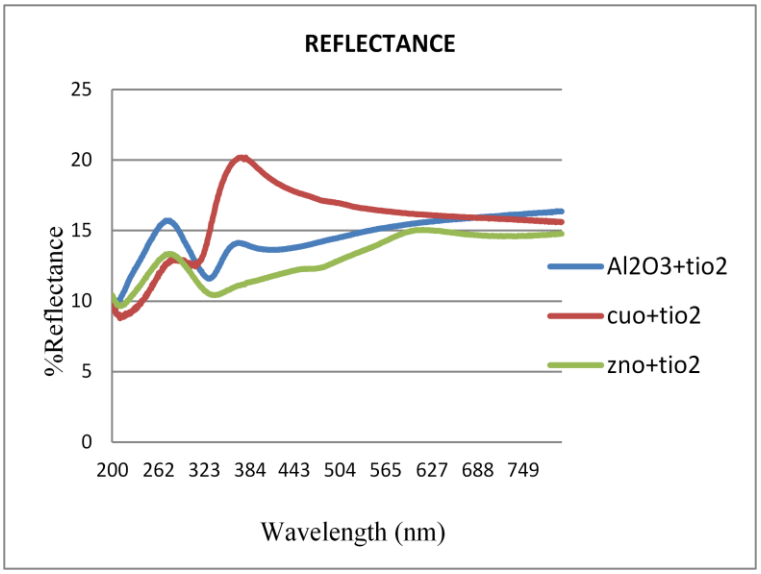

Fig. 6.14: UV-Visible reflectance spectra of spin coated TiO_2 on copper coated solar cell with nano additives

The UV absorption spectra shown in Fig. 6.13 showed sharp absorption peaks with a blue shift for ZnO nano additive, due to mono dispersity and lower particle size of zinc oxide. The zinc oxide curve shows two peaks in the UV region and uniform absorbance in the visible range.

6.3 SUMMARY

This chapter discuss about the study of various properties of the copper solar cell coated with the addition of nano additives such as CuO, Al_2O_3 and ZnO to the electroless copper bath. As the second session in this chapter the copper coated solar with nano additives was again spin coated with TiO_2. The comparative study was made with respect to SEM, EDAX and UV-Visible spectroscopy analysis. The conclusion and the future scope of the research are presented in the next chapter.

CHAPTER 7 : CONCLUSION

The electroless coating on the multicrystalline solar cell creates the texturing of silicon surface with copper nano particles which acts itself as an anti reflective coating and the dense copper layer on the gridlines adds the property of good corrosion resistance, good absorbance of sunlight and anti bacterial properties.

7.1 EFFECT OF COPPER TEXTURING

The absorbance of the cell was increased to 1.5% with reference to that of 1.1% in case of reference cell and the reflectance of the cell was decreased from 46% to 35 % .The fill factor of the cell was increased to 61.15 % which leads to the efficiency of 11.06 % which is 4% increase when compared to that of the reference cell.

7.2 OPTIMIZATION OF ELECTROLESS PROCESS

The optimum operating conditions for electroless coating of copper on solar cell for maximum green energy consumption was obtained, when the pH was 9-10 and at the temperature of 85 ^{o} C with the surfactant concentration of 1.2g/l, with the activation time of 2 minutes and immersion time of one hour.

7.3 EFFECT OF TiO_2 COATING

The efficiency of the solar cell coated with TiO_2 shows the efficiency of 14.86% which is 3 % increase from the copper coated solar cell. The efficiency of the solar cell has increased to 50% when compared to the reference cell.

7.4 OPTIMIZATION OF SPIN COATING

From the DOE results of TiO_2 coating process, the spinning speed influences the surface roughness and the coating thickness is affected by the spinning speed and temperature. The major effect on the electrical properties is by the spinning time and minor effect by temperature. The optimum operating conditions for spin coating of TiO_2 on copper coated solar cell was obtained at the spinning speed of 4000rpm, spinning time of 20 sec and at the annealing temperature of 100^{o}C.

7.5 ADDITION OF NANO ADDITIVES

Maximum voltage was obtained with the 0.1% of CuO and Al_2O_3 nano additive and 2% of ZnO nano additive. As the coating thickness increases, the voltage decreases in case of CuO due to the synergistic effects of the electron back-transport reaction and the resistive losses.

The addition of zinc oxide nano additives with TiO_2 coating shows better absorbance of 1.1% and the reduction in the reflectance to 13% when compared to other results derived from the addition of nano additives aluminium oxide and copper oxide with TiO_2 coating.

7.6 FUTURE SCOPE

1. Electroless coating can be carried out on solar cell using other metals such as zinc and aluminium
2. The electroless solutions can be chosen such that the oxide formation can be avoided
3. Various coating techniques can be employed to develop thin film solar cell.

APPENDIX

MINITAB RESULTS FOR THE ANALYSIS OF ELECTROLESS COPPER COATING

General Linear Model: surfacerough versus pH, temperature, surfactant c

```
Factor                    Type   Levels  Values
pH                        fixed       2  4, 10
temperature               fixed       2  65, 85
surfactant concentration  fixed       2  0.0, 1.2
Analysis of Variance for surfaceroughness(µm), using Adjusted SS for
Tests
Source                    DF   Seq SS   Adj SS   Adj MS     F      P
pH                         1  0.00605  0.00605  0.00605  0.18  0.700
temperature                1  0.00045  0.00045  0.00045  0.01  0.915
surfactant concentration   1  0.31205  0.31205  0.31205  9.27  0.056
pH*temperature             1  0.08405  0.08405  0.08405  2.50  0.212
Error                      3  0.10095  0.10095  0.03365
Total                      7  0.50355
S = 0.183439   R-Sq = 79.95%   R-Sq(adj) = 53.22%
```

The regression equation is
surfaceroughness(µm) = 0.850 - 0.0092 pH - 0.00075 temperature- 0.329 surfactant concentration

General Linear Model: coating thic versus pH, temperature, surfactant c

```
Factor                    Type   Levels  Values
pH                        fixed       2  4, 10
temperature               fixed       2  65, 85
surfactant concentration  fixed       2  0.0, 1.2
Analysis of Variance for coating thickness(µm), using Adjusted SS for Tests
Source                                DF  Seq SS  Adj SS  Adj MS     F      P
pH                                     1   1.523   1.523   1.523  0.41  0.587
temperature                            1   0.030   0.030   0.030  0.01  0.936
surfactant concentration               1  35.322  35.322  35.322  9.54  0.091
pH*temperature                         1   5.831   5.831   5.831  1.58  0.336
temperature*surfactant concentration   1   1.931   1.931   1.931  0.52  0.545
Error                                  2   7.404   7.404   3.702
Total                                  7  52.040
S = 1.92401   R-Sq = 85.77%   R-Sq(adj) = 50.21%
```

The regression equation is
coating thickness(µm) = 8.07 + 0.145 pH - 0.0061 temperature+ 3.50 surfactant concentration

General Linear Model: current(Amps versus pH, temperature, surfactant c

```
Factor                    Type   Levels  Values
pH                        fixed       2  4, 10
temperature               fixed       2  65, 85
surfactant concentration  fixed       2  0.0, 1.2
Analysis of Variance for current(Amps), using Adjusted SS for Tests
Source                    DF     Seq SS     Adj SS     Adj MS     F      P
pH                         1  0.0000781  0.0000781  0.0000781  0.82  0.432
temperature                1  0.0000451  0.0000451  0.0000451  0.47  0.541
surfactant concentration   1  0.0002101  0.0002101  0.0002101  2.20  0.235
pH*temperature             1  0.0004651  0.0004651  0.0004651  4.87  0.114
Error                      3  0.0002864  0.0002864  0.0000955
Total                      7  0.0010849
S = 0.00977028   R-Sq = 73.60%   R-Sq(adj) = 38.41%
```

The regression equation is
current(Amps) = 0.0649 + 0.00104 pH + 0.000237 temperature+ 0.00854 surfactant concentration

General Linear Model: Voltage(Volt versus pH, temperature, surfactant c

```
Factor                    Type   Levels  Values
pH                        fixed       2  4, 10
temperature               fixed       2  65, 85
surfactant concentration  fixed       2  0.0, 1.2
Analysis of Variance for Voltage(Volts), using Adjusted SS for Tests
Source                       DF     Seq SS     Adj SS     Adj MS      F      P
pH                            1  0.0044651  0.0044651  0.0044651   6.07  0.091
temperature                   1  0.0010351  0.0010351  0.0010351   1.41  0.321
surfactant concentration      1  0.0051511  0.0051511  0.0051511   7.00  0.077
pH*surfactant concentration   1  0.0077501  0.0077501  0.0077501  10.53  0.048
Error                         3  0.0022084  0.0022084  0.0007361
Total                         7  0.0206099
S = 0.0271316   R-Sq = 89.28%   R-Sq(adj) = 75.00%
```

The regression equation is
Voltage(Volts) = 0.349 + 0.00788 pH + 0.00114 temperature + 0.0423 surfactant concentration

General Linear Model: power(Watts) versus pH, temperature, surfactant c

Factor	Type	Levels	Values
pH	fixed	2	4, 10
temperature	fixed	2	65, 85
surfactant concentration	fixed	2	0.0, 1.2

Analysis of Variance for power(Watts), using Adjusted SS for Tests

Source	DF	Seq SS	Adj SS	Adj MS	F	P
pH	1	0.0001201	0.0001201	0.0001201	1.40	0.358
temperature	1	0.0000451	0.0000451	0.0000451	0.53	0.543
surfactant concentration	1	0.0002101	0.0002101	0.0002101	2.45	0.258
pH*temperature	1	0.0001531	0.0001531	0.0001531	1.79	0.313
pH*surfactant concentration	1	0.0001201	0.0001201	0.0001201	1.40	0.358
Error	2	0.0001713	0.0001713	0.0000856		
Total	7	0.0008199				

S = 0.00925338 R-Sq = 79.11% R-Sq(adj) = 26.89%

The regression equation is

power(Watts) = 0.0176 + 0.00129 pH + 0.000238 temperature
+ 0.00854 surfactant concentration

MINITAB RESULTS FOR THE ANALYSIS OF SPIN COATING OF TiO_2

General Linear Model: power(watts) versus spinning spe, spinningtime, ...

Factor	Type	Levels	Values
spinning speed(rpm)	fixed	2	2000, 4000
spinningtime(sec)	fixed	2	20, 100
temperature(oC)	fixed	2	100, 150

Analysis of Variance for power(watts), using Adjusted SS for Tests

Source	DF	Seq SS	Adj SS	Adj MS	F
spinning speed(rpm)	1	0.0000379	0.0000379	0.0000379	2.02
spinningtime(sec)	1	0.0002398	0.0002398	0.0002398	12.80
temperature(oC)	1	0.0000401	0.0000401	0.0000401	2.14
spinning speed(rpm)*temperature(oC)	1	0.0001988	0.0001988	0.0001988	10.61
Error	3	0.0000562	0.0000562	0.0000187	
Total	7	0.0005727			

Source	P
spinning speed(rpm)	0.250
spinningtime(sec)	0.037
temperature(oC)	0.240
spinning speed(rpm)*temperature(oC)	0.047
Error	
Total	

S = 0.00432855 R-Sq = 90.19% R-Sq(adj) = 77.10%

Regression Equation

power(watts) = 0.0496578 - 2.17548e-006 spinning speed(rpm)
- 0.000136877spinningtime(sec) + 8.95178e-005 temperature(oC)

General Linear Model: Current(Amps versus spinning spe, spinningtime, ...

Analysis of Variance for Current(Amps), using Adjusted SS for Tests

Source	DF	Seq SS	Adj SS	Adj MS	F
spinning speed(rpm)	1	0.0000088	0.0000088	0.0000088	3.24
spinningtime(sec)	1	0.0001378	0.0001378	0.0001378	50.59
temperature(oC)	1	0.0000445	0.0000445	0.0000445	16.34
spinning speed(rpm)*temperature(oC)	1	0.0001066	0.0001066	0.0001066	39.14
Error	3	0.0000082	0.0000082	0.0000027	
Total	7	0.0003058			

Source	P
spinning speed(rpm)	0.170
spinningtime(sec)	0.006
temperature(oC)	0.027
spinning speed(rpm)*temperature(oC)	0.008
Error	
Total	

S = 0.00165025 R-Sq = 97.33% R-Sq(adj) = 93.77%

Regression Equation

Current(Amps) = 0.0894417 - 1.05e-006 spinning speed(rpm) - 0.00010375 spinningtime(sec) + 9.43333e-005Temperature(oC)

General Linear Model: voltage(Volt versus spinning spe, spinningtime, ...

Analysis of Variance for voltage(Volts), using Adjusted SS for Tests

Source	DF	Seq SS	Adj SS	Adj MS	F
spinning speed(rpm)	1	0.002211	0.002211	0.002211	1.94
spinningtime(sec)	1	0.010296	0.010296	0.010296	9.04
temperature(oC)	1	0.000861	0.000861	0.000861	0.76
spinning speed(rpm)*temperature(oC)	1	0.008515	0.008515	0.008515	7.47
Error	3	0.003418	0.003418	0.001139	
Total	7	0.025302			

Source	P
spinning speed(rpm)	0.258
spinningtime(sec)	0.057
temperature(oC)	0.449
spinning speed(rpm)*temperature(oC)	0.072
Error	
Total	

S = 0.0337559 R-Sq = 86.49% R-Sq(adj) = 68.48%

Regression Equation

voltage(Volts) = 0.550188 - 1.6625e-005 spinning speed(rpm) - 0.000896875spinningtime(sec) + 0.000415 temperature(oC)

General Linear Model: surface roug versus spinning spe, spinningtime, ...

Factor	Type	Levels	Values
spinning speed(rpm)	fixed	2	2000, 4000
spinningtime(sec)	fixed	2	20, 100
temperature(oC)	fixed	2	100, 150

Analysis of Variance for surface roughness(µm), using Adjusted SS for Tests

Source	DF	Seq SS	Adj SS	Adj MS	F	P
spinning speed(rpm)	1	0.25920	0.25920	0.25920	15.77	0.029
spinningtime(sec)	1	0.03380	0.03380	0.03380	2.06	0.247
temperature(oC)	1	0.00845	0.00845	0.00845	0.51	0.525
spinningtime(sec)*temperature(oC)	1	0.05445	0.05445	0.05445	3.31	0.166
Error	3	0.04930	0.04930	0.01643		
Total	7	0.40520				

S = 0.128193 R-Sq = 87.83% R-Sq(adj) = 71.61%

Regression Equation

surface roughness(µm) = -0.14 + 0.00018 spinning speed(rpm) + 0.001625spinningtime(sec) + 0.0013 temperature(oC)

General Linear Model: coating thic versus spinning spe, spinningtime, ...

Factor	Type	Levels	Values
spinning speed(rpm)	fixed	2	2000, 4000
spinningtime(sec)	fixed	2	20, 100
temperature(oC)	fixed	2	100, 150

Analysis of Variance for coating thickness(µm), using Adjusted SS for Tests

Source	DF	Seq SS	Adj SS	Adj MS	F	P
spinning speed(rpm)	1	2.7966	2.7966	2.7966	5.43	0.102
spinningtime(sec)	1	0.0171	0.0171	0.0171	0.03	0.867
temperature(oC)	1	0.8515	0.8515	0.8515	1.65	0.289
spinningtime(sec)*temperature(oC)	1	0.5886	0.5886	0.5886	1.14	0.363
Error	3	1.5456	1.5456	0.5152		
Total	7	5.7995				

S = 0.717783 R-Sq = 73.35% R-Sq(adj) = 37.81%

Regression Equation

coating thickness(µm) = 7.00312 - 0.00059125 spinning speed(rpm) - 0.00115625spinningtime(sec) - 0.01305 temperature(oC)

REFERENCES

1. **Ali Bahrami et al**., 'Optimized Single and Double Layer Antireflection Coatings for GaAs Solar Cells' International Journal of Renewable Energy Research, Vol.3, No.1, **2013**.

2. **Andrew Yeh J-L et al.,** "Copper encapsulated silicon micro machined structures", Journal of Microelectromechanical Systems, Vol. 9, No. 3, September **2000.**

3. **Astha Kukreja**, "Application of Full Factorial Design for Optimization of Feed Rate of Stationary Hook Hopper", International Journal of Modeling and Optimization, Vol. 1, No. 3, August **2011.**

4. **Balakrishnan Kavitha*, Muthusamy Dhanam** "Determination of Optimum Film Thickness and Composition of Cu(InAl)Se2 Thin Films as an Absorber for Solar Cell Applications", World Journal of Nano Science and Engineering, Vol. 1, pp.108-118, **2011**.

5. **Bard, A. J. J.** Phys. Chem. **1982,** 86, 172**; J.** Photochem. **1979,** 10, 59**;** Science **1980,** 207, 139**.**

6. **Battiston.G.A, R.Gerbasi, M. Porchia, A. Morigo**,, Thin Solid Films,Vol. 239, pp. 186, **1994.**

7. **Brinker.C.F and G. W. Scherer**, sol-gel science, The Physics and Chemistry of sol-gel processing, Academic press, London, **1990**.

8. **Brinker, M.S. Harrington**, Solar Energy Mater. S, pp 159, **1981.**

9. **Buck . P and L. R. Griffith,** "Voltammetric and chronopotentiometric study of the anodic oxidation of methanol, formaldehyde, and formic acid", J. Electrochem. Soc., Vol. 109, No. 11, pp.1066–1068, Nov. **1964.**

10. **Carp.O, C. L. Huisman and A. Reller,** Prog. Solid State. Chem, Vol. 32, No.33, **2004**.
11. **Coombs.C.F**, Printed Circuit Handbook, 3rd ed., McGraw-Hill, NewYork, pp. 12.1–45 and 13.1–18, **1988**.

12. **Deckert.C.A**, Plating and Surface Finishing 82 (2) (1995) 48; Plating and Surface Finishing 82 (3) (**1995**) 58.

13. **Eea, Y.C., Chen, Z. et al**., "Effect of processing parameters on electroless Cu seed layer Properties", Thin Solid Films, ICMAT 2003 Conference Issue, Vol. 462–463, pp.197–201, **2004**.

14. **Elansezhian, R et al** .,'The influence of SDS and CTAB surfactants on the surface morphology and surface topography of electroless Ni–P deposits', Journal of Materials Processing Technology, Vol. 209, No. 14, pp.233–240, **2009**.

15. **Fernandez L.A, Z. P. Espinos, T. R. Belderrain, and A. R. Gonzalez-Elipe**,, Thin Solid Films, Vol. 241, No. 154, **1994.**

16. **Fleisher.M, H. Meixner**, Sensor Actuators B 4, 437,**1999.**

17. **Fujishima.A, Hashimoto.K and Watanabe.T**: TiO_2 photocatalysis, fundamentals and applications (BKC, Tokoyo, **1999**).

18. **Fujishima, A**, Honda, K. Nature, Vol. 37, No. 238**, 1972.**

19. **Funda Sayilkan et al.,** "Characterization of TiO_2 Synthesized in Alcohol by a Sol-Gel Process: The Effects of Annealing Temperature and Acid Catalyst" Turk J Chem, Vol. 29, pp. 697- 706, **2005**.

20. **Fujishima.A** and K. Honda, Natura 238, 38, **1972**.

21. **Fujishima.A, T. N. Rao, and D. A. Tryk.** Titanium Dioxide Photocotalysis. J. Photochem. Photobio. C: Photochem. Rev, Vol. 1, pp. 1-21, **2000**.

22. **Forro.L, O. Chauvet, D. Emin, L. Zupplioli, H. Berger, and F. Levy**J.Appl. Phys. Vol. 75, No. 1, pp 633-635, **1994**.

23. **Gratzel,** M., Ed. Energy Resources through Photochemistry and Catalysis; Academic Press: New York, **1983.**

24. **Graetzel.M**, Comments Inorg. Chem. Vol. 12, No. 93, **1991.**

25. **Guan-Jun Yang et al.,** "Influence of pore structure on ion diffusion property in porous TiO_2coating and photovoltaic performance of dye- sensitized solar cells" surface and coatings technology, Vol. 205, pp. 3205-3210, **2011**.

26. **Gugliemi.M, P. Colombo, and D. Mancielli**, 1992, J. Nan- Cryst. Sol. Vol. 147, No. 641, **1992**.

27. **Hanna, F., Abdel Hamid, Z. et al**., "Controlling factors affecting the stability and rate of electroless copper plating", Materials Letters, Vol. 58, No. 1–2, pp.104–109, **2003**.

28. **Henrich.V.E**, Rep, Prog. Phys. Vol. 48, pp. 1481, **1985**.

29. **Hilton B. de Aguiar et al**.,"Surface Structure of Sodium Dodecyl Sulfate Surfactant and Oil at the Oil-in-Water Droplet Liquid/Liquid Interface: A Manifestation of a Nonequilibrium Surface State", J. Phys. Chem. Vol. 115, pp. 2970–2978, **2011**.

30. **Hocine1.D, MS. Belkaid**, "3% absolute efficiency gain on multicrystalline silicon solar cells by TiO_2 antireflection coatings derived by APCVD process" European Association for the Development of renewable Energies, Environment and Power Quality (EA4EPQ), International conference on Renewable Energies and Power Quality (ICREPQ'12) Santiago de Compostela (Spain), 28th to 30th March, **2012**.
31. **Hung.A**, Journal of the Electrochemical Society Vol.132, No.1047, **1985.**

32. **Innes.W.P, J.J. Grunwald, E.D. Ottavio, W.H. Toller, C. Armicheal**, Plating, Vol. 56, No. 51, **1969**.

33. **Janczuk.B, M.** L. Gonzalez-martın, and J. M. Bruque, "Wettability of fluorite in the presence of an anionic and a non-ionic surfactant", Canadian Metallurgical Quarterly, Vol. 35, No. 1, pp.17–21, **1996**.

34. **Jeremy Barbe et al.,** "Nanoimprinted TiO_2 sol–gel passivating diffraction gratings for solar cell applications" progress in photovoltaics: research and applications Prog. Photovolt: Res. Appl. (**2011**).
35. **Kubota.Y, C. Niwa, T. Ohnuma, Y. Ohko**, T. Talsuma, T. Mori, and A.Fujishima, J. Photochem. Potoboil. A, Vol. 141, No. 225, **2001.**

36. **Landoft – Bornstein**, New Series, Semiconductors: Physics of Non-Terahedrally Bonded Binary Compounds, III, 179, Springer, Verlag, Berlin, pp. 133-150,**1984**.
37. **Lobl.P, M. Huppertz, D. Mergel**, Thin Solid Films, Vol. 251, No. 72, **1994**.

38. **Lowenheim.F.A**, Modern Electroplating, 3rd ed., Wiley, New York, pp. 636, **1974**.

39. **Lukes.R.M**,"Chemistry of autocatalytic reduction of copper by alkaline formaldehyde,"Plating,Vol.51, No.11, pp.1066-1068, **Nov.1964**.
40. **Mandich.N.V**, **G.A. Krulik**, Plating and Surface Finishing, 80 (**1993**) 68.

41. **Manea.E**, E. Budianu, M. Purica, C. Podaru, A. Popescu, I. Cernica, F.Babarada, and C. C. Parvalecu, "SnO_2 thin films prepared by sol-gel method

for honeycomb textured silicon solar cell", Romanian Journal of information science and technology, Vol.10, No.1, **2007**.

42. **Manjunatha Pattabi et al.,** " Preparation and characterization of copper indium diselenide films by electroless deposition" Solar Energy Materials & Solar Cells, Vol. 63, pp. 315-323, **2000**.
43. **Martin.N**, C, Rousselot, C. Savall, and F. Polmino, Thin Solid Films, Vol. 287, No.154, **1994**.
44. **Medina-Valtierra, J**., Claudio, F.-R., Calixto, S., Bosch, P., Lara, V.H., "The influence of surfactants on the roughness of titania sol–gel films", Mater. Charact, Vol.58, pp. 233–242, **2007**.

45. **Mechiakh.R** "TiO_2 thin films prepared by sol-gel method for wave guiding applications: correlation between the structural and optical properties" optical materials, Vol.30, pp. 645-651, **2007**.

46. **Narasimha Rao.K et al.,** "Some Studies on TiO_2 Films Deposited by Sol-Gel Technique" Advances in Thin-Film Coatings for Optical Applications, Proc. of SPIE Vol. 7067, 70670F, **2008**. Doi: 10.1117/12.799923.

47. **Nathan Fritz et al**., "Electroless Deposition of Copper on Organic and Inorganic Substrates Using a Sn/Ag Catalyst" Journal of The Electrochemical Society, Vol.159 , No.6, pp. D386-D392, **2012.**

48. **NuzziF.J**, Plating and Surface Finishing ,Vol.70, No.51, **1983**.

49. **Ollis, D. F., Al-Ekabi, H.,** Eds. Photocatalytic Purification andTreatment of Water and Air; Elsevier: Amsterdam, **1993.**
50. **Oregan.B and M. Gratzal**, Natura, Vol. 353, No.737, **1991**.

51. **Oskam, J G. Long** "Electrochemical deposition of metals onto silicon" J. Phys. D: Appl. Phys, Vol. 31, pp. 1927–1949, **1998**.

52. **Paily.R, A. DasGupta, N. DasGupta, P. Bhattacharya,** T. Inisra, LM.Kukkeja, AK. Balamurugan, S. Rajagopalun, and AK. Tyagi, Applied Surface Sicience, Vol. 187, pp 297- 304, **2002**.

53. **Parmon V. N, Zamareav, K. I**. In Photocatalysis –Fundamentals and Applications; Serpone, N., Pelizzetti, E., Eds.; Wiley Interscience : New York, pp. 565**, 1989.**

54. **Pelizzetti.E, Schiavello. M**., Eds. Photochemical Conversion and Storage of Solar Energy; Kluwer Academic Publishers: Dordrecht, **1991.**

55. **Paunovic.M**, "Electrochemcial aspects of electroless deposition of metals," Plating, Vol. 55, No. 11, pp. 1161–1167, Nov **1968**.

56. **Paunovic .M and M. Schlesinger**, Fundamentals of Electrochemical Deposition. Pennington, NJ: Electrochem. Soc., **1998**.
57. **Rancourt.J**, Optical Thin Films (user's Handbook), McGraw-Hill, NewYork, **1987**.

58. **Raseshwar.K and J. G. Ibanez**., "Electrochemical Aspects of Photocatalys D: Application to Detoxification and Disinfection Scenarios" , J. Chem, Edu. Vol. 72, pp. 1044-1049, **1995**.

59. **Rati Saluja et al.,** "Modeling and Parametric Optimization using Factorial Design Approach of Submerged Arc Bead Geometry for Butt Joint" International Journal of Engineering Research and Applications (IJERA) ISSN: 2248-9622 www.ijera.com Vol. 2, Issue 3, pp. 505-508 ,May-Jun **2012**.
60. **Riedel Wolf**, Electroless Plating, ASM International, Ohio, pp. 287, **1991**.

61. **Saveninije.T.J, J. M. Warman and A. Goosens**, Chem. Phys. Lett, Vol. 287, No. 148, **1998**.

62. **Schiavello, M**., Ed. Photocatalysis and Enuironment; Kluwer Academic Publishers: ordrecht, **1988.**

63. **Sze S.M** " Physics of semiconductor devices" 5th edition ,Wiley publishers, **2008**.

64. **Sonawane .R.S**., "Preparation of titanium(IV) oxide thin film photocatalyst by sol–gel dip coating" Materials Chemistry and Physics, Vol .77, pp.744–750, **2002**.

65. **Sahrul Saehana et al** .,"Efficiency improvement in TiO_2-particle based solar cells after deposition of metal in spaces between particles" International Journal of Basic & Applied Sciences IJBAS-IJENS. Vol. 11 No. 06.

66. **Sunada,T.Watanabeand K.Hashimoto**:Environmental Science and Technology,Vol.37, No.4785, **2003**.

67. **Tang.H, K. Poasad, R. Sunjines, P. E. Schmid, and F. Levy**, J. Appl.Phys, Vol. 75, No. 4, pp 2042, **1994**.
68. **Tripathy**B.C., Das S.C., Hefter G.T., Singh P., "Electro winning from acidic sulfate solution Part I Effects of SLS", Journal of Applied Electrochemistry, Vol. 27, pp.673–674, **1997**.

69. **Tryl.D.A, A. Fujishima, and K. Honda,** "Recent Topical in Photo electrochemistry: Achievements and Future Prospects" Electrochim.Acta, Vol. 45, pp. 2363-2376, **2000**.

70. **Twite R. L. ,GP. Bierwagon,** prog. Coat. Vol. 33, No. 91, **1998**.

71. **Yongxiang Li et al.,** "Titanium dioxide films for photovoltaic cells derived from a sol-gel process" Solar Energy Materials and Solar Cells, Vol.56, pp.167 -174, **1999**.

LIST OF PUBLICATIONS

(a)International Journals (5):

1. **M.Jeevarani**, R.Elansezhian and, N.karpagavalli "Study on the effect of process parameters in the electroless copper coating on solar photovoltaic cell" international journal of Engineering and Innovative Technology, ISO 9001:2008 Certified,ISSN:2277-3754, Volume 2, Issue 7, January 2013. (Published)
2. **M.Jeevarani** and R.Elansezhian,(2014) "Development of self cleaning and energy efficient solar cells using two different coating techniques" International journal of Computer Aided Engineering and Technology, Inderscience enterprises ltd. (published)
3. **M.Jeevarani** and R.Elansezhian "Optimizing the process parameters in spin coating of sol-gel TiO_2 on copper textured solar cells using full factorial method" journal of Sol-Gel Science and Technology –Springer (Accepted) Ref. No: JSST-S-14-00002
4. **M.Jeevarani** and R.Elansezhian "Texuring of solar cell using electroless copper coating to increase the green energy consumption" Journal of Green Energy – Taylor and Francis(Communicated)
5. **M.Jeevarani** and R.Elansezhian(2014) "Comparative study on the effects of surfactants on the electroless copper coated solar cell and optimizing its process parameters"Advances In Chemistry-Hindawi publication(Published)

(b) International conferences (6):

1. **M.Jeevarani**, R.Elansezhian, and N.Sathyaprasanna "Study on optimizing the process parameters in the electroless copper coating on solar PV cells using full factorial method" The 3rd Asian Symposium on Materials & Processing ASMP – 2012(IIT,MADRAS).
2. **M.Jeevarani** and R.Elansezhian "Study on the process parameters in the electroless copper coating on solar pv cell to increase its green energy consumption" 1st international conference on Bio energy, Environment and Sustainable Technologies(BEST2013),jan27-30,2013.(Arunai Engg College, Thiruvannamalai).
3. **M.Jeevarani** and R.Elansezhian "Study on developing photocatalytic solar cell by electroless process and optimizing its process parameters to improve the energy absorbing efficiency" "Second International Conference on Advances in Materials Processing and Characterization (AMPC) 2013 February, 6-8, 2013 (ANNA UNIVERSITY,CHENNAI).
4. **M.Jeevarani** and R.Elansezhian "Study on developing electroless coated solar photovoltaic cell and optimizing its process parameters using full factorial method" IEEE - International Conference on Research and Development Prospectus on Engineering and Technology(ICRDPET-2013)29-30March2013(EGS-Pillai-Engg College, Nagapattinam).
5. **M.Jeevarani** and R.Elansezhian "Development of self-cleaning and energy efficient solar cells using two different coating techniques" International

conference on Advanced Materials and Manufacturing-2013, 11-12 April 2013(Cape Institute, kanyakumari).

6. **M.Jeevarani** and R.Elansezhian "Study on the effects of surfactants on the electroless Copper coated solar pv cells and optimizing its process parameters" International Conference on Green Technology in Engineering and Applied Science, 2013. 29th to 30th March 2013. (Adiparasakthi Engg College, Melmaruvathur.)